Adsorption of oxygen molecules on platinum surfaces modified with subsurface atoms of vanadium: A DFT study

A thesis submitted to the Faculty of Engineering and Built Environment, University of Cape Town, in fulfilment of the requirements of the degree of Master of Science in Engineering.

Department of Mechanical Engineering

Centre for Materials Engineering

Prepared by:

Rutendo Matengaifa

Supervisors:

Prof C. I. Lang

Dr. H. Sithole

DECLARATION

I know the meaning of plagiarism and declare that all the work in the document, save for that which is properly acknowledged, is my own.

…… ……..

Rutendo Matengaifa Date

ABSTRACT

The aim of this work was to investigate changes in the electronic structure of platinum as a result of alloying with vanadium, and the effects of these changes on O_2 adsorption. This is important for the further development of hydrogen fuel cells, because the oxygen reduction reaction (ORR) presently requires O_2 adsorption to occur on pure platinum, which is a prohibitively expensive material. A computational study has therefore been undertaken on alloying platinum (which reduces cost) with vanadium (for which there is plentiful experimental data) and the consequences for O_2 adsorption.

The first moment of the d-band of platinum alloy DOS was used to represent the d-band centre. The d-band centre of Pt-PDOS became lower as a result of hybridisation between platinum and vanadium. The d-band centre of a pure platinum surface with respect to the Fermi level is -1.99eV, but it is shifted to -3.23eV when vanadium atoms are added to the subsurface layer.

The adsorption energies of O_2 are sensitive to a combination of calculation parameters used. In this work, the calculations were executed using the CASTEP code. This is a plane wave pseudo potential code. The most stabilised geometry of an adsorbed molecule on pure Pt (111) was at the fcc site and had an adsorption energy of -1,91eV. The adsorption energy at the bridge site of Pt (111) is -1.81eV. When subsurface vanadium atoms were introduced, the equilibrium surface-molecule bond lengths increased. The adsorption energy at the fcc site shifted to -1.37eV, -1.43 for the bridge site and -1.45eV for the hcp site.

It was concluded that the presence of vanadium atoms in the surface region destabilises an adsorbed oxygen molecule but a more detailed study is needed to show the effect of the solute atoms on the thermodynamics and kinetics of the whole oxygen reduction reaction chain.

ACKNOLEDGEMENTS

I am indebted to several individuals and organisations who contributed their expertise and resources to make this project a success.

Firstly my sincere and profound gratitude goes to my supervisor, Professor Candice Lang, for the guidance and encouragement she offered throughout the work. She allowed me to pursue a project of my choice and I appreciate the constructive suggestions and corrections she offered.

I also greatly appreciate the support and assistance offered by my co-supervisor Dr. Happy Sithole and for giving me a chance to learn the art of ab initio calculations and high performance computing. Thank you for all the time and so much effort spend teaching me Density Functional Theory.

Professor Eric Van Steen, thank you for helping me during the revision process. The guidance, 'searching questions' that you always posed, and the constructive criticism helped me to stay on course.

I am grateful for all the resources and support provided by the Centre of Materials Engineering (CME). A million thanks goes to the CME staff and students for their support and friendship.

I also would like to thank Professor David J. Simbi for helping me in various aspects of my work and Chinhoyi University of Technology Staff Development Committee for funding my studies.

CSIR's Centre for High Performance Computing in Rosebank in Cape Town was such an invaluable resource for this project. I would like to thank CHPC staff for giving access to the computational resources and software.

TABLE OF CONTENTS

LIST OF FIGURES

LIST OF TABLES

CHAPTER 1

1.1 Introduction

Platinum, which has high catalytic efficacy and stability, is widely used as a solid catalyst. The main disadvantage is its price. When it is used in energy technologies, the price of platinum becomes an important issue because of the complex nature of energy markets (Gasteiger et al., 2005). Thus, in fuel cell technologies utilising platinum as their electrodes, there is a need to reduce the loading of the noble metal without compromising performance.

1.1.1 Catalysis

Catalysis is a process in which the rate of chemical reactions is altered by using other chemical substances. Catalysts themselves are not consumed in the process; they participate in reactions and are regenerated at the end of each chain to start another reaction cycle. The action of catalysts is to provide alternative reaction pathways with lower reaction barriers (Atkins, 2006).

Catalysis plays a very important role in natural processes as well as in industry. Enzymes catalyse biochemical processes that make life and other natural phenomena possible. Industrial catalytic processes are essential in many areas including food production, fuels, pharmaceuticals and environmental emissions control. Adams (2009) estimated that the catalysis industry that supports manufacturing and refining had an annual turnover of about US$15 billion and produced goods worth about US$15 trillion.

There are three types of catalytic processes: (1) enzyme (biological), (2) homogeneous and (3) heterogeneous. Of these three processes, heterogeneous catalysis is the most used in industry. The process takes place with reactants and products being in a different state of aggregation to the catalyst.

A catalysed reaction proceeds through a series of elementary processes. Figure 1.1 outlines the elementary processes of a heterogeneous catalytic reaction. First, a gaseous molecule is adsorbed onto the catalyst surface yielding adsorbed intermediates. The adsorbed intermediates in turn may diffuse across the surface and meet other species with which they may react to form new adsorbed species. Upon desorption from the surface, product molecules are formed. A good catalyst should be able to perform all the processes efficiently.

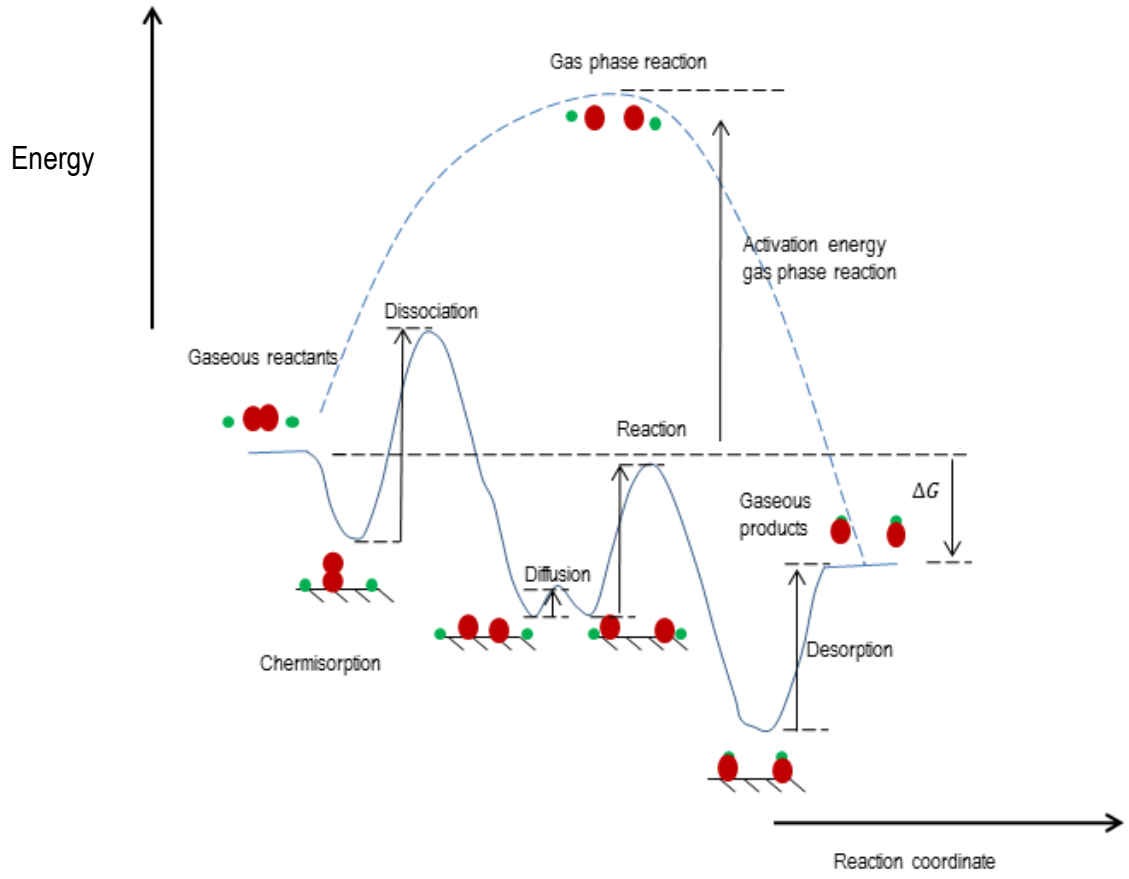

Figure 1.1: Elementary processes in heterogeneous catalysis (Chorkendorff and Niemantsverdriet, 2006).

Two reaction pathways are shown in Figure 1.1: the gas phase reaction (not catalysed) and the surface reaction (catalysed).The activation energy needed for the gas phase reaction can be high and as a result, it is very slow. For the surface reaction proceeding through a series of elementary steps, the overall activation energy may not be that high. However, if any of the elementary processes is sluggish, it may become a bottleneck for the whole reaction. The efforts in catalysis research are aimed at identifying the bottlenecks for particular reaction pathways and finding ways of eliminating them.

1.1.2 Fuel cells

A fuel cell is an electrochemical device that converts chemical energy direct to electricity. It consists of two electrodes separated by a medium that conducts ions but not electrons. The electrodes are then connected to an external electrical circuit that draws out the power. At the cathode, oxygen is reduced and at the anode, hydrogen is oxidised. The overall products of the two half-cell reactions are electrical energy and water. However, because of the thermodynamic irreversibility of processes taking place during reactions, not all energy is produced as electricity. Some is converted to heat and appears as wasted energy. This lowers the efficiency of the fuel cells.

There are several types of low temperature fuel cells. Figure 1.2 shows a schematic layout of a Proton Exchange Membrane (PEM) fuel cell. A common feature in all low temperature electrodes is the presence of platinum as catalyst. However, even with the platinum catalyst present, the energy needed for the Oxygen Reduction Reaction (ORR) is still significant. The amount of platinum needed to obtain practical operating current densities makes the whole fuel cell system uneconomic, yet platinum remains the best known catalyst for both half-cell reactions. A publication reviewing state-of-the-art fuel cell catalysis in 2005 reported that the lowest platinum loading possible in fuel cell electrodes was $0.6 \text{ to } 0.8 \text{ mg/cm}^2$ at a power density of 0.7 W/cm^2 (Gasteiger et al., 2005). This translates to $72 - 94\text{g}$ of platinum for a 75kW automobile. A five-fold reduction in platinum loading was required to make fuel cell economically viable. This issue still remains unsolved. There have been extensive efforts to find a catalyst that performs better than platinum. The most successful systems tested to date are alloys of platinum itself. The performance of non-platinum based catalysts is much lower and they are not stable in the reaction fuel cell environment (Stamenkovic et al., 2007, Serov and Kwak, 2009, Adams, 2009).

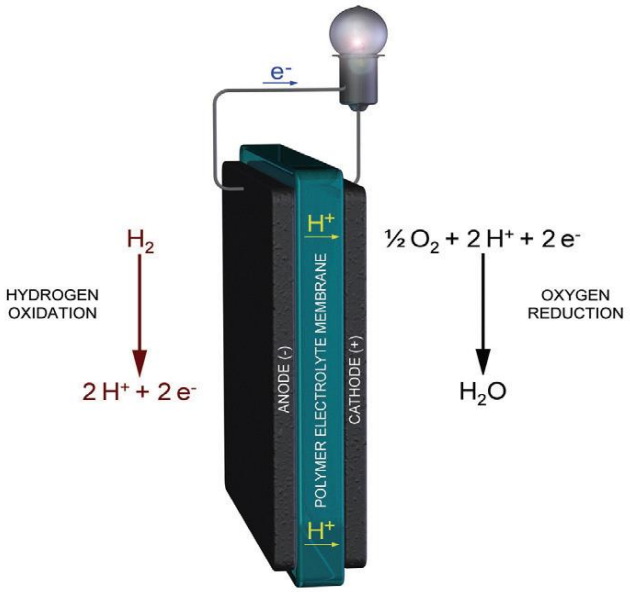

Figure 1.2: Basic structure of a proton exchange membrane fuel cell.

(Bashyam and Zelenay, 2006)

1.2 Literature review

Electrochemical measurements of ORR rates on pure platinum and platinum alloy surfaces in conjunction with Density Functional Theory (DFT) calculated reaction pathways have been used to improve the performance of fuel cell cathode catalysts. The reaction on Pt (111) is the well-studied. The initial step of the reaction is adsorption of molecular oxygen.

1.2.1 Adsorption of oxygen on Pt (111)

It is believed that the dissociative adsorption of oxygen on Pt (111) is mediated through precursor states (Eichler and Hafner, 1997, Zambelli et al., 1997). A molecular oxygen species exists on the surface in physisorbed and chemisorbed states preceding dissociation. In fact, the trapped molecule may either dissociate or desorb depending on the thermal conditions of the substrate. Nolan *et al.* (1998, 1999) proposed an adsorption scheme illustrated by the one dimensional potential energy surface (Figure 1.3), showing the local minima as possible precursor states.

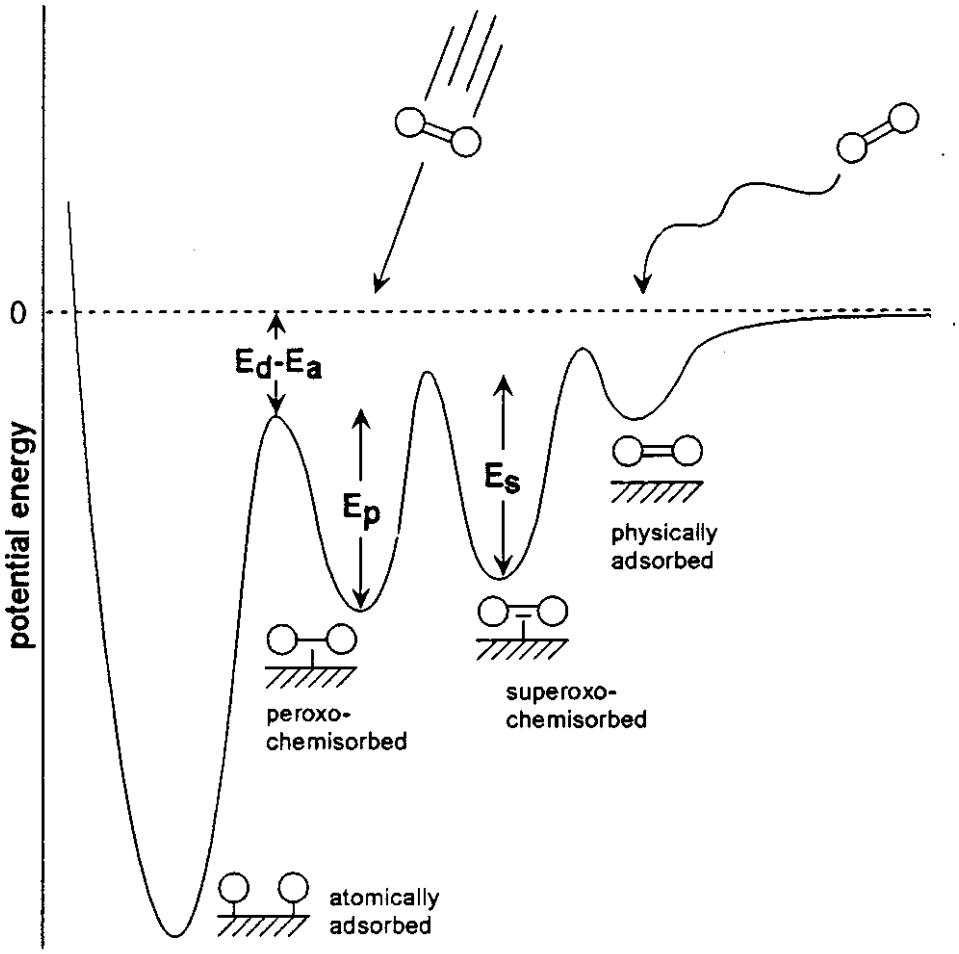

Figure 1.3: One dimensional potential energy diagram for dissociative adsorption of oxygen on platinum. Species with low translational kinetic energy may initially physisorb (Nolan et al., 1999, Nolan et al., 1998).

1.2.2 Dissociative adsorption of oxygen on Fuel Cell electrodes

There are two possible oxygen reduction mechanisms for fuel cell electrodes, the direct/dissociative and the associative mechanisms (Nørskov et al., 2004):

Dissociative mechanism

$$\frac{1}{2}O_2 + \quad ^* \rightarrow O^* \qquad (1.1)$$

$$O^* + H^* + e^- \rightarrow OH^* \qquad (1.2)$$

$$HO^* + H^* + e^- \rightarrow H_2O \qquad (1.3)$$

Associative mechanism

$$O_2 + \quad ^* \rightarrow O_2^* \qquad (1.4)$$

$$O_2^* + H^* + e^- \rightarrow HOO^* \qquad (1.5)$$

$$HOO^* + H^* + e^- \rightarrow H_2O^* + O^* \qquad (1.6)$$

$$O_2^* + H^* + e^- \rightarrow OH^* \qquad (1.7)$$

$$OH^* + H^* + e^- \rightarrow H_2O^* \qquad (1.8)$$

where *denotes the surface.

It can be seen that in the dissociative mechanism, oxygen dissociation precedes protonation while in the associative mechanism, dissociation follows protonation. The question of which mechanism dominates depends on several factors. DFT calculations performed by Nørskov and co-workers showed that the associative mechanism is dominant at high O_2 coverage (Nørskov *et al*., 2004). Ford *et al.* also performed calculations to determine energetics of ORR intermediates. They proposed that the intrinsic reactivity of the substrate also contributes to the favoured mechanism and reported that for Rh, Ir, Ni and Cu the dissociation mechanism dominates whilst on Pt, Pd, Au and Ag, the dissociative mechanism dominates (Ford *et al*., 2010).

1.2.3 Factors affecting adsorption and dissociation of oxygen on platinum surfaces

Factors that affect adsorption and dissociation energies of oxygen include co-adsorption (presence of spectator ions) and the effect of a strong potential due to an electric double layer at the electrode surface (Nørskov *et al.*, 2004). Intrinsic reactivity of the surface also plays an important role as highlighted by Ford *et al.* (2010) and is the subject of the present study. The substrate interacts with oxygen electronically. Several models have been developed to study this interaction. One early model was developed by Newns (1969) using a mathematical technique proposed by Anderson (1961).

Normally, bonding is explained in terms of molecular orbital theory (Atkins, 2006). It is possible to enumerate orbitals in small molecules because there are not many. However, the number of electronic states on a metal surface is very large such that it is not practical to count them one by one. A practical way to enumerate the large number of surface electronic states is to use a mathematical concept called the density of states (Ashcroft and Mermin, 1976). Newns used the density of states to describe surface-molecule interactions.

The Newns-Anderson model

The Newns-Anderson model clearly distinguishes physisorption and chemisorption. In physisorption, each system keeps its electronic states, they are only weakly perturbed and there is no hybridisation. Physisorption is a result of Van der Waals attraction due to induced dipoles and the bond is weak. An equilibrium physisorption interaction is a bond that only balances induced dipoles and Pauli repulsion. Sometimes a molecule is able to reach very close to a surface such that a covalent interaction may occur. Covalent bonding involves the formation of new hybrid orbitals. Thus, an equilibrium covalent interaction is a bond that balances induced dipoles, hybridisation energy and Pauli repulsion.

Newns (1969) considered the surface to be a jellium of electrons into which a hydrogen atom was embedded (Anderson, 1961). Two simple results of Newns-Anderson analysis relevant to catalysis were summarised (Chorkendorff and Niemantsverdriet, 2006): the first case explains the changes to molecule electronic states as a result of interacting with a metal that has s and p electrons only and the second case considers the interaction of the atom's states with d states in transition metals.

The interaction between oxygen molecule states and the substrate s and p states leads to formation of a bond in which all molecule states are lowered in energy and broadened as it moves closer and closer to the surface (Figure 1.4). All energy levels that fall below the Fermi level automatically become occupied with electrons (Chorkendorff and Niemantsverdriet, 2006). This interaction is almost equal in all metals, with the hydrogen energy levels being lowered by approximately $5\mathrm{eV}$.

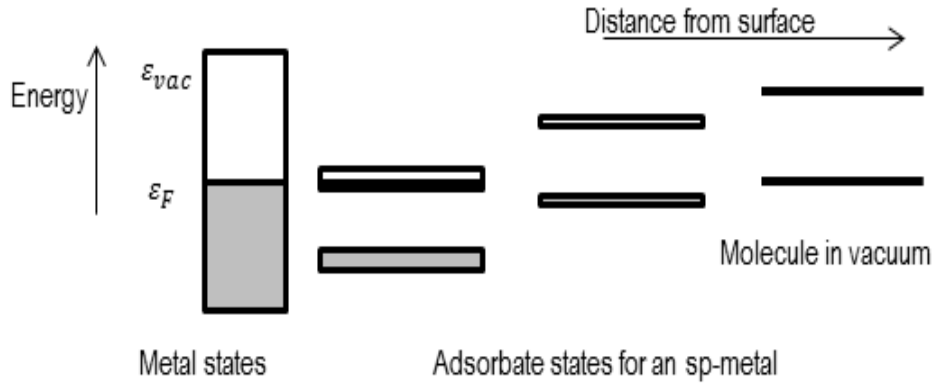

Figure 1.4: Molecule states are broadened and lowered in energy as the molecule approaches a surface (Adapted from (Chorkendorff and Niemantsverdriet, 2006)).

A transition metal has both sp and d-states. The transition metal sp-states will interact with the molecule states just like a simple metal. Narrow d-bands with half-filled orbitals and a significant density of states at the Fermi level interact strongly with the molecule states. The interaction is covalent, resulting in hybridisation of states forming bonding and anti-bonding levels (see Figure 1.5). The formerly molecular anti-bonding states now fall below the Fermi level, resulting in weakening of the intra-molecular bond. In this way, the metal surface is able to dissociate molecule bonds. Since the properties of d-bands vary considerably across and down the Periodic Table, the interaction of molecule states with metal d-states is thought to be responsible for variations in catalytic performance of different metals (Hammer and Nørskov, 1995).

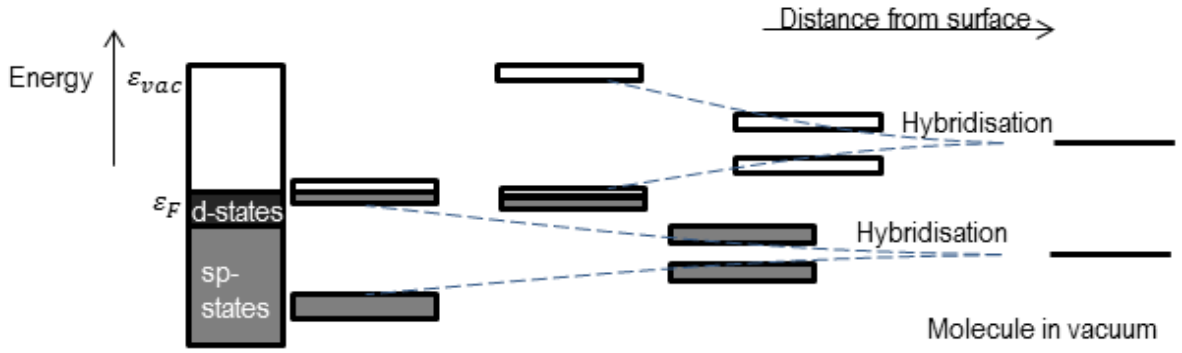

Figure 1.5: Interaction of molecular states with metal d-states result in formation of hybrid bonding and antibonding states (Adapted from (Chorkendorff and Niemantsverdriet, 2006)).

Chemisorption on transition metal surfaces can be summarised as having two contributing factors (Figure 1.6) (Greeley et al., 2009). The first step is the interaction of molecule states with the metal sp states. This interaction results in lowering and broadening of the energy levels of the molecule states. The second step is the interaction of molecule states with the metal d-states. This interaction results in splitting of molecule states into bonding and anti-bonding levels. Hybridisation of the molecule anti-bonding states causes them to fall below the Fermi level, weakening the intra-molecular bond.

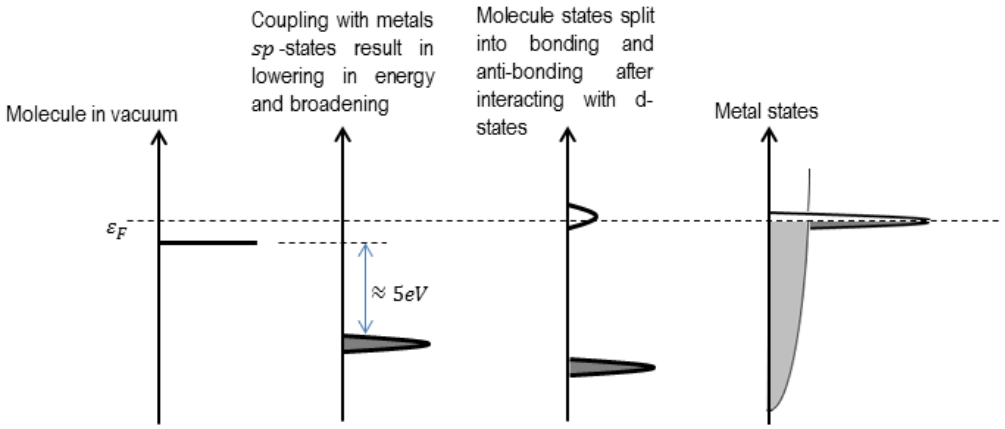

Figure 1.6: Interaction of a molecule with a transition metal (Greeley et al., 2009).

It is difficult to find one single electronic descriptor of surface reactivity for a substrate surface with electronic states being described by a band structure. For example, Figure 1.7 is a plot of the catalytic performance versus d-band filling for the ammonia synthesis. A resulting volcano curve shows that d-band filling is a factor influencing adsorption and dissociation. The local density of states at the Fermi level and average energy of d-bands were all individually correlated with catalytic performance (Feibelman and Hamann, 1985). Hammer and Norskøv (1995) summed up the contributions of the three individual factors and proposed a reactivity model called the d-band model.

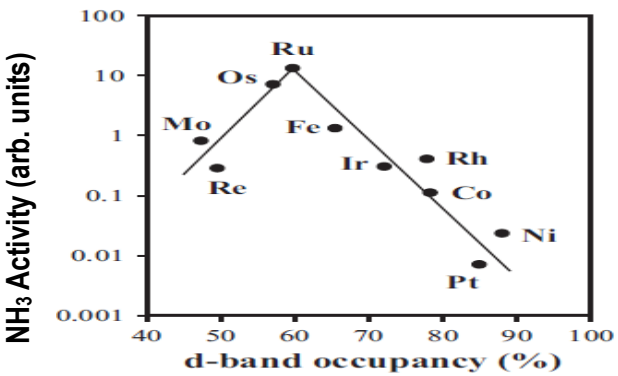

Figure 1.7: Volcano curve of electronic properties for ammonia synthesis (Ozaki, 1981).

In formulation of the **d**-band model, Hammer and Nørskov used the example of a hydrogen molecule interacting with a metal surface to develop the approximate relationship in Equation (1.9) (Hammer and Nørskov, 1995):

$$\Delta \mathrm{E_{bond}} = \alpha |\mathrm{V_{ad}}|^2 - 2(1-\mathrm{f})\frac{|\mathrm{V_{ad}}|^2}{\varepsilon_\mathrm{d} - \varepsilon_\mathrm{a}} \qquad (1.9)$$

where

$\boldsymbol{\alpha}$ is a constant of proportionality,

$\mathbf{V_{ad}}$ is the coupling matrix element,

$\mathbf{f}$ is the level of filling for d-orbitals,

$\boldsymbol{\varepsilon_d}$ is the average energy of the d-band,

$\boldsymbol{\varepsilon_a}$is the energy of the adsorbate states.

The first term is renormalisation energy (readjustment of states to fulfil Pauli repulsion requirements). It increases with the square of the coupling matrix element. The coupling matrix element is a measure of the strength of covalent interaction between any two atoms. The second term is the hybridisation energy. Hybridisation energy increases with the filling of bonding orbitals and decreases with the filling of antibonding orbitals. The approximate relationship in Equation 1.9 completely ignores contributions from metal sp states, and hence it was named the d-band model.

Three factors affecting the value of chemisorption and dissociation can be isolated. These are:

- Degree of filling of surface-molecule anti-bonding states (f)
- A measure of coupling strength between the surface states and the molecule states (the coupling matrix element (V_{ad}).
- The position of the surface states relative to molecular states ($\varepsilon_d - \varepsilon_a$).

Of these factors, the average energy of the d-band (ε_d) can easily be manipulated by alloying, through strain and ligand effects. Strain results when a surface adopts a lattice parameter different from that of its parent solid. A change of lattice parameter causes the overlap between d-orbital ligands to change. Strained ligands are shown in Figure 1.8. Compressive strain results in a bigger overlap of orbitals. This increases the range of energy of electrons in the d-band. The increase of range of energies is

manifested by wider bandwidth on a density of states diagram. Tensile strain has an opposite effect (Mavrikakis et al., 1998).

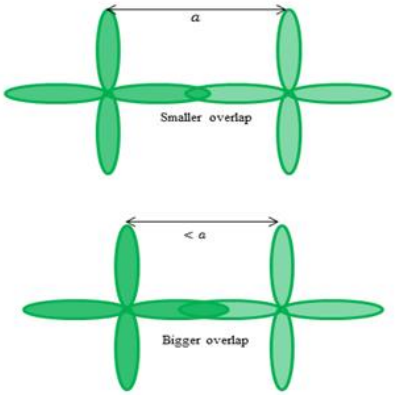

Figure 1.8: Strained ligands (Xin *et al*., 2012).

Ligand effects result when the orbitals of the solute element have a different spatial extent (Bligaard and Nørskov, 2007). Introducing solute elements that have large spatial extent of d-orbitals result in wider bandwidth. Conversely, alloying with an element that has small d-orbitals result in a narrower bandwidth. In Figure 1.9, the parent atom (in green) has been replaced by an atom that has larger d-bands (in red) resulting in a bigger overlap.

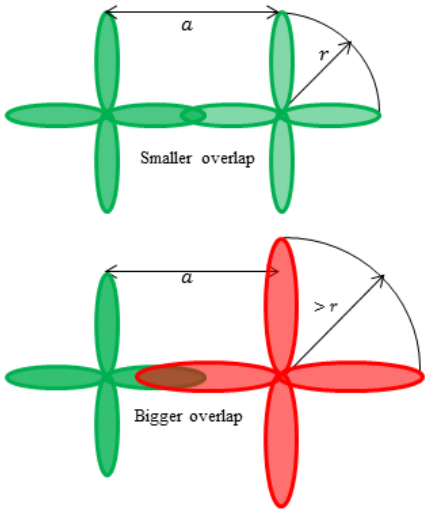

Figure 1.9: Ligand effect due to a foreign atom (Xin et al., 2012).

An increase or decrease of d-band orbital overlap changes the range of energies of electrons in the d-band (the d-band is broadened or made narrower). Each metal maintains its Fermi level (Bligaard and Nørskov, 2007). Thus change of bandwidth results in shifting of the average energy (ε_d in equation 2.1)

as shown in Figure 1.10. These effects can be used to explain reactivity trends observed in platinum alloy surfaces.

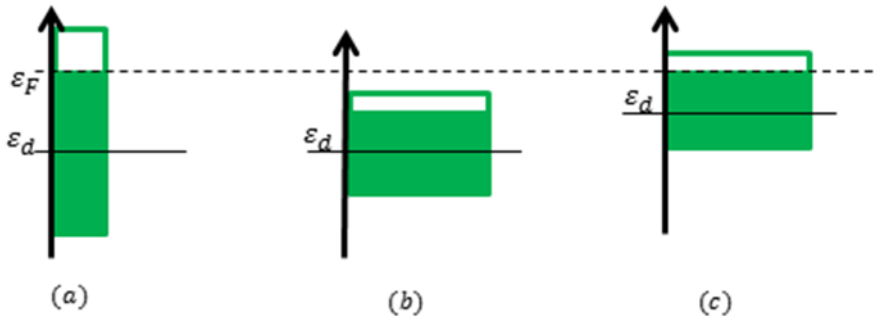

Figure 1.10: The rectangular band model (Bligaard and Nørskov, 2007).

Thus adsorption properties of the Pt (111) surface can be modified by introducing subsurface solute atoms.

1.3 Objectives of the study

Novel platinum vanadium surface alloy and nanoparticle alloy systems have been successfully synthesized (Leteba, 2013). These systems are being tested for use as fuel cell catalysts. The aim of this study is to provide an in-depth insight on the effect of subsurface vanadium atoms on adsorption properties of a platinum surface. The study is attempting to answer the following questions:

How does alloying platinum with vanadium modify its electronic structure?

What is the effect of subsurface vanadium atoms on the equilibrium geometry of O_2^*, and adsorption energy?

CHAPTER 2

COMPUTATIONAL METHODS

Modern methods of calculating solid state properties are based on quantum theory. Computation of the properties is made complicated by many-body interactions among electrons and nuclei. A special technique to resolve the problem is called Density Functional Theory (DFT). Whilst other electronic structure methods are highly successful for molecular systems, density functional theory makes the solution of Schrodinger's equation for solid state materials tractable.

2.1 Schrödinger's equation

In classical mechanics, variables are directly related to observable physical properties. In quantum mechanics, however, variables are represented by mathematical operators that produce physically measurable quantities only when they act on a state function called a wave function, usually denoted ψ. The wave function, assuming that it exists, contains all information about a system.

A Hamiltonian ($\mathbf{H}$) is a total energy operator from which all chemical and physical properties of a system can be derived. Determining microscopic properties of any system requires operating the Hamiltonian on the wave function.

$$\mathbf{H}\psi = \varepsilon\psi \qquad (2.1)$$

where $\mathbf{H}$ is the Hamiltonian operator, ψ is the wave function and $\boldsymbol{\varepsilon}$ is total energy of the system. Equation (2.1) is called Schrodinger's equation.

For a solid state system, the Hamiltonian that enters Schrodinger's equation is a sum of kinetic and potential energy operators. These operators are for the kinetic energy of the nuclei ($\mathbf{T_n}$), kinetic energy of electrons ($\mathbf{T_e}$), energy from electrostatic interactions between nuclei ($\mathbf{V_{nn}}$), energy from interactions between electrons ($\mathbf{V_{ee}}$) and energy from interactions between nuclei and electrons ($\mathbf{V_{en}}$).

$$\mathbf{H} = \mathbf{T_n} + \mathbf{T_e} + \mathbf{V_{nn}} + \mathbf{V_{ee}} + \mathbf{V_{en}} \qquad (2.2)$$

The Hamiltonian in equation (2.2) is simplified using the Adiabatic Approximation, also called the Born-Oppenheimer Approximation, by neglecting the kinetic energy of the nuclei.

2.2 The Born-Oppenheimer Approximation

The Born-Oppenheimer approximation allows motion of electrons to be considered independently to that of the nuclei. The wave function is separated into a nuclei part (ψ_n) and an electronic part (ψ_e).

$$\psi = \psi_n(\mathbf{R})\psi_e(\mathbf{r}) \quad (2.3)$$

This approximation is valid because the nucleus is massive and moves at a velocity much lower than that of electrons. For any perturbation on nuclear coordinates, electrons are expected to follow instantaneously. For each set of nuclei coordinates **R**, the potential due to electrons is determined independently. When the electronic potential is evaluated for a series of nucleus sets of coordinates $\mathbf{R_1}, \mathbf{R_2}, \ldots, \mathbf{R_n}$, a potential energy surface for the system is mapped and nuclei are said to move in a potential determined by the electron distribution. Motion of electrons is considered quantum mechanically and nuclei are treated classically.

The Born-Oppenheimer approximation reduces the dynamical problem to a simpler one of electrons moving in a frozen configuration of nuclei. The Hamiltonian is greatly simplified:

$$\boldsymbol{H} = (\mathbf{T_e} + \mathbf{V_{en}}) + \mathbf{V_{ee}} + \quad \mathbf{V_{nn}} \quad (2.4)$$

2.3 Wave function based calculations

To obtain the total energy of a system from equation 2.1, the wave function must be evaluated first. The wave function can be determined if the external potential (V_{ext}) is known. Thus, the external potential specifies the wave function. Once the wave function is known, any property can be calculated by taking the expectation value (Figure 2.1).

$$V_{ext} \longrightarrow \psi \longrightarrow \rho(\boldsymbol{r})$$

Figure 2.1: Wave function based methods.

For example electron density is calculated as follows:

$$\rho(\mathbf{r}) = \sum_i^N |\psi_i(\mathbf{r})|^2 \quad (2.5)$$

Unfortunately it is not possible to know the exact form of the wave functions due to many-body interactions. There are several methods of approximating wave functions. The most successful of these is called the Hartree-Fock approximation. This approximation follows from Hartree's proposition that the wave function of a system with many electrons can be written as a product of wave functions for each electron present (Hartree, 1928):

$$\psi(\mathbf{r_1}, \mathbf{r_2}, \ldots, \mathbf{r_N}) = \psi_1(\mathbf{r_1})\,\psi_2(\mathbf{r_2}) \ldots \psi_N(\mathbf{r_N}) \quad (2.6)$$

where $\mathbf{r_i}$ are position coordinates. Each electron is thought to be moving in a potential determined by all other electrons. The single electron wave functions generated are called one electron wave functions because there are no direct electron-electron interactions. This is an independent electron approximation.

An extension of Hartree-Fock theory may be made by including a non-classical coordinate $\boldsymbol{\sigma}$, called spin.

$$\psi(\mathbf{r_1\sigma_1}, \mathbf{r_2\sigma_2}, \dots, \mathbf{r_N\sigma_N}) = \psi_1(\mathbf{r_1\sigma_1})\, \psi_2(\mathbf{r_2\sigma_2}) \dots \psi_N(\mathbf{r_N\sigma_N}) \qquad (2.7)$$

where $\boldsymbol{\sigma_i}$ are spin coordinates to represent either spin up or spin down. Spin introduces two non-classical effects, correlation and exchange. The effects are both summed up by the Pauli Exclusion Principle: two electrons in a system cannot be in the same quantum state. Hartree-Fock theory partially fulfils the exclusion requirement by accounting for exchange effects. Being fermions, electrons are antisymmetric under exchange:

$$\psi(\mathbf{r_1\sigma_1}, \mathbf{r_2\sigma_2}, \dots, \mathbf{r_N\sigma_N}) = -\psi(\mathbf{r_2\sigma_2}, \mathbf{r_1\sigma_1}, \dots, \mathbf{r_N\sigma_N}) \qquad (2.8)$$

All allowed wave functions should fulfil the above requirement (Equation 2.8). A special way of getting normalised antisymmetric wave functions is through the use of Slater determinants (1951,1960)

$$\psi(\mathbf{r_1\sigma_1}, \mathbf{r_2\sigma_2}, \dots, \mathbf{r_N\sigma_N}) = \frac{1}{\sqrt{N}} \begin{vmatrix} \phi_1(\mathbf{r_1\sigma_1}) & \phi_2(\mathbf{r_1\sigma_1}) \dots & \phi_N(\mathbf{r_1\sigma_1}) \\ \phi_1(\mathbf{r_2\sigma_2}) & \phi_2(\mathbf{r_2\sigma_2}) \dots & \phi_N(\mathbf{r_2\sigma_2}) \\ & \vdots & \\ \phi_1(\mathbf{r_N\sigma_N}) & \phi_2(\mathbf{r_N\sigma_N}) \dots & \phi_N(\mathbf{r_N\sigma_N}) \end{vmatrix} \qquad (2.9)$$

where **N** is the number of electrons.

Starting with a trial wave function, the solution of Hartree-Fock equations must be sought iteratively until self-consistence is attained (the output wave function between consecutive iterations no longer changes) (Figure 2.2). The output of a Hartree-Fock calculation is a self-consistent wave function from which properties are deduced.

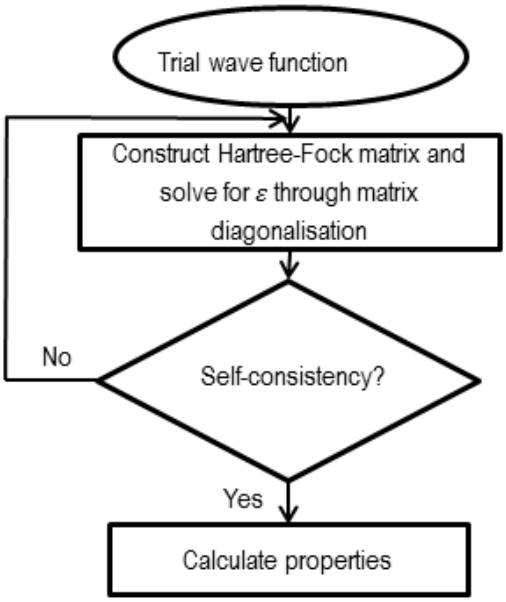

Figure 2.2: Hartree-Fock self-consistent procedure (Martin, 2004).

Although Hartree-Fock theory accounts for exchange, it does not include electron correlation. Efforts to include correlation effects to Hartree-Fock equations yields a method called Configuration Interaction (Slater et al., 1960). However, the CI method involving many electrons is computationally demanding. It is only effective for molecules with few nuclei.

2.4 Density functional theory

Density functional theory maps a system of interacting electrons into that of independent electrons moving in a fictitious effective external potential. The theory is exact in principle. It originated with ideas by Thomas (1927) and Fermi (1927) who expressed electron density as a functional of the external potential. Since the external potential specifies the wave function, Thomas and Fermi sought to solve Schrodinger's equation by expressing electron density in terms of the external potential without calculating the wave function.

Use of electron density instead of wave functions to calculate properties of materials is a great simplification. Electron density does not depend on the size of the system, but on symmetry. Modern formulations of the density functional theory are based on a framework developed by Hohenberg and Kohn (1964) and Kohn and Sham (1965).

2.4.1 Hohenberg and Kohn Theory

Hohenberg and Kohn (1964) proposed two theorems in which they proved that the ground state energy of a system is a unique functional of electron density.

Theorem 1: The external potential is a unique functional of electron density. Since the external potential specifies ψ as well as H, it also follows that total energy is a functional of electron density.

Theorem 2: For any external potential, the electron density that minimises the energy functional is the exact ground state density. Thus ground state energy can be determined though variation minimisation.

Knowledge of the electron density enables one to determine a unique external potential and hence the wave function as shown in Figure 2.3:

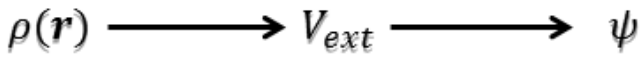

Figure 2.3: Electron density approach.

The Hohenberg and Kohn theory identifies the electron density as a basic variable for determination of total energy of the system.

$$\mathrm{E} = \mathrm{E}[\rho(\mathbf{r}), \mathbf{R}] \tag{2.10}$$

The total energy functional is expanded in terms of the electro-static electro nuclei and a term $\mathrm{F}[\rho(\mathbf{r})$ as shown in Equation 2.11:

$$\mathrm{E}[(\rho(\mathbf{r})] = \int \mathrm{V_{en}}\rho(\mathbf{r})\mathrm{d}r + \mathrm{F}[\rho(\mathbf{r})]\,. \tag{2.11}$$

The functional $\mathrm{F}[\rho(\mathrm{r})]$ consists of kinetic energy and an electron-electron interaction term.

$$\mathrm{F}[\rho(\mathbf{r})] = \mathrm{T_e}[\rho(\mathbf{r})] + \mathrm{V_{ee}}[\rho(\mathbf{r})] \tag{2.12}$$

The electron-electron interaction ($\mathrm{V_{ee}}[\rho(\mathbf{r})]$) can be separated into a classical Coulomb term (also called Hartree energy) and a non-classical term $\mathrm{U_C}$:

$$\mathrm{V_{ee}}[\rho(\mathbf{r})] = \frac{1}{2}\iint \frac{\rho(\mathbf{r})\rho(\mathbf{r}')}{|\mathbf{r}-\mathbf{r}'|}\mathrm{d}\mathbf{r}\mathrm{d}\mathbf{r}' + \mathrm{U_C}[\rho(\mathbf{r})] \tag{2. 13}$$

The term U_C is called correlation energy. It is non-classical because it arises due to the Pauli exclusion requirement: two electrons cannot occupy the same point in space at the same time, so when one electron moves, the other electron has to move so that they avoid each other. Exact energy differs from Coulomb interaction energy by the correlation term U_C. Explicit determination of the correlation energy terms remains a great challenge.

2.4.2 Kohn-Sham Equations

The unknowns in equation (2.13) are kinetic energy and the correlation term. Kohn and Sham (1965) introduced kinetic energy of non-interacting effective electrons, $T_s[\rho(\mathbf{r})]$, defined so that their corresponding one particle wave functions generate the exact density of the interacting many-body system,

$$T_s[\rho(\mathbf{r})] = -\frac{1}{2}\sum_i^N \langle \Psi_i | \boldsymbol{\nabla}^2 | \Psi_i \rangle \qquad (2.14)$$

where ψ_i are orbitals of a non-interacting system (Ψ_i form an orthonormal set of independent particle wave functions).

This energy differs from the exact energy by a non-classical term called exchange energy. Just like correlation energy, exchange energy is a result of many-body interactions and restrictions imposed by the Pauli Exclusion Principle. The anti-symmetry property of interacting electrons reduces Coulomb energy by an amount equal to the exchange energy.

Having determined major explicit terms, kinetic and potential energies, non-classical many-body interaction terms are lumped together into a functional called correlation and exchange ($E_{XC}[\rho(\mathbf{r})]$).

$$E_{XC}[\rho(\mathbf{r})] = (T_e[\rho(\mathbf{r})] - T_s[\rho(\mathbf{r})]) + (U_{ee}[\rho(\mathbf{r})] - U_C[\rho(\mathbf{r})]) \qquad (2.15)$$

Thus the total energy functional becomes a sum of the kinetic energy of non-interacting particles, classical Coulomb energy for electron-electron interactions, energy from Coulomb potential due to fixed nuclei, and all non-classical residuals collected into the correlation and exchange functional.

$$E[(\rho(\mathbf{r})] = T_s[\rho(\mathbf{r})] + \frac{1}{2}\iint \frac{\rho(\mathbf{r})\rho(\mathbf{r}')}{|\mathbf{r}-\mathbf{r}'|} d\mathbf{r}d\mathbf{r}' + \int V_{en}\rho(\mathbf{r})d\mathbf{r} + E_{XC}[\rho(\mathbf{r})] \qquad (2.16)$$

By applying variation minimisation to equation (2.16), the Kohn-Sham equation is obtained:

$$\left(-\frac{\boldsymbol{\nabla}_i^2}{2} + V_{KS}\right)\Psi_i = \epsilon_i \Psi_i \qquad (2.17)$$

Kohn-Sham theory reduces the many-body Schrödinger's equation into an equation of independent electrons in an effective external potential V_{KS}. The many-body effects are contained in the effective external potential through the correlation and exchange potential μ_{XC} .

$$V_{KS} = \frac{1}{2}\int \frac{\rho(\mathbf{r}')}{|\mathbf{r}-\mathbf{r}'|}\mathrm{d}\mathbf{r} + V_{en} + \mu_X \tag{2.18}$$

The correlation and exchange potential is defined by equation (2.19) below:

$$\mu_{XC} = \frac{\delta E_{XC}[\rho(\mathbf{r})]}{\delta\rho(\mathbf{r})} \tag{2.19}$$

2.4.3 Approximating correlation and exchange

The benefit of the Kohn-Sham equation is that it contains wave functions of non-interacting particles, and terms that can be determined explicitly (kinetic energy and classical Coulomb potential) have been separated from the unknown exchange and correlation energy. Non-classical many-body effects are gathered together in the correlation and exchange functional. This makes the problem tractable. Since $E_{XC}[\rho]$ is the only unknown term, approximations of it can be made to a reasonable degree of accuracy.

Correlation and exchange is so important that it is often referred to as the glue of nature (Perdew and Schmidt, 2001). Without it the calculated values of cohesion would be much lower than reality. Approximations of exchange and correlations can be arranged into a ladder hierarchy in which complexity varies from the simplest at the first rung to the most sophisticated on top of the ladder (Figure 2.4). At the lowest level, local densities are used to calculate correlation and exchange. Gradients of densities are included at the next level and more improvements are added at each rung going up the ladder. It is expected that moving up the ladder the correlation and exchange functionals become more accurate.

Approximating the correlation and exchange functional is still an active area of research. The simplest approach is the Local Density Approximation (LDA) (Kohn and Sham, 1965). Improvements by Perdew (Perdew, 1986), Becke (Becke, 1988), and Perdew, Burke and Ernzerhof (Perdew et al., 1996) yielded the Generalised Gradient Approximations (GGA). Meta-gradient methods containing higher orders of the electron density gradient have recently been added to DFT codes. A brief description of the LDA and GGA functionals is given in subsections 2.4.3.1 and 2.4.3.2

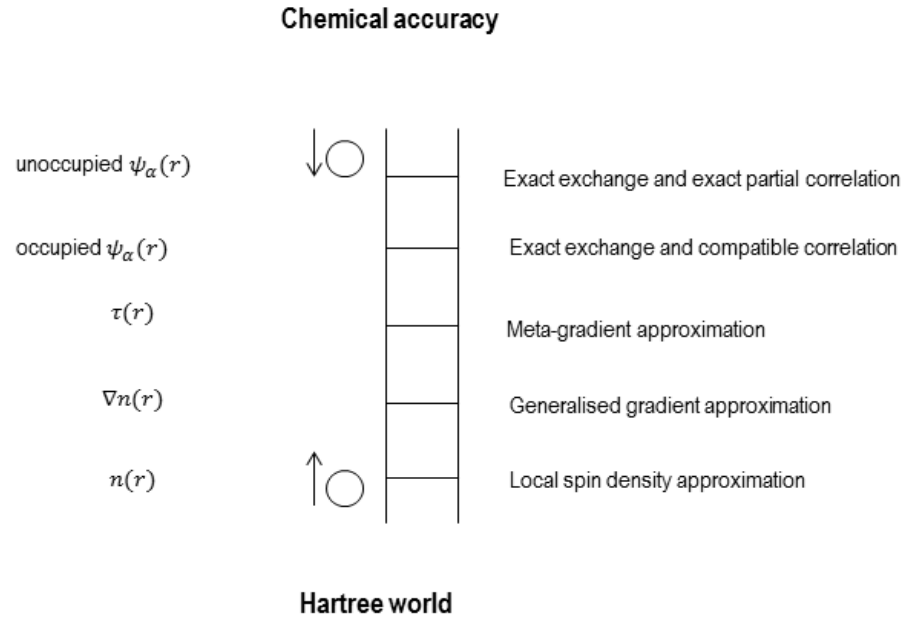

Figure 2.4: Jacob's ladder for correlation and exchange (adapted from Perdew and Schmidt, 2001).

2.4.3.1. Local Density Approximation (LDA)

In the lowest rung of the ladder is the LDA. Correlation and exchange energy depend on local density of particles. If in a volume $\mathrm{d}\mathbf{r}$, the electron density is $\rho(\mathbf{r})$, the LDA correlation and exchange energy is given by equation (2.20):

$$\mathrm{E_{XC}}[\rho] = \int \rho(\mathbf{r})\epsilon_{\mathrm{XC}}\,\mathrm{d}\mathbf{r} \qquad (2.20)$$

where the factor ϵ_{XC} is the exchange-correlation energy per particle. This factor can be determined accurately from Monte Carlo calculations (Ceperley and Alder, 1980). LDA approximations are valid for systems that are largely homogeneous. They are not appropriate for systems in which electron density gradient changes rapidly. The LDA tends to under-predict ground state energies and ionisation energies while over-predicting binding energies (Haas *et al*., 2011).

2.4.3.2. Generalised Gradient Approximation (GGA)

GGA approximations seek to improve on the LDA by including a term that depends on the gradient of electron density.

$$\mathrm{E_{XC}} = \mathrm{E_{XC}}[\rho(\mathbf{r}), \nabla\rho(\mathbf{r})] \qquad (2.\ 21)$$

They are suitable for systems which are not homogeneous, where electron densities change rapidly like molecules and surfaces. There are several variants of the GGA approximations.

2.4.4 Solving the Kohn-Sham equation

The Kohn-Sham equation

$$\left(-\frac{\nabla_i^2}{2} + V_{KS}(\mathbf{r})\right)\psi_i(\mathbf{r}) = \epsilon_i\psi_i(\mathbf{r}) \quad (2.22)$$

is solved self consistently with electron density

$$\rho(r) = \sum_i^N |\psi_i(\mathbf{r})|^2. \quad (2.23)$$

The unknown wave function is expanded in terms of a known set of functions called the basis set with unknown coefficients.

$$\Psi_i(\mathbf{r}) = \sum_j c_{ij}\,\phi_j(\mathbf{r}) \quad (2.24)$$

To determine the unknown coefficients c_{ij}, a matrix of the form

$$(H - \varepsilon S)c = 0 \quad (2.25)$$

is solved using the variation minimisation procedure where H and S are matrix elements

$H_{ij} = \int \phi_i^*(\mathbf{r})\left[-\frac{\nabla_i^2}{2} + V_{KS}(\mathbf{r})\right]\phi_j(\mathbf{r})d\mathbf{r}$ and

$S_{ij} = \int \phi_i^*(\mathbf{r})\phi_j(\mathbf{r})d\mathbf{r}$ respectively and

$\boldsymbol{\varepsilon}$ is the eigenvalue column vector.

Two common methods of expanding the wave function into a basis set are the plane wave pseudo potential and the tight binding methods. Plane wave expansions are made simple through using Bloch's Theorem.

2.4.5 Bloch's Theorem and the plane wave basis set

In a solid, the number of electrons is extremely large, practically infinity. Accordingly, by the Kohn-Sham formulation, there is an almost-infinite number of non-interacting electrons (Ashcroft and Mermin, 1976). A wave function must be calculated for each of these electrons. Moreover, since each wave function extends over the entire solid, the basis set required to expand it is very large. Different methods vary in

the way they expand each wave function into a basis set and also the way they treat valence and core electrons. In many cases different methods give complementary information required to build a complete picture of the situation. A brief description of two methods, the plane wave pseudo potential and tight binding approach, will be presented. First a description is made of how Bloch's theorem is used to reduce the infinite number of wave functions into a finite set. Each wave function is then expanded into a basis set depending on the method used and some approximations are employed to make the basis set finite.

The wave function for a system in a periodic potential can be chosen to have the form of a plane-wave, multiplied by a function of the periodicity of the Bravais lattice.

$$\psi_{n,k}(\mathbf{r}) = e^{i\mathbf{k}\cdot\mathbf{r}} U_{n,k}(\mathbf{r}) \quad (2.26)$$

Since the function $U_{n,k}(\mathbf{r})$ has the periodicity of the Bravais lattice, it can be expressed as a basis set using Fourier expansion, for each wave function $\mathbf{n}$.

$$U_{n,k}(\mathbf{r}) = \sum_G c_{n,G} e^{i\mathbf{G}\cdot\mathbf{r}} \quad (2.27)$$

G is a lattice vector for the reciprocal space. So each wave function can be written as a sum of plane waves.

$$\psi_{n,k}(\mathbf{r}) = \sum_G c_{n,G} e^{i(\mathbf{k}+\mathbf{G})\cdot\mathbf{r}} \quad (2.28)$$

For each electron n there is an infinite number of electronic states. Also, there are infinite electrons, and so there are an infinite number of allowed **k**-points. Applying periodic boundary conditions to equation (2.28) results in a discrete set of allowed states (Ashcroft and Mermin, 1976). Considering the variation of $\psi_{n,k}(\mathbf{r})$ with $\mathbf{k}$, for a region close to a given k, the change in the wave function is very small. Thus wave functions over a region of k-space can be represented by wave functions at a single point and only a finite number of k-points are required for a calculation (Payne et al., 1992). The question of how many points are required for a given problem was addressed by Chadi and Cohen (1973) and Monkhorst and Pack (Monkhorst and Pack, 1976)(1976). Determination of the proper set of $\mathbf{k}$-points to be used in a calculation is called $\mathbf{k}$-point sampling. Errors introduced by k-point sampling can be reduced by increasing their density.

2.4.5.1. Cut-off energy

The basis set required to expand each wave function is infinite. However, plane waves with small kinetic energy are more significant compared to those with higher kinetic energy. The basis set is made

finite by truncating it to include only wave functions with less than a given value called cut-off energy (E_{cut}).

$$E_{cut} = \frac{\hbar^2 |k+G|^2}{2m} \quad (2.29)$$

The error introduced by truncating the basis set this way can be reduced by increasing the cut off energy.

2.4.5.2. Pseudo potentials

Plane wave expansion is not well suited to express core electrons and valence electrons in the core region. Wave functions of valence electrons oscillate rapidly in the core region to maintain orthogonality with core electrons and the plane wave basis set required to represent them is extremely large. In the pseudo potential approximation, core electrons are removed and replaced with a weaker potential that acts on a set of pseudo wave functions of valence electrons. This is reasonable since properties of materials mainly depend on interactions of valence electrons. The pseudo-potential and pseudo-wave function are constructed in such a way that they conserve the important properties of the true potential and the wave functions. Therefore the space is divided into the core region occupied by pseudo-waves and pseudo-potential, and the interstitial region where delocalised states are represented by the plane wave basis set (see Figure 2.5).

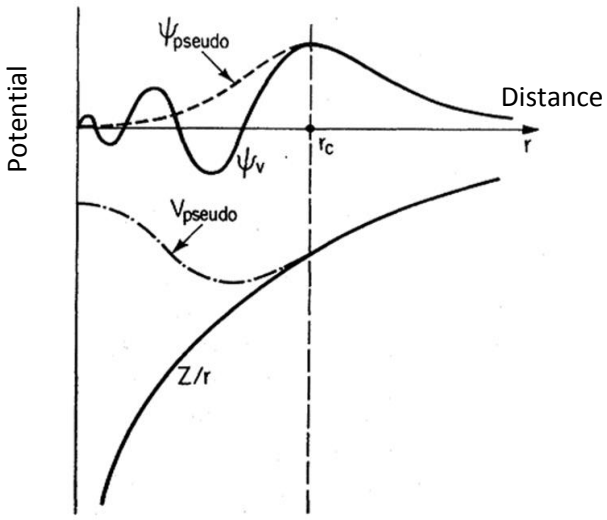

Figure 2.5: Pseudopotentials and pseudo wave functions

(adapted from Payne *et al.*, 1992)

2.4.5.3. Tight Binding Approximation

In the tight binding approximation electrons are strongly bound to the nucleus and interact weakly with electrons from neighbouring nuclei. The basis set is expanded in terms of radial functions $\phi_{\mathrm{RmL}}(\mathrm{r})$.

$$\psi_{\mathrm{n,k}}(\mathrm{r}) = \mathrm{c}_{\mathrm{Rml,n}}\phi_{\mathrm{Rml}}(\mathrm{r}) \qquad (2.30)$$

The function $\phi_{\mathrm{RmL}}(\mathrm{r})$ interacts strongly with nuclei and resembles atomic orbitals and so the tight binding approximation is also called the Linear Combination of Atomic Orbitals (LCAO). The subscript R is for nuclear coordinates and m and l are quantum numbers. The model is suitable for description of properties of tightly bound states like d-bands and covalent interactions.

2.5 Self-Consistent Field iterative procedure for Kohn-Sham equations

To obtain eigenvalues, the matrix $(\mathrm{H} - \varepsilon S)$ is diagonalised. The external potential and the correlation and exchange potential required for the matrix can be determined if the charge density is known. The charge density in turn can be determined from Kohn-Sham independent wave functions, and the wave functions are determined by diagonalising the matrix. The problem is cyclic. An iterative technique shown in Figure 2.6 is used to break the cycle, starting with a clever guess of the electron density.

The stages in the iteration process may be described as follows:

1. Trial densities for initiating the iteration are constructed from superposition of atomic densities. Geometrical data about the system obtained in experiments is used to construct the start densities. Then for the following iterations, densities from previous calculation are fed back as restart parameters until self-consistence is achieved.

2. The charge densities are then used to construct the potentials, both Coulomb and correlation and exchange.

3. From the potentials the Kohn-Sham equation can now be constructed and matrix elements are determined. The matrix is diagonalised to obtain eigenvalues and the basis set coefficients so that the Kohn-Sham wave functions can be synthesized.

4. Synthesised Kohn-Sham equations are used to build a new charge density that is fed back to step 2. This cycle continues until the change in the new charge density from the previous one is less than a predefined tolerance value. This is called self-consistency.

5. The output of the iterative procedure is a self-consistent charge density. Ground state properties are determined from this charge density.

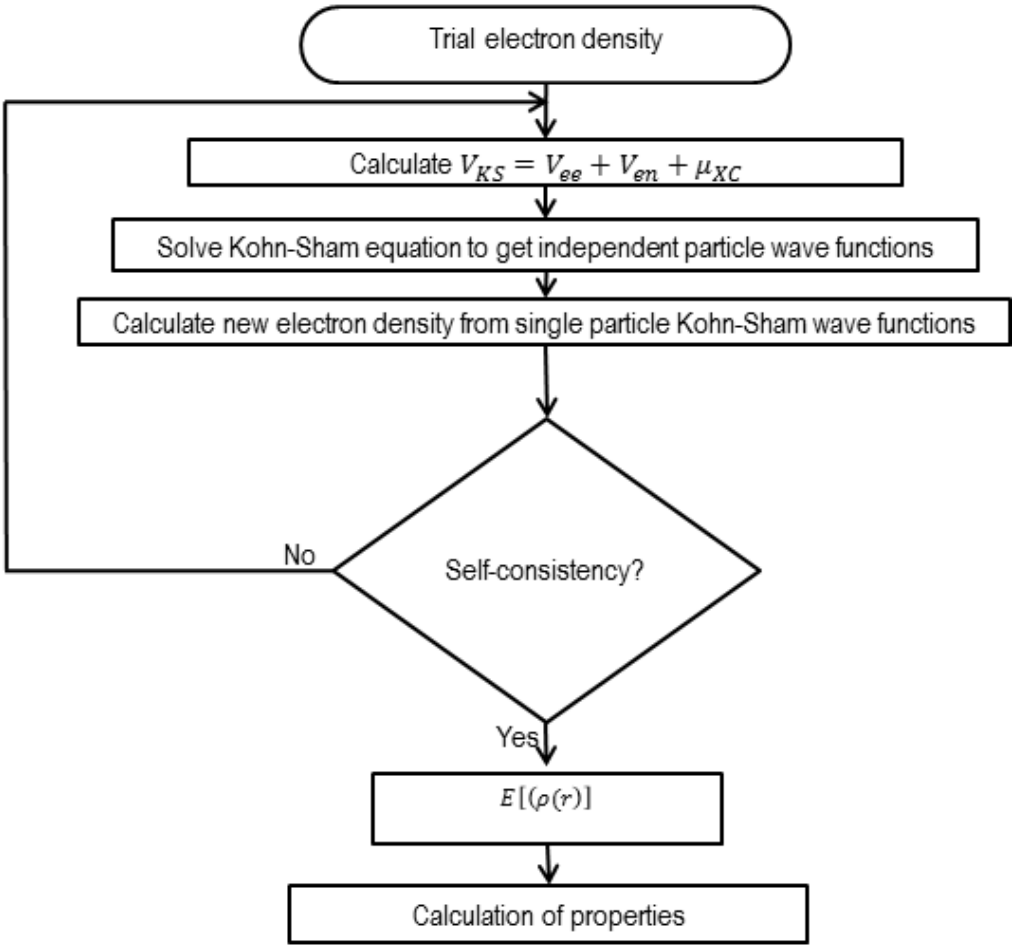

Figure 2.6: Kohn-Sham iterative technique (Martin, 2004).

2.6 Calculation of properties

Total energy of a system is obtained from the charge density through variation minimisation. The ground state properties are obtained at minimum total energies.

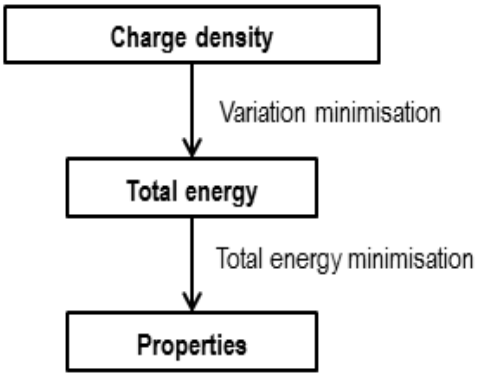

Figure 2.7: Calculation of properties from DFT total energies.

To determine the ground state value of a property, a series of total energy calculations is made for a range of values of that property. The ground state value is the one corresponding to the lowest total energy. For example Figure 2.8 is a graph of lattice parameter against total energy, showing the equilibrium lattice parameter at the lowest total energy.

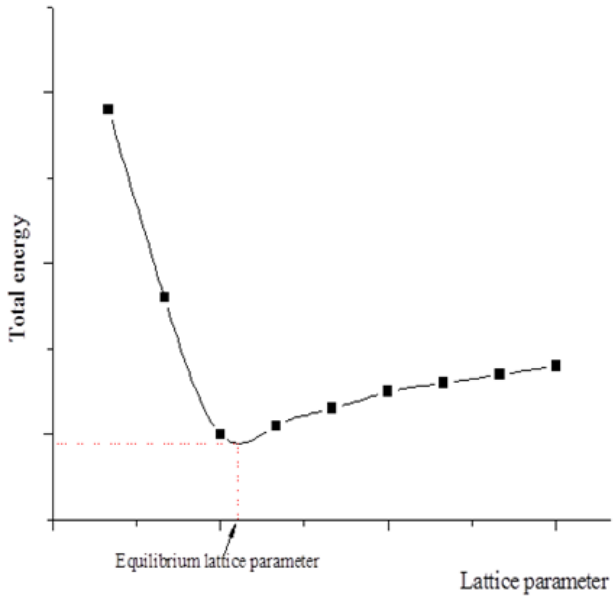

Figure 2.8: The value that minimises total energy is the ground state value.

For any DFT calculation, there is need to verify if model parameters describe the properties of a physical system as accurately as possible. The important ones include Brilliun zone parameters, exchange and correlation functionals, the potentials and supercell parameters. However, accuracy increases with computational costs. Thus, model parameters are chosen by optimising accuracy with computational costs.

2.6.1 Bulk properties

Surfaces are obtained by cleaving bulk materials. Surface properties depend on the bulk from which it was created. Thus, to have a surface model that accurately describes physical properties, an accurate bulk model has to be constructed first. In this work, the following bulk model parameters were considered: the number of irreducible k-points, cut-off energy, and exchange and correlation functionals. All calculations were performed using the Cambridge Serial Total Energy Programme (CASTEP, (Clark *et al.*, 2005). The chosen model parameters must be fully converged and can be verified by comparing calculated properties with values obtained from experiments. The equilibrium lattice parameters and bulk modulus were obtained by fitting calculated values to the Birch Murnaghan equation (Birch, 1947, Murnaghan, 1944):

$$E(V) = \frac{9}{16} B_0 V_0 \left[\left(\left(\frac{V}{V_0} \right)^{\frac{2}{3}} - 1 \right)^3 B_0' + \left(\left(\frac{V}{V_0} \right)^{\frac{2}{3}} - 1 \right)^2 \left(4 - 6 \left(\frac{V}{V_0} \right)^{\frac{2}{3}} \right) \right] \quad (2.30)$$

where E is total energy, V is the unit cell volume, B_0 the bulk modulus, V_0 the equilibrium cell volume, and $B_0'$is the first derivative with respect to pressure of the bulk modulus.

2.6.2 Clean surface properties

Surface energy and relaxation of surface interlayer distance were used to verify convergence of modelling parameters. The surface energy is the energy needed to split an infinite crystal into two semi-infinite crystals. The surface energy per surface atom (σ) is given by:

$$\sigma = \frac{1}{2} (E_T^{slab} - N E_T^{bulk}) \quad (2.31)$$

where E_T^{slab} is the total energy per atom of the surface slab, E_T^{bulk} the total energy per atom for bulk atoms. N is the number of layers.

Upon creation of a surface, the topmost atoms may remain at higher energy levels compared to atoms buried deep in the material. These atoms may redistribute the excess energy by changing the surface geometry. The Pt (111) surface is more stable than other facets and it was found that the surface relaxes by increasing the interlayer distance of the topmost atoms (Bøgh and Stensgaard, 1978).

Creation of a surface destroys periodicity in the direction perpendicular to it. Thus periodicity should be imposed in DFT surface models. One way of imposing surface periodicity is to use slabs of material separated by layers of vacuum. The thickness of the slab must enable it to mimic properties of a real surface accurately. The vacuum layer must be thick enough to allow the electron density due to the

lower surface to tail off to zero before the electron density from the top layer starts. The factor $\frac{1}{2}$ is used in equation (2.31) to account for the existence of two equivalent surfaces.

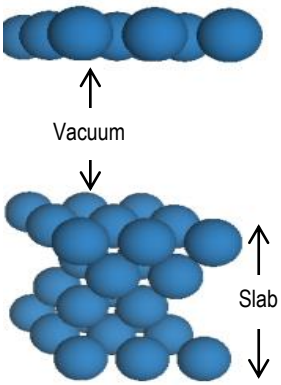

Figure 2.9: Periodicity is imposed on the surface by using layers separated by vacuum space.

2.6.3 Adsorption

Convergence of adsorption energies of an oxygen atom with respect to the number of slab layer was also investigated. On a Pt (111) surface, there are four special adsorption sites. These are the top, bridge, face centred cubic and hexagonal close packing sites. Convergence of adsorption energy was considered for the ontop site.

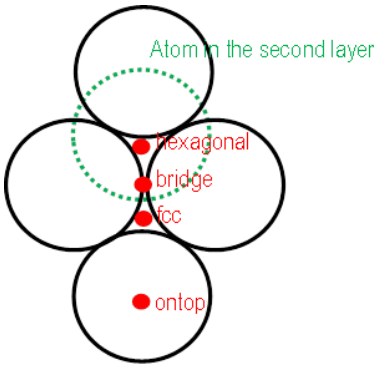

Figure 2.10: Adsorption site on a (111) surface.

The adsorption energy of the oxygen atom can be calculated as follows:

$$E_{ads} = E_{slab+O} - E_{slab} - E_o \qquad (2.32)$$

where E_{ads} is the adsorption energy, E_{slab+O} is total energy of a supercell with an adsorbed oxygen molecule, E_{slab} is the total energy of a clean surface and E_o the energy of an oxygen atom.

2.7 Model parameters results

Results for calculations to determine model parameters are presented in this section. The results include Brillouin zone parameters for bulk platinum, bulk vanadium, and Pt (111) surface, exchange and correlation functionals, and supercell parameters for surfaces.

2.7.1 Bulk properties

2.7.1.1 Brillouin zone parameters

Single point energy calculations were performed and plotted to show convergence of total energy with respect to the number of irreducible points and cut-off energy. Convergence of k-points was considered successful when the difference in energy between successive steps was below $5\ meV$ per atom. Total energy converged below $5meV$ at 56 irreducible k-points for bulk platinum and 120 irreducible k-points for bulk vanadium (Figures 2.11 (*b*) and 2.12 (*b*)). Convergence of cut-off energy below $5meV$ per atom was at 400 eV for both bulk platinum and bulk vanadium (Figures 2.11 (*a*) and 2.12 (*a*)). Thus, 120 irreducible k-points and cut-off energy of 500 eV were chosen for further calculations.

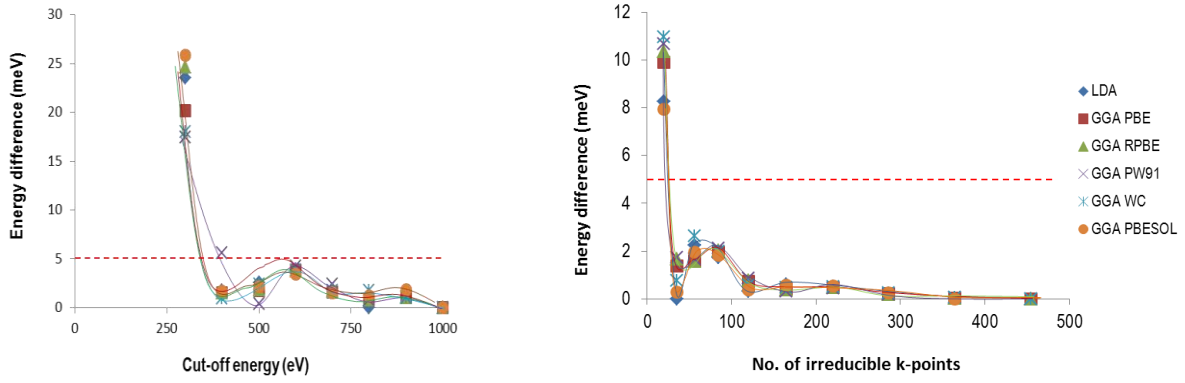

(a) (b)

Figure 2.11: (a) Convergence of total energy with respect to cut-off energy for bulk platinum. The number of irreducible k-points was maintained at 120. (b). Convergence of total energy with respect to the number of irreducible k-points for bulk platinum. The cut-off energy was maintained at 600 eV

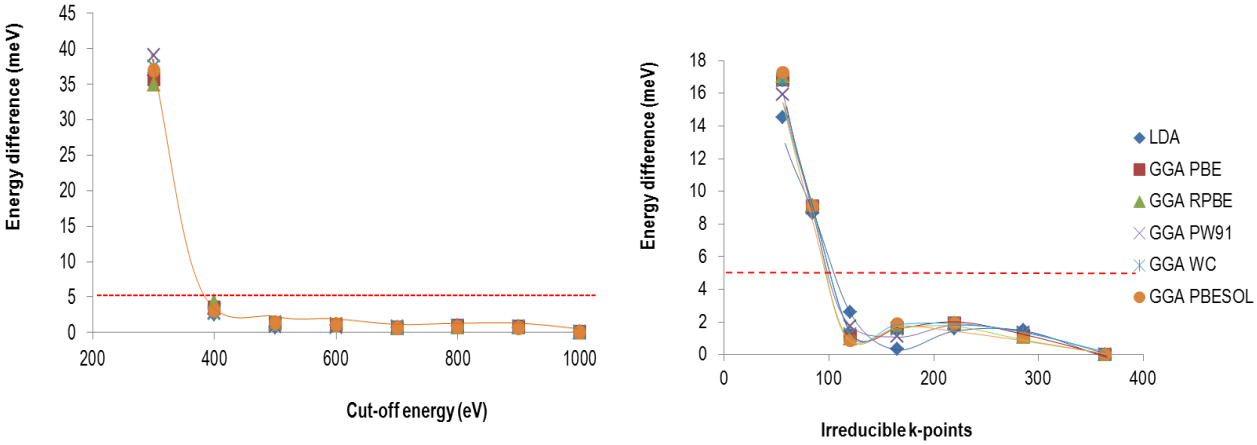

Figure 2.12: (a) Convergence of total energy with respect to cut-off energy for bulk vanadium; the number of irreducible k-points was maintained at 120 (b). Convergence of total with respect to k-points for bulk vanadium; the cut-off energy was maintained at 600 eV

2.7.1.2 Correlation and exchange functionals

All functionals available in CASTEP were tested. These are the LDA and variants of GGA which include PBE, RPBE, PW91, WC and PBEsol. The aim of the exercise was to find out how the lattice parameters and bulk modulus calculated using the different functionals compare to values obtained from experimental measurements.

Generally, LDA underestimates lattice parameters and overestimates ionisation energies. GGA corrects LDA by overestimating the lattice parameter and softening bonds. The overestimation of ionisation energies by GGA functionals is not as large as those from LDA. Results of CASTEP calculations for lattice constants and bulk modulus for platinum and vanadium are recorded in Tables 2.1 and 2.2 respectively. The bulk modulus as well as equilibrium lattice constant and volume were determined by fitting CASTEP results to the Birch Munaghan equation.

The Birch Murnaghan fit for GGA PBE results is shown in Figures 2.13(a) for bulk platinum. The calculated equilibrium lattice parameter from LDA is 3.92Å; the values from PBE, RPBE and PW91 were about 4Å while WC and PBEsol gave 3.97 and 3.96 Angstroms respectively. Table 2.1 shows the calculated values of the bulk modulus. The bulk modulus value from LDA calculations is 299 GPa, about 8% overestimation. The LDA pressure derivative is underestimated. Most GGA values of the bulk modulus are much lower than those determined experimentally (See Table 2.1). PBE functionals give a value of 244 GPa compared to the measured value of 278 GPa (Ashcroft and Mermin, 1976). In fact, the experimental value was measured at 300 K, if extrapolated to 0K, an even higher value is expected. The pressure derivative is overestimated by all GGA functionals. The GGA PBEsol functional

was specially constructed to give more accurate lattice constants compared to other GGA functionals. The bulk modulus from the PBEsol functional is 279 GPa. This is the closest to the experimental value.

Figure 2.13 (b) shows the Birch Murnaghan fit for vanadium using the PBE. Equilibrium parameters from different functionals are shown in Table 2.2. LDA, GGA PBE, and GGA PBEsol slightly overestimate the bulk modulus. GGA RPBE and GGA WC underestimate the bulk modulus. All lattice parameters are overestimated. For vanadium, values from GGA WC and GGA PBEsol are the most accurate.

LDA, GGA PBEsol and PBE WC are able to predict bulk properties more accurately compared to GGA PBE and GGA RPBE. However the later functionals (PBE and RPBE) describe surface properties better. This project is about interaction of molecules and surfaces, a compromise between bulk properties and surface properties is necessary, and the PBE functional was chosen for use in further calculations.

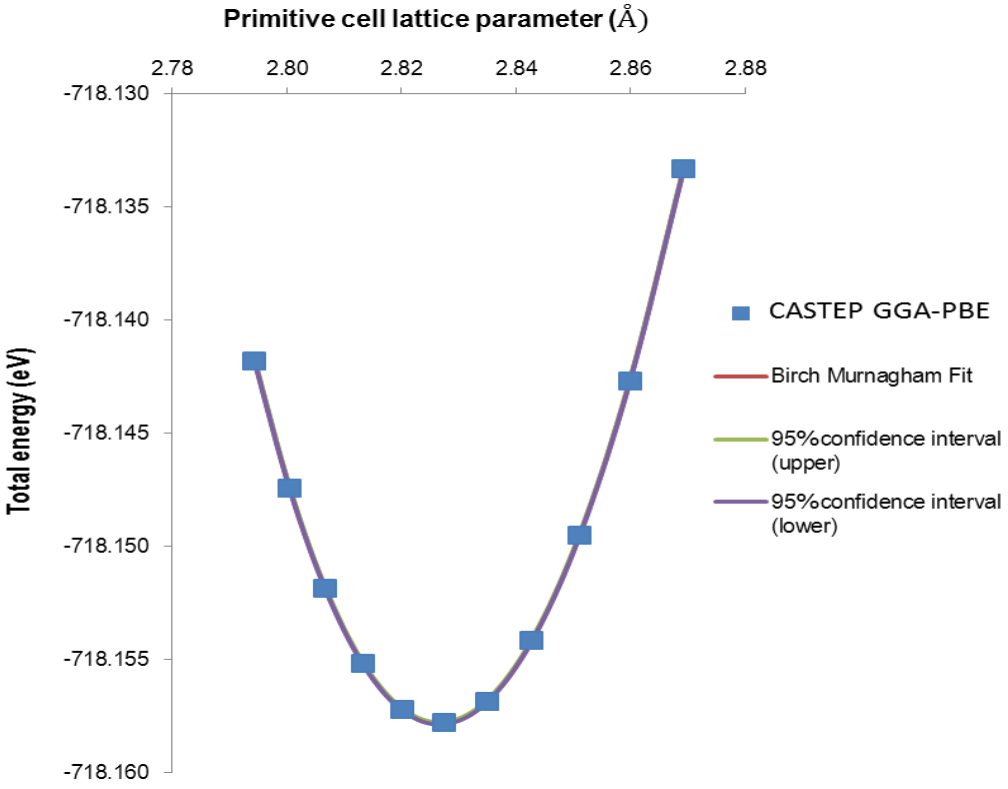

(a)

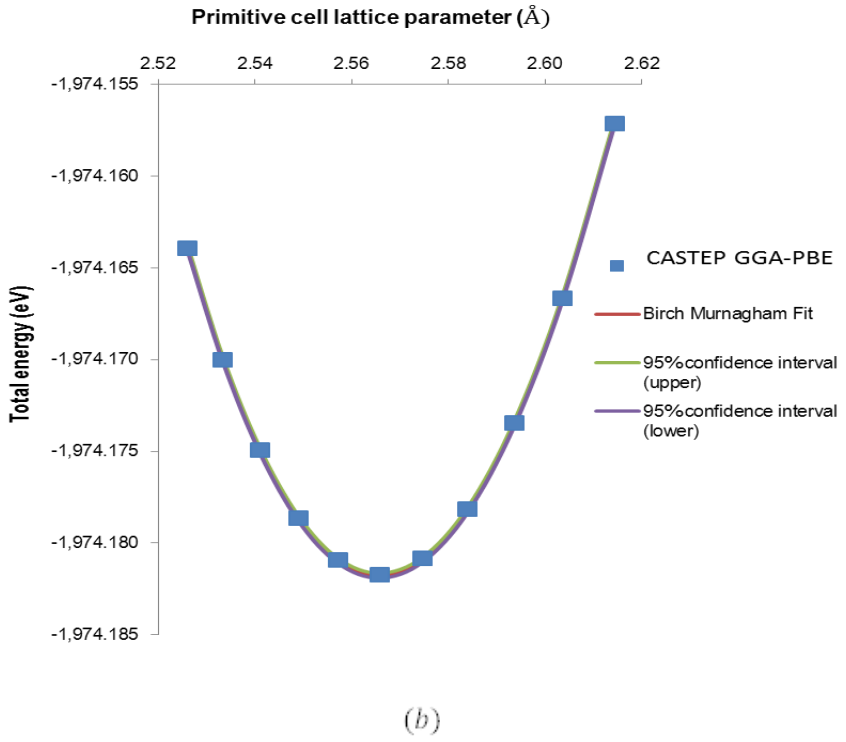

(b)

Figure 2.13: *(a)* Birch Murnaghan fit for bulk platinum at 120 irreducible k-point and 500 with GGA PBE functionals *(b)* Birch Murnaghan fit for bulk vanadium at 120 irreducible k-point and 500 with GGA PBE functionals.

Table 2.1: Calculated values of lattice parameter for fcc Pt obtained by fitting Birch Murnaghan equation. Values from experiments were taken from Ashcroft and Mermin (1976).

Method	Bulk modulus (B_0) (GPa)	Pressure Derivative (B_0')	Primitive cell equilibrium volume (Å)	Primitive cell equilibrium lattice parameter (Å)	Unit cell equilibrium lattice parameter (Å)
Experimental	278	5.61	15.10	2.775	3.92
CASTEP DFT					
LDA	299	5.36	15.97	2.77	3.920
GGA PBE	244	5.99	16.94	2.83	3.997
GGA RPBE	232	6.12	17.09	2.84	4.009
GGA PW91	242	6.00	17.03	2.83	4.004
GGA WC	269	5.47	16.64	2.81	3.974
GGA PBEsol	279	5.83	16.50	2.80	3.962

Table 2.2: Calculated values of lattice parameter for bcc vanadium obtained by fitting Birch Murnaghan equation. Values from experiments were taken from Ding *et al*. (2007).

Method	Bulk modulus (B_0) (GPa)	Pressure Derivative (B_0')	Equilibrium Volume (Å)	Equilibrium lattice parameter (Å)
Experimental	165	3.50	13.92	3.03
CASTEP DFT				
LDA	178	3.25	14.51	3.587
GGA PBE	170	3.34	15.01	3.629
GGA RPBE	149	3.37	15.95	3.702
GGA PW91	157	3.79	15.53	3.883
GGA WC	168	3.54	15.05	3.632
GGA PBEsol	170	3.34	15.01	3.629

2.7.2 Surfaces

Model parameters were also tested for surface properties. The first test was to determine the Brillion zone parameters required to accurately describe the surface properties. Then, the vacuum layer thickness and the number of slab layers were tested for convergence of total energy and their ability to reproduce physical surface properties which include surface energy, surface geometry (interlayer relaxation) and adsorption properties. The ability of all functionals available in CASTEP to predict the surface properties was tested.

2.7.2.1 Brillouion zone sampling

The convergence criteria for the surface Brillouion zone parameters was made more stringent compared to that of the bulk model from which it was created. A (Pt111) surface model with a slabs consisting of six layers separated by vacuum spaces 12 Angstroms thick was used. Thus, the unit cell had six atoms. All atoms were constrained to their fractional positions. Converging total energy below $10meV$ translates to a convergence criterion of below 2 meV per atom (see Figure 2.14). 120 irreducible k-points and a cut –off energy of 500 eV were chosen.

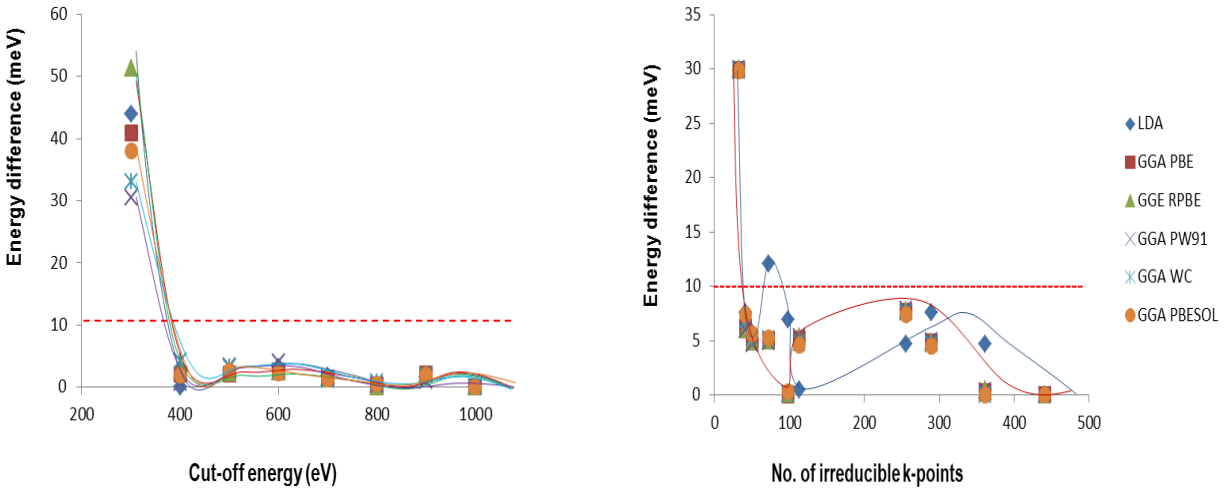

(a) (b)

Figure 2.14: *(a)* Convergence of total energy with respect to the number of irreducible k-points for a surface unit cell consisting of six Pt atoms separated by a 12Å thick vacuum layer; the cut off energy was maintained at 600 eV while varying the number of irreducible k-points. *(b)* Convergence of total energy with respect to the cut-off energy; the number of irreducible k-points was maintained at 120 while varying the cut-off energy.

2.7.2.2 Vacuum spacing

An infinite vacuum slab is always desired. However, computational costs put a restriction on the thickness of the vacuum that should be used in a calculation. Figure 2.15 shows convergence of total slab energy with respect to the vacuum thickness for a Pt (111) surface. A vacuum layer 12Å thick was chosen for use in further calculations.

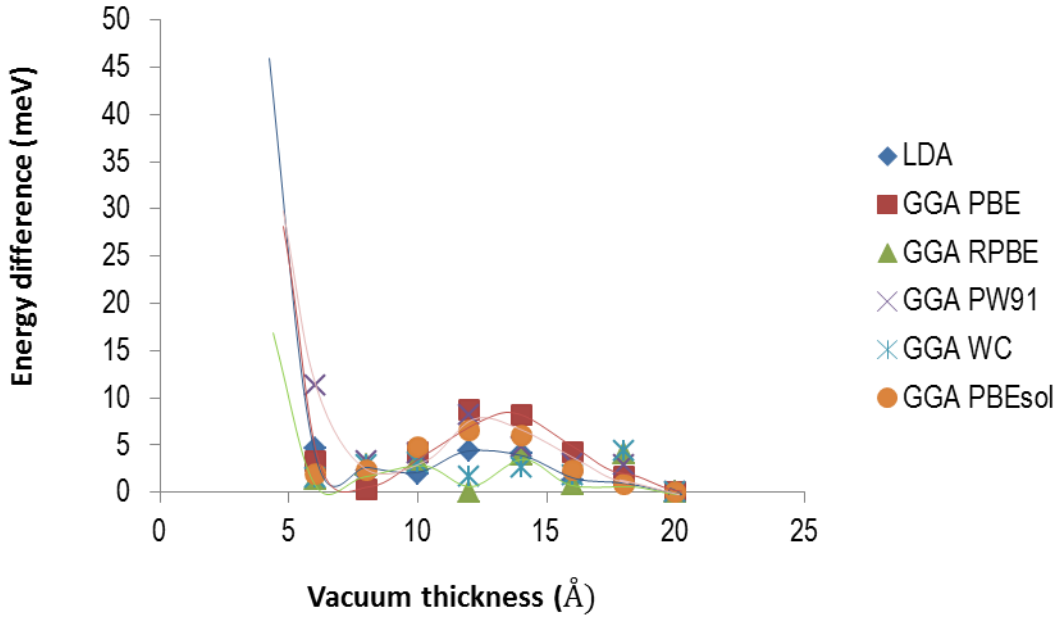

Figure 2.15: Convergence of total energy of Pt (111) with respect to the vacuum layer thickness; a layer consisted of six Pt slab layers, and 120 irreducible k-points and a cut off energy of 500 eV were used.

2.7.2.3 Surface energy

The value of surface energy of the Pt (111) surface measured by Tyson and Miller (Tyson and Miller, 1977) using the surface tension method was $2.49\,J/m^2$. The present calculation gave a value of about 0.65 eV per atom using the PBE functional. A similar value was obtained by Da Silva et al.(0.71 $eV\ per\ atom$) (Da Silva et al., 2006). These calculated values are 40 to 50 percent smaller than experimental values. LDA give more accurate values of the surface energy compared to GGA functionals (Da Silva et al., 2006).

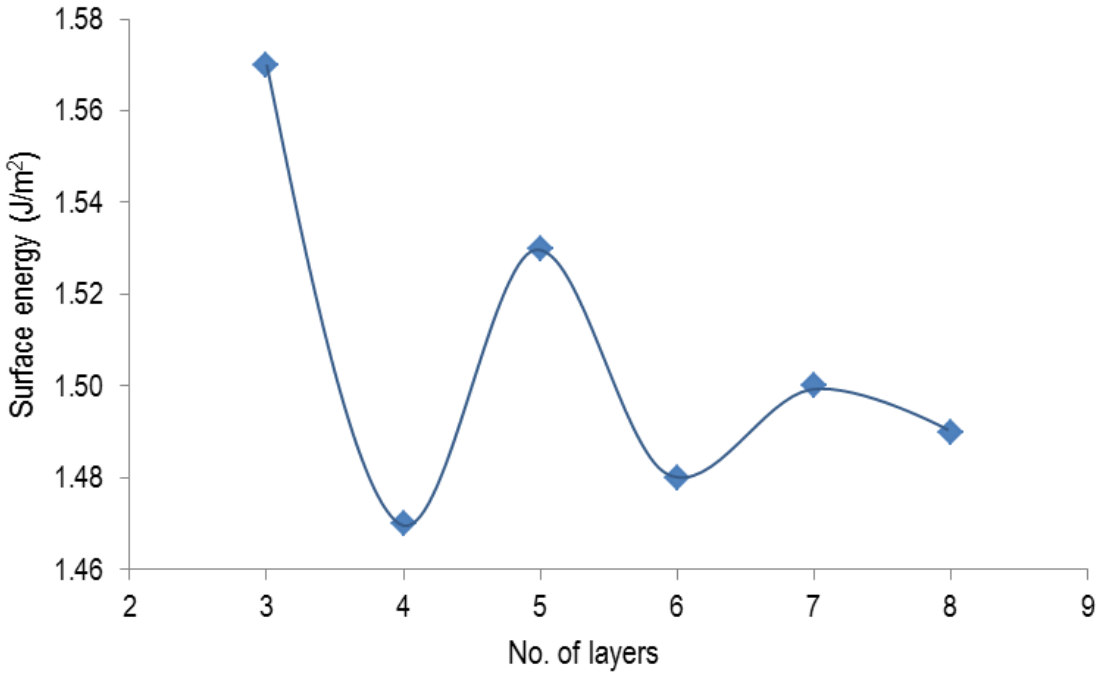

Figure 2.16: Convergence of surface energy with respect to the number of slab layers using GGA PBE. The vacuum thickness was fixed at 12 Å. 120 irreducible k-points and energy of up to 500 eV were used. Top two layers were allowed to relax.

2.7.2.4 Interlayer relaxation

The top two layers were allowed to relax to mimic surface properties and the rest were fixed to their fractional position to mimic bulk properties. Low energy electron diffraction measurements showed that the top most interlayer distance expands by up to 1.7% (Somorjai and Li, 2010). All functionals produced Pt (111) with the interlayer distance of the top most surface expanded. PBE and RPBE functionals showed higher expansion compared to PBEsol and WC.

Table 2.3: Interlayer spacing for Pt (111) surface. The supercell consisted of six slab layers separated by a vacuum layer 12 Å thick.

Source		**Interlayer relaxation**		
		Bulk (Å)	Surface (Å)	% expansion of surface layer
Somorjai and Li (2010)		2.26	0-2.30	0-1.77
Some previous calculations				
Da Silva et al. (2006)	LDA			1.3
	PBE			1.14
Present study (CASTEP DFT)				
GGA PBE		2.308	2.337	1.26
GGA RPBE		2.316	2.342	1.12
GGA PW91		2.313	2.338	1.07
GGA WC		2.295	2.315	0.85
GGA PBEsol		2.289	2.310	0.91

2.7.2.5 Adsorption properties

The final test performed on the surfaces was adsorption of an oxygen atom on Pt (111) for different slab thicknesses as shown in Figure 2.17. Adsorption energy of atomic oxygen was computed using equation 2.32.The number of slab layers was varied from 3 to 8. The only functional used is the GGA PBE. For slab thickness of up to 10 layers, adsorption energy of atomic O converged below 10 mV at 7 layers.

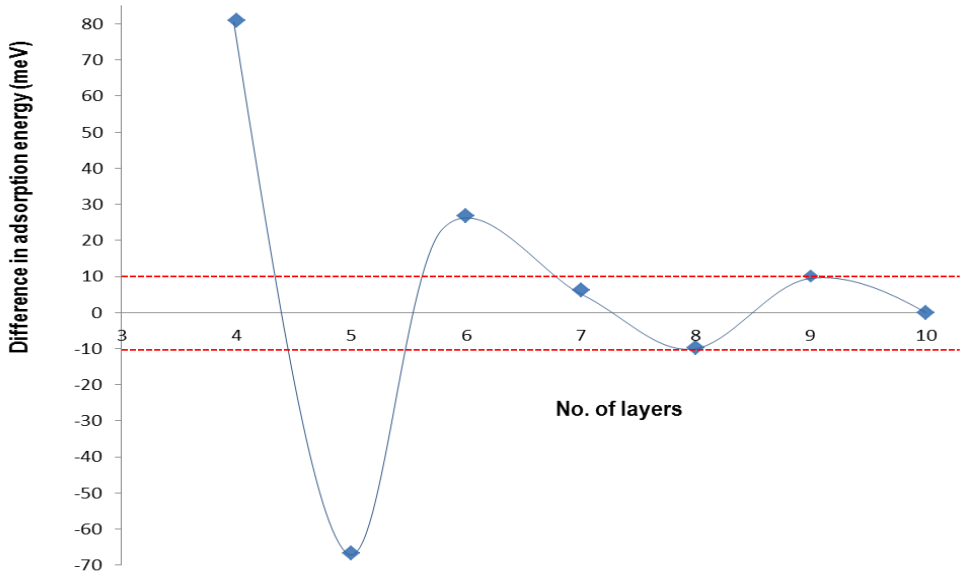

Figure 2.17: Convergence of adsorption energy of atomic O on Pt (111) with respect to the number of slab layers. The vacuum thickness was fixed at 12 Å. 120 irreducible k-points and energy of up to 500 eV were used.

2.7.2.6 Number of layers

The number of slab layers of the surface model was tested for reproduction of physical properties including surface energy, interlayer surface relaxation and adsorption energy. Strict convergence of these properties with respect to the number of slab layers was not possible for the maximum number of layers considered. After six layers, the surface energies and adsorption energies converged below $50meV$. Also, interlayer surface distances had sufficiently converged after six layers (See Table A9 in Appendix A). Therefore a slab consisting of six layers was chosen for further calculations.

2.7.2.7 Selection of correlation and exchange functionals

Five GGA functionals available in CASTEP were compared for both convergence of total energy and reproduction of physical properties for both bulk materials and surface. Convergence of total energy was almost similar for all functionals considered. LDA, GGA PBEsol and GGA WC gave equilibrium lattice parameters close to values determined experimentally. However, the bulk modulus estimated was much lower than experimental values for all functionals, meaning that the model material is much softer than the real material. GGA PBE gave a highest value of 242 GPa compared to the experimentally measured value of 278 GPa for pure platinum. For surface energies the predicted values were also much lower than measured values. LDA, PBEsol and WC perform well in predicting

properties of bulk materials, and PBE and RPBE perform well for adsorption energies. GGA PBE was chosen for further calculations.

2.7.3 Conclusion

Although density functional theory is exact in principle, its application is made possible by making use of several approximations. For a practical calculation, the Brillouion zone is represented by a finite number of k-points and the wave functions are expanded into a finite basis set determined by the cut-off energy. For platinum surfaces, a k-point mesh of $12 \times 12 \times 2$ corresponding to 120 irreducible k-point was considered sufficient. The cut off energy chosen was $500eV$. The GGA PBE functional was chosen as a good compromise between bulk and adsorption properties. A surface was modelled by a supercell containing six slab layers separated by a vacuum 12Å thick.

CHAPTER 3

ELECTRONIC PROPERTIES OF PLATINUM VANADIUM ALLOYS

Studying the electronic structure of alloys is important since adding solute atoms like vanadium to a platinum catalyst may change its catalytic performance (Jalan, 1980). The improved performance may be a result of changes in the electronic structure caused by alloying. Main factors affecting the electronic structure of alloys are composition and crystal geometry, but these two are interdependent. In this chapter, the electronic density of states of stable Platinum-Vanadium phases is analysed.

3.1 Crystal structure of intermetallic compounds

Most pure metals crystallise into face centred cubic (fcc), body centred cubic (bcc) or hexagonal close packed (hcp) structures. When two or more metallic elements are present, they can form a homogenous solid solution to make an alloy depending on their mutual solubility limits (See Figure 3.1). If they are miscible, an interstitial or substitutional alloy can be formed. Interstitial alloys form when the solute atoms occupy lattice voids because of their small size. Substitutional alloys are usually formed when the atomic radii of the metal atoms is almost equal. The atomic radius of platinum is 1.53Å (Xin et al., 2012) and that of vanadium is 1.49Å (Xin et al., 2012), hence a substitutional alloy is expected in Platinum-Vanadium alloy systems. In substitutional alloys, there is little or no disruption of the original crystal structure. Alloys can be ordered or disordered. In disordered alloys, the elements are arranged in a random manner. Conversely, in ordered alloys, the atoms of each element are arranged on preferred lattice sites.

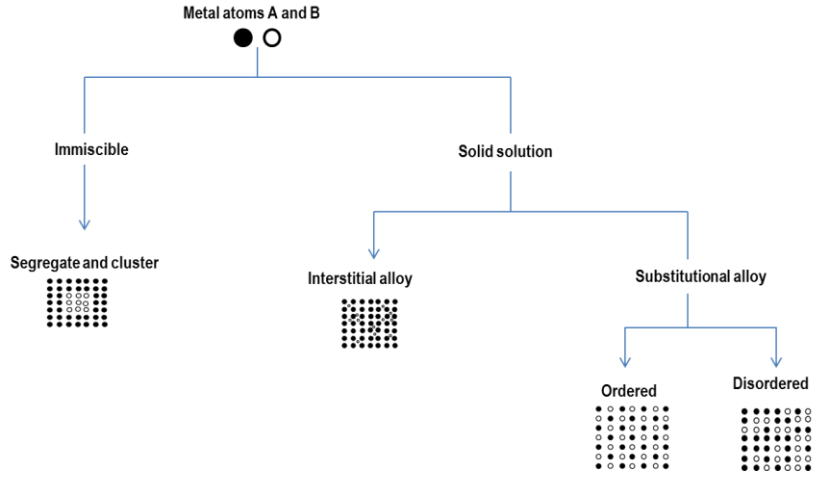

Figure 3.1:Interaction of two metal species to form metallic compounds

The likelihood of formation of solid solutions depends on thermodynamic variables, although sometimes thermodynamically stable phases do not form because of sluggish kinetics. Alloys crystallise into

geometries that minimise their Gibbs free energy. Thus structures with the most negative Gibbs free energy are the most stable:

$$\Delta G = \Delta H - T\Delta S \quad (3.1)$$

where the formation energy ΔH is the difference between the average enthalpy per atom in pure form and the average energy per atom in alloy form. At 0K, the Gibbs free energy of formation is equal to the enthalpy of formation, which for solids is almost equal to the internal energy and can be calculated from the electronic energy (Equation 3.2).

$$\Delta \mathrm{H}(\mathrm{A_mB_n}) = \frac{1}{\mathrm{m+n}}[\mathrm{E_{tot}}(\mathrm{A_mB_n}) - \mathrm{mE_{tot}}(\mathrm{A_m}) - \mathrm{nE_{tot}}(\mathrm{B_n})] \quad (3.2)$$

where m is the number of species A atoms in the unit cell, n the number of species B atoms and E_{tot} is the total energy of a given unit cell.

3.1.1. Platinum –vanadium intermetallic structures

Temperature-composition phase diagrams are usually used to characterise the solid solutions. Ordered phases are observed at lower temperatures. The Platinum-Vanadium phase diagram was originally constructed by Waterstrat (1973). The solubility of vanadium in platinum is appreciable, but the solubility of platinum in vanadium is very small. Several intermediate ordered phases have been reported: Pt_3V, Pt_2V, PtV and PtV_3 at composition ranges and temperatures shown in the revised phase diagram in Figure 3.2 (Okamoto, 2009). Earlier first principle calculations determined that Pt_8V can form a stable phase of the Pt_8Ti prototype structure (Turchi et al., 1988) and this structure was successfully synthesised (Nxumalo and Lang, 2006).

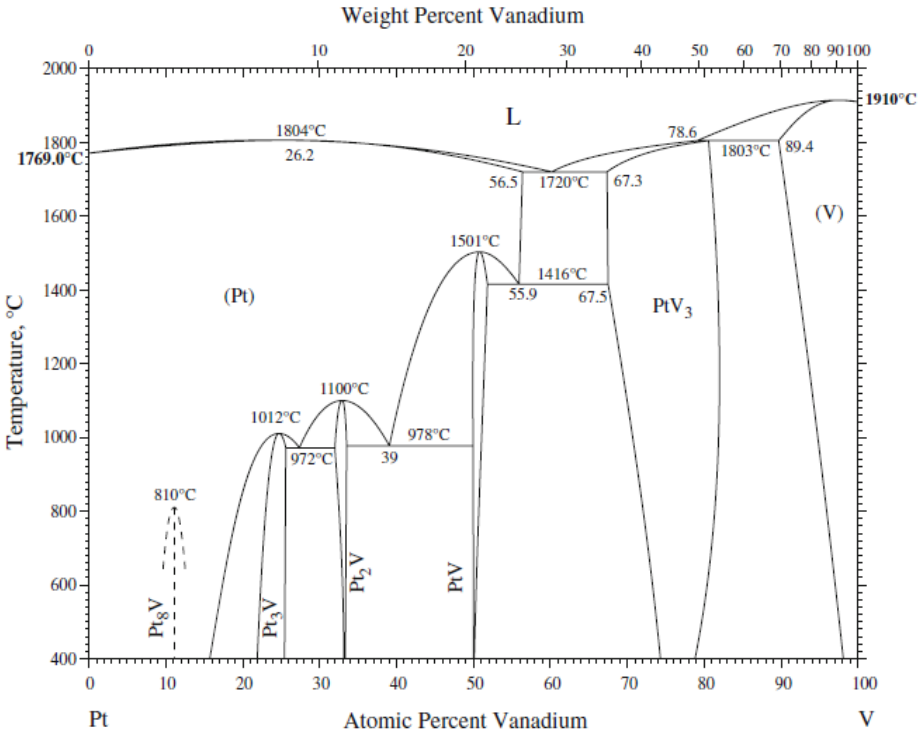

Figure 3.2: Platinum-vanadium phase diagram (Okamoto, 2009)

3.1.2. Electronic structure of platinum-vanadium alloys

As the two elements come together, all electronic states adjust themselves in order to maintain orthonormality. New states are also created by hybridisation, when new bonds are formed (Atkins, 1998). The total density of states of the alloy is composed of all states available in the structure. In Pt-V alloys these include states in platinum-platinum bonds, vanadium-vanadium bonds, platinum-vanadium bonds and states localised on the atoms and delocalised states. Delocalised states are mainly sp-states (Ashcroft and Mermin, 1976). Platinum localised and platinum-platinum bond states and vanadium localised and vanadium-vanadium bond states are displayed on respective PDOS. Hybridisation creates states that have a more stable configuration called bonding states. It also creates repulsive states called anti-bonding states. Thus, the structures become more stable when the bonding orbitals are occupied. They become less stable when anti-bonding orbitals are occupied. The nature of created states and the position and filling of states is important in solid state chemistry.

The d-band filling at the Fermi level and average energy of d-electrons are important for gas-solid reactions that take place in catalysis. The aim of this chapter is to analyse the way these properties are modified when platinum is mixed with vanadium to form ordered alloys.

3.2 Calculation details

Ordered structures of known substitutional Pt-V were considered. Ordered phases are naturally suited to be studied using DFT calculations since they are less computational demanding compared to disordered phases. Another motivation in studying the electronic structure of alloy ordered phases is that catalytic properties of metal surfaces were found to correlate with the level of ordering (Xiong and Manthiram, 2005).

Geometry optimisation calculations were performed by minimising forces (See Chapter 2).GGA PBE functionals for exchange and correlation and ultrasoft pseudopotentals were used throughout. The unit cell volume varied according to the crystal structure and the number of k-points was adjusted accordingly. First, the stability of phases was verified by comparing formation energy (Equation 3.2) of related crystal structures. Since platinum is fcc and vanadium is bcc, for each of the ordered phases, Pt_8V, Pt_3V, Pt_2V, PtV, and PtV_3, bcc and fcc superstructures were considered. Then, the DOS was calculated and presented for the most stable phases. The DOS was plotted against the electronic energy relative to the Fermi level ($E-E_F$). The d-band centre was calculated by determining the first moment and the d-band width is represented by the second moment. The reported values of the d-band centre are relative to $E-E_F$. The Fermi energy was computed for all stable phases.

3.3 Results and discussions

The formation energies of platinum-vanadium alloy at vanadium compositions 11% (Pt_8V), 25% (Pt_3V), 50% (PtV), 25% (PtV_3) are displayed in Figure 3.3. Generally fcc superstructures ($D0_{22}$, $L1_2$, $D0_{19}$) are more stable at high platinum concentrations and bcc superstructures are more stable at high vanadium concentrations. This is in agreement with experimentally determined structures (Wang et al., 2008). This implies that the experimentally determined structures are the actual thermodynamically stable phases, and not quasistable ‘frozen’ structures.

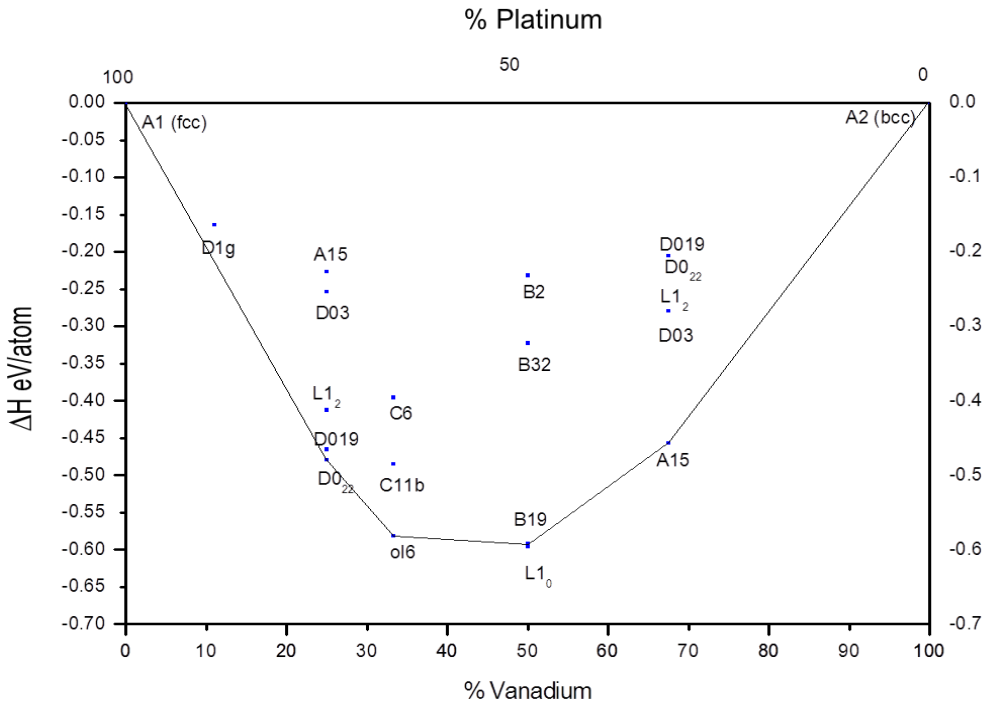

Figure 3.3: Ground state formation energies of platinum vanadium structures at stoichiometric ratios Pt_3V, Pt_2V, PtV, PtV_3**.**

3.3.1. Pure elements: platinum and vanadium

3.3.1.1. Platinum

Platinum is a 5d transition metal in group VIIIC of the periodic table. It is silvery-white in colour and lustrous. The crystal structure of solid platinum is face-centred cubic. The calculated value of the optimised lattice parameter is overestimated by 2% compared to the experimental value (Predel, 1998). The valence d-orbital of platinum is almost fully occupied. The DOS for platinum is shown in Figure 3.4.

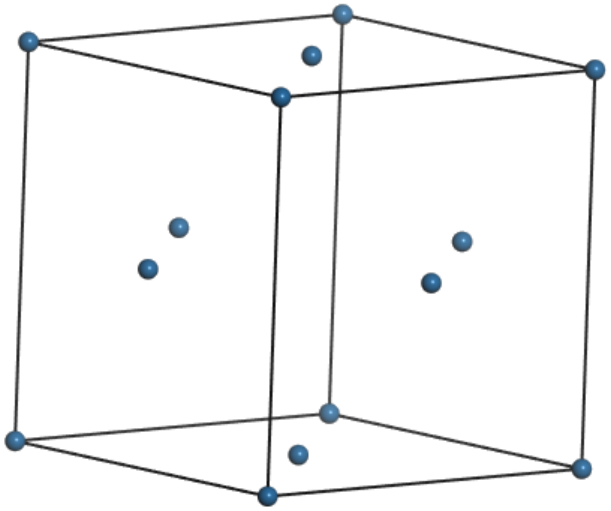

(a)

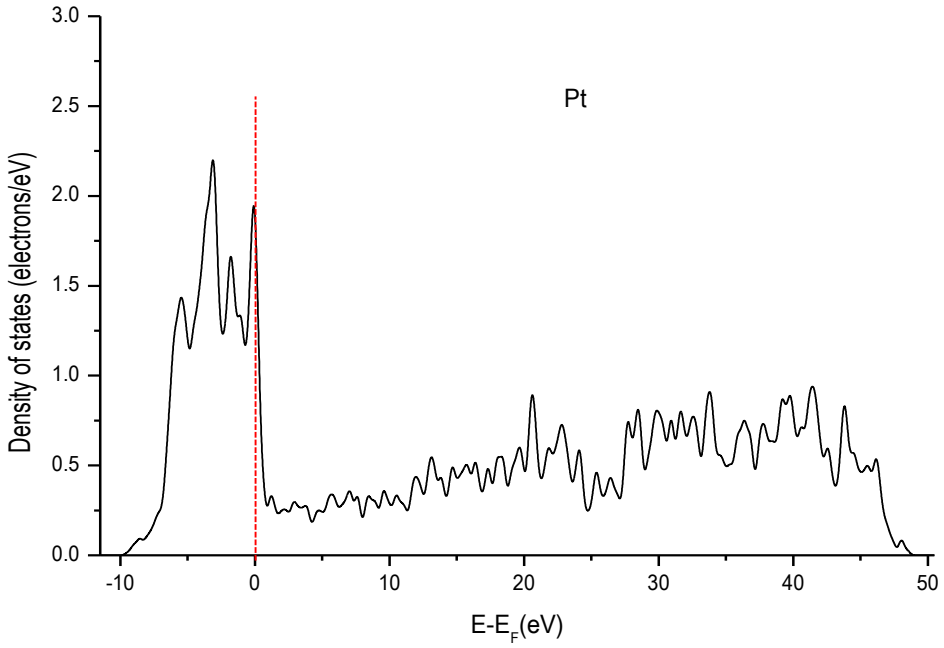

(b)

Figure 3.4: (a) Face centred cubic crystal structure for pure platinum; **(b)** the valence d-band of platinum.

Table 3.1: Optimised properties for pure platinum

Property	CASTEP	Experiment
Lattice parameter (Å)	3.99	3.92*
Crystal structure (Strukturbericht)	A1	
d-band centre(eV)**	-2.068	
d-band width (eV)	3.130	
Fermi energy (eV)	-11.96	

*(Predel, 1998)

**The value of the d-band centre is relative to $E\text{-}E_F$.

3.3.1.2. Vanadium

Vanadium is a 3d transition element. It exhibits a bright white colour, and has a body centred cubic crystal structure. Its valence d-orbital has fewer electrons compared to that of platinum as shown in the DOS (Figure 3.5). Thus, there are many empty d-band states in a pure vanadium structure.

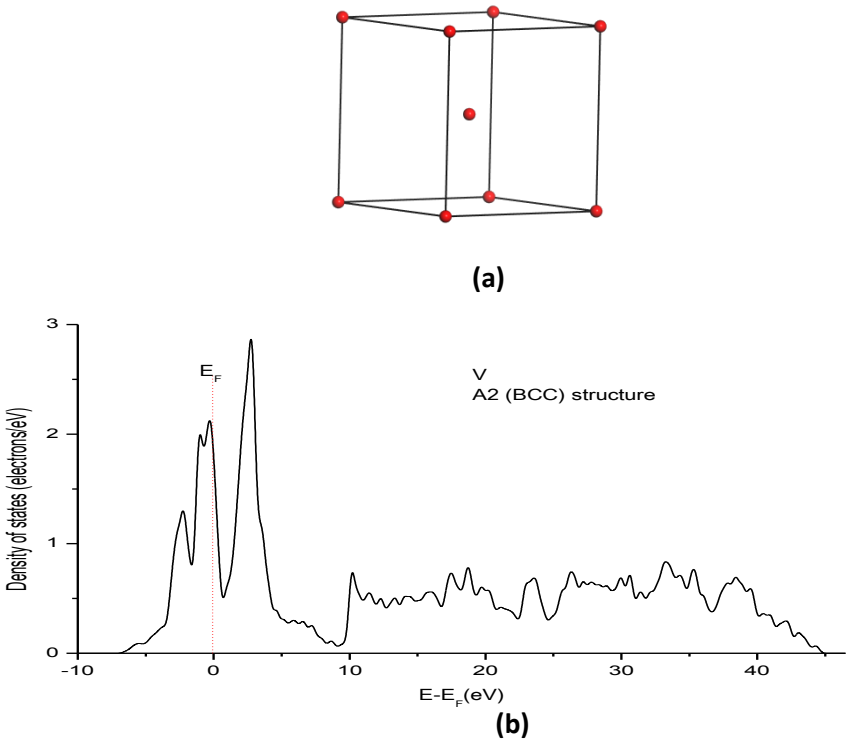

Figure 3.5: (a) Body centred cubic crystal structure for pure vanadium; **(b)** the valence d-band of vanadium.

Table 3.2: Optimised properties for pure vanadium

Property	CASTEP	Experiment
Lattice parameter (Å)	3.00	3.00*
Crystal structure (Strukturbericht)	A2	
d-band centre(eV)	-1.630	
d-band width (eV)	-2.610	
Fermi energy (eV)	9.50	

*(Predel, 1998)

3.3.2. Pt_8V

A_8B compounds like Pt_8V are few in nature and all known structures order into a crystallographic configuration shown in Figure 3.6. This is a bcc tetragonal structure of space group 139. However, to show relationship with the parent pure platinum structure, an fcc superstructure can be described by considering unit cells with faces lying on the (110) plane as shown in Figure 3.6. Optimised properties for Pt_8V are displayed in Table 3.3 and the electronic DOS is shown in Figure 3.7. Although there are two symmetrically different positions for platinum atoms, the difference between their electronic populations is very small and their projected DOS are similar. The total DOS for the alloy is dominated by platinum states. The empty d-band states contributed by hybridisation between platinum and vanadium are shown in Figure 3.7(c). The d-band centre of electrons in Pt_8V has a value of average energy -2.165 eV, 0.097 lower than that of pure platinum.

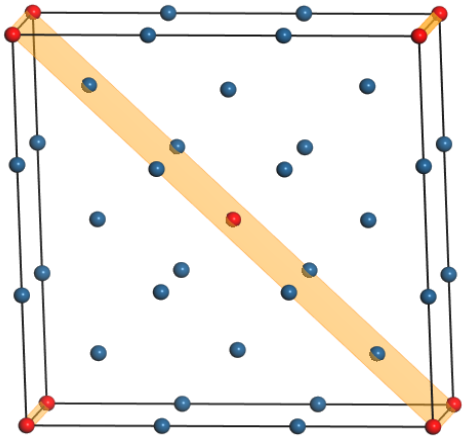

Figure 3.6: The fcc superstructure for Pt_8V can be viewed by looking on the (110) projection.

Table 3.3: Optimised properties for Pt_8V

Property	**CASTEP**	**Experiment**
Lattice parameter (Å)	10.16 2.77	-
Crystal structure (Strukturbericht)		
Atomic position (fractional)	Pt: $\frac{1}{3}, \frac{1}{3}, 0$ Pt: $\frac{1}{3}, 0, 0$ V: $0, 0, 0$	
Formation energy (eV)	-0.16	-
d-band centre (Pt PDOS) (eV)	-2.165	
Shift in average energy of the d-band (Pt PDOS) (eV)	-0.097	
d-band width (eV)	3.14	
Fermi energy (eV)	-9.64	

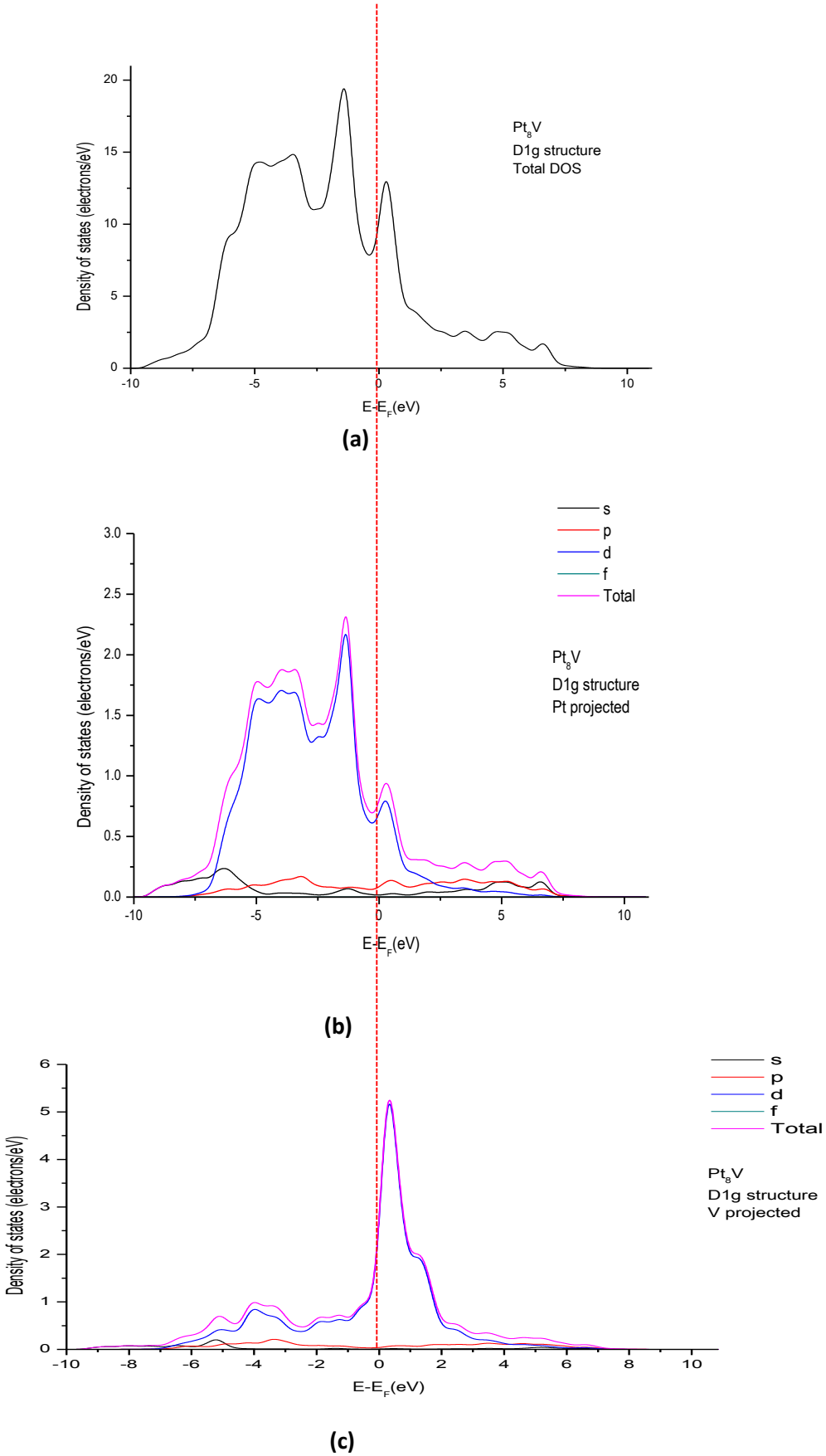

Figure 3.7: Density of states for Pt_8V is dominated by states from platinum, (a) total DOS, (b) PDOS platinum; (c) PDOS vanadium.

3.3.3. Pt_3V

The formation energies of face centred cubic superstructures ($D0_{22}$, $L1_2$), bcc based superstructures ($D0_3$ and A15) and hcp superstructure $D0_{19}$ is compared in Figure 3.3. The $D0_{22}$ structure has the most negative formation energy. This is in agreement with experimental results (Waterstrat, 1973). The $D0_{22}$ structure is shown in Figure 3.8. It belongs to space group 139. Optimised properties of the structure were recorded in Table 3.4. The calculated lattice parameters in Figure 3.4 are overestimated by 1.8% and 1.9% respectively, compared with experimental data (Predel, 1998).

The DOS for $D0_{22}$ structure is shown in Figure 3.9. The PDOS for a platinum atom in Pt_3V has a d-band 121 meV wider than that of an atom in a pure platinum crystal. The average energy of d-electrons centred on the platinum atom in Pt_3V is 0.205 eV lower than those in pure platinum.

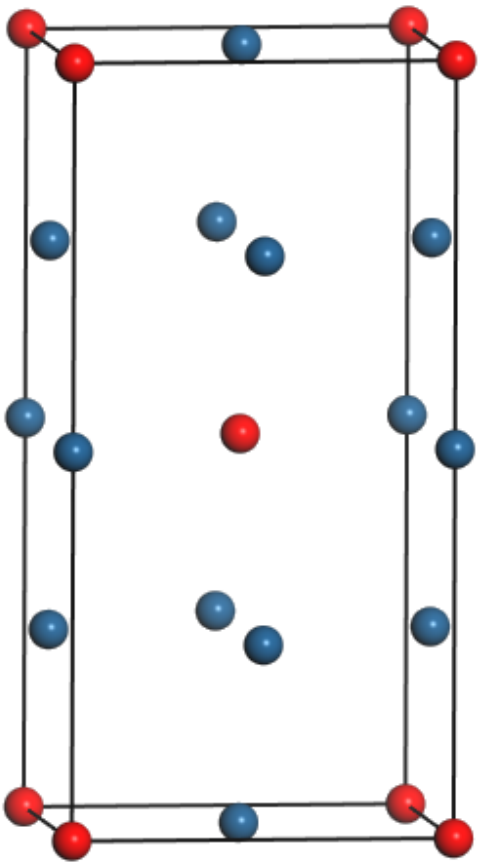

Figure 3.8: The Pt_3V $D0_{22}$ superstructure

Table 3.4: Optimised properties for Pt_3V

Property	**CASTEP**	**Experiment**
Lattice parameter (Å)	3.91 7.95	3.84 7.80*
Crystal structure (Strukturbericht)	$D0_{22}$	
Atomic positions (fractional)	Pt: $0, 0, \frac{1}{2}$ Pt: $0, \frac{1}{2}, \frac{1}{4}$ V: $0, 0, 0$	
Formation energy (Pt PDOS)(eV)	-0.48	-
d-band centre (eV) (Pt PDOS)	-2.27	
Shift in average energy of the d-band (eV)	-0.21	
d-band width (Pt PDOS) (eV)	3.25	
Fermi energy (eV)	-6.85	

*(Predel, 1998)

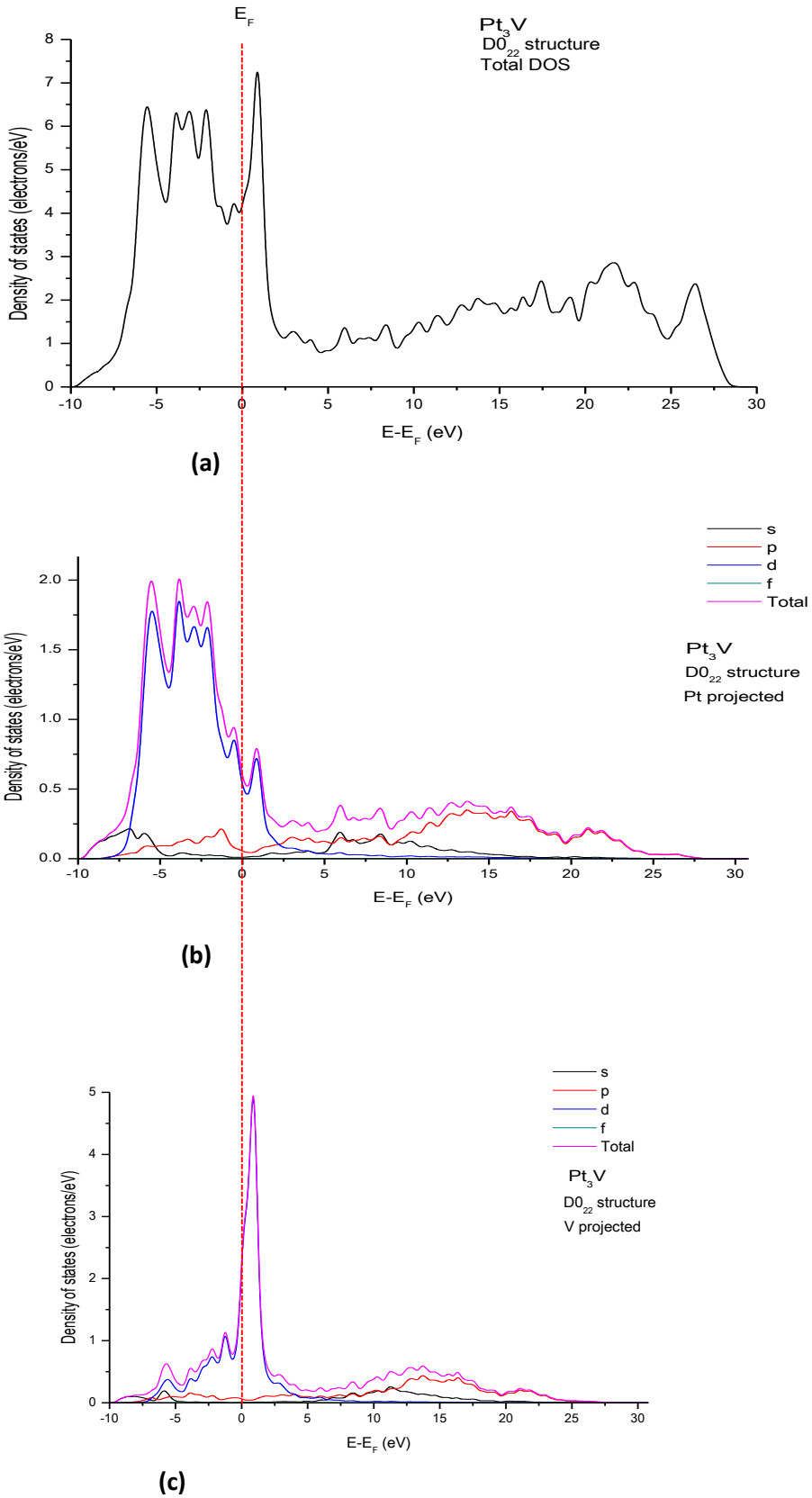

Figure 3.9: (a) The DOS of the DO_{22} structure for Pt_3V; (a) total DOS; (b) Pt projected; (c) V projected.

3.3.4. Pt_2V

The Pt_2V alloy crystallises in a structure described by the Pearson symbol oI6. The structure belongs to space group number 71. This is also the most stable structure from DFT energies (See Figure 3.3). The crystal structure is displayed in Figure 3.10. The calculated lattice parameters are overestimated by 1.5%, 1.7% and 0.8% respectively (Predel, 1998).

DFT optimised properties and DOS are displayed in Table 3.5 and Figure 3.11 respectively. The d-bandwidth of platinum atoms in Pt_2V is 90 meV greater compared to platinum in a pure crystal. The d-band centre is 0.22 eV lower in Pt_2V.

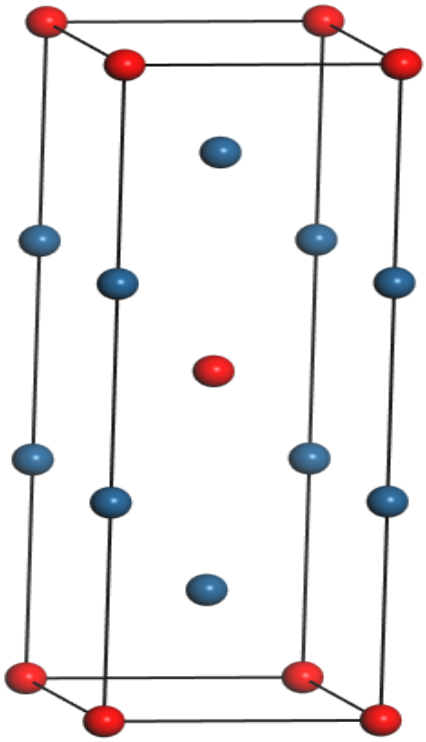

Figure 3.10: The Pt_2V oI6 superstructure

Table 3.5: Optimised properties for Pt_2V structure

Property	CASTEP	Experiment
Lattice parameters (Å)	2.76 8.49 3.82	2.72 8.35 3.79*
Crystal structure (Pearson symbol)	oI6	
Atomic positions (fractional)	Pt: $0, \frac{1}{3}, 0$ V: $0, 0, 0$	
Formation energy (eV)	-0.58	-
d-band centre (Pt PDOS) (eV)	-2.29	
Shift in average energy of the d-band (Pt PDOS) (eV)	-0.22	
d-band width (eV)	3.22	
Fermi energy (eV)	-5.194	

*(Predel, 1998)

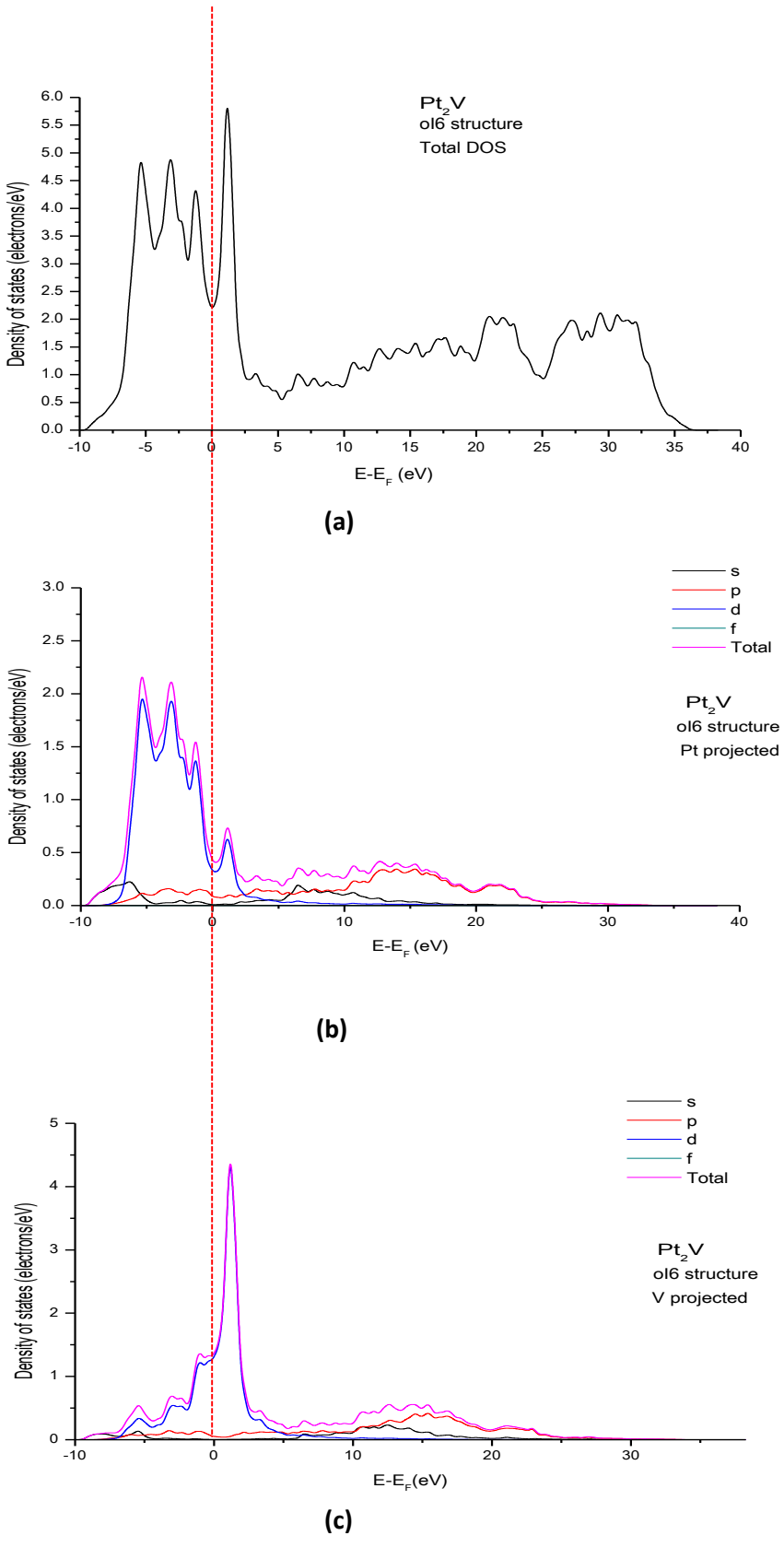

Figure 3.11: (a) The Pt_2V DOS (a) total; (b) Pt projected; (c) V projected.

3.1.1. PtV

The $L1_0$ and B19 structures are the most stable of PtV. In practice, the B19 (space group 51) is most stable and the $L1_0$ (space group 123) is metastable. However, from the present calculations, the formation energy of $L1_0$ is more negative compared to that of the B19 by 4 meV. Calculated properties are recorded in Table 3.6. The B19 structure and their DOS are displayed in Figures 3.12 and 3.13 respectively.

The calculated lattice parameters for the B19 structure are 0.5%, 0.7% and 0.8% larger than experimental values. The Fermi level lies exactly on the pseudogap, and the d-band centre of the platinum atom in PtV is 0, 27 eV lower.

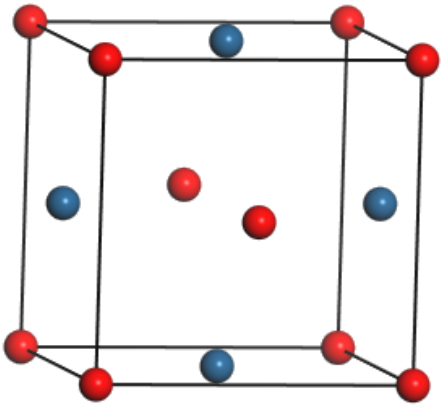

(a)

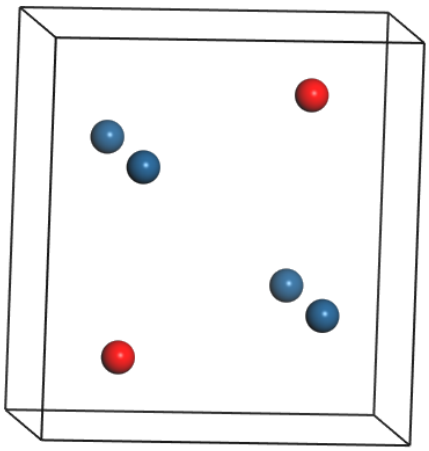

(b)

Figure 3.12: Stable PtV structures (a) the L10 structure and (b) the B19 crystal structure

Table 3.6: Optimised properties for PtV

Property	CASTEP	Experiment
Crystal structure (Strukturbericht)	B19	
Lattice parameters (Å)	4.43 2.71 4.81	4.41 2.69 4.77*
Atomic positions (fractional)	Pt: $0, 0, \frac{1}{8}$ V: $0, 0, -\frac{3}{8}$	
Formation energy (eV)	-0.59	-
d-band centre (eV)	-2.34	
Shift in average energy of the d-band (eV)	-0.27	
d-band width (eV)	3.22	
Fermi energy (eV)	-1.57	

*(Predel, 1998)

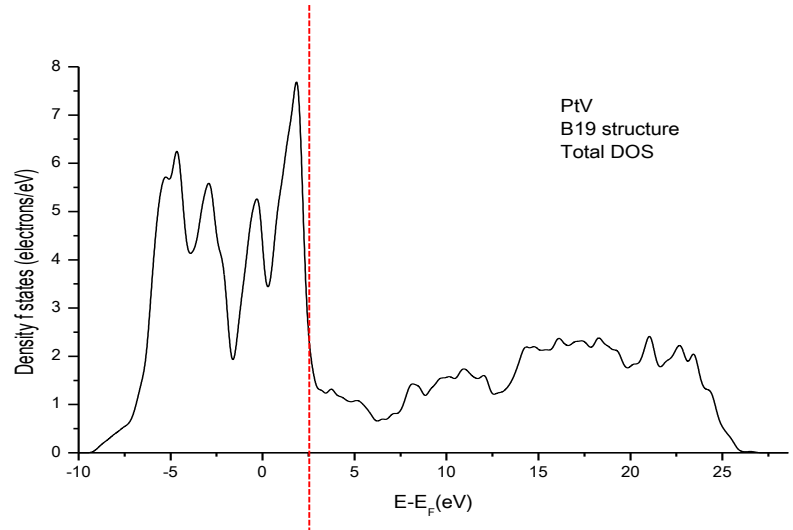

(a)

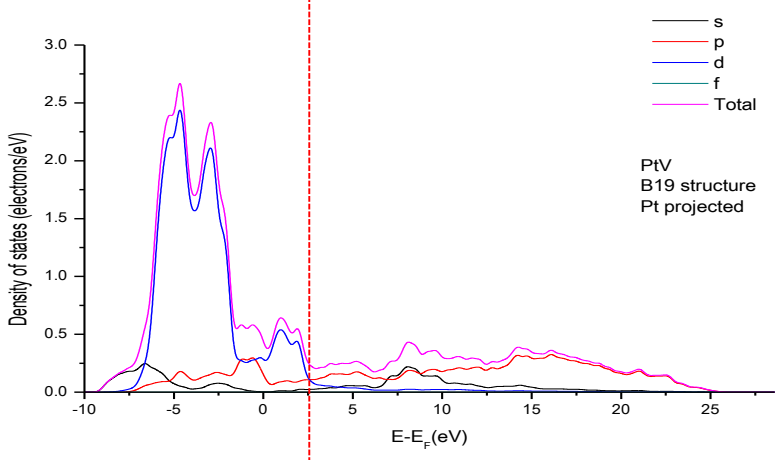

(b)

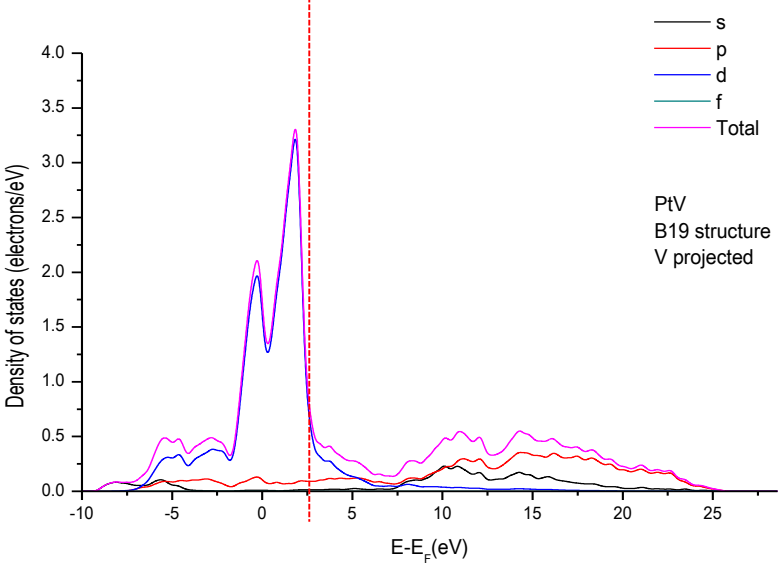

(c)

Figure 3.13: (a) DOS for the PtV B19 structure (a) total; (b) Pt projected; (c) V projected

3.1.2. PtV_3

PtV_3 crystallises into an A15 structure. The A15 polyhedron is basically a bcc skeleton structure and is displayed in Figure 3.14. It belongs to space group 223. The contribution to the DOS from Vanadium states is very significant as shown in Figure 3.15. The d-band centre is 0.31 eV lower. Optimised structural and electronic properties are shown in Table 3.7.

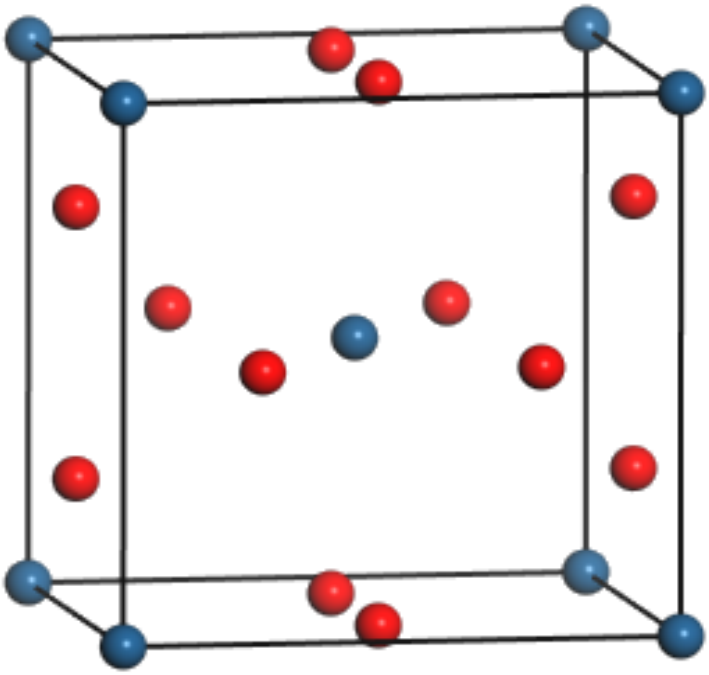

Figure 3.14: Crystal structure of PtV_3 A15 structure

Table 3.7: Optimised properties for PtV_3

Property	**CASTEP**	**Experiment**
Lattice parameters (Å)	4.82	4.81*
Crystal structure (Strukturbericht)	A15	
Atomic positions (fractional)	Pt: $\frac{1}{4}, 0, \frac{1}{2}$ V: $0, 0, 0$	
Formation energy (eV)	-0.46	-
d-band centre (eV)	-2.38	
Shift in average energy of the d-band (eV)	-0.31	
d-band width (eV)	3.20	
Fermi energy (eV)	4.09	

*(Predel, 1998)

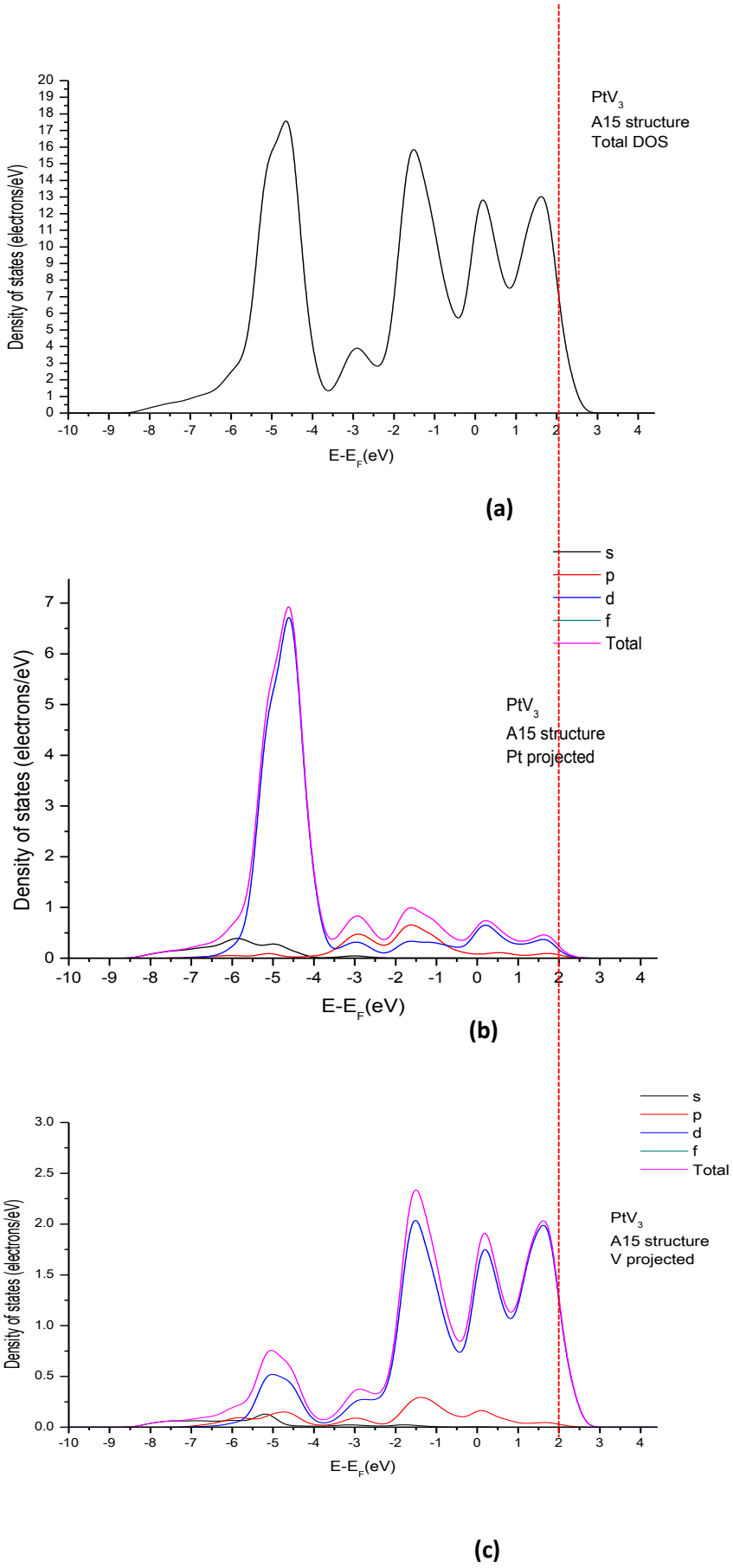

Figure 3.15: DOS of the A15 PtV_3 structure (a) total; (b) Pt projected; (c) V projected

3.4 Summary and conclusion

The density of states diagrams displayed in the preceding section shows the changes that result in the electronic structure upon alloy formation. By considering the relative positions of energy levels on the total and PDOS, it is likely that the alloy valence DOS is composed of states from platinum and anti-bonding states from vanadium. Platinum states in the 5-d band react with vanadium states in the 3-d band to produce anti-bonding orbitals that overlap with platinum 5-d states.

The d-band centres for the stable configurations were calculated by determining the first moment. The d-band centres for Pt DOS in eV for platinum vanadium structures become stabilised as the concentration of vanadium increases as shown in Figure 3.16. Thus, alloying can be used effectively to manipulate the electronic structure of parent metal, platinum in this case.

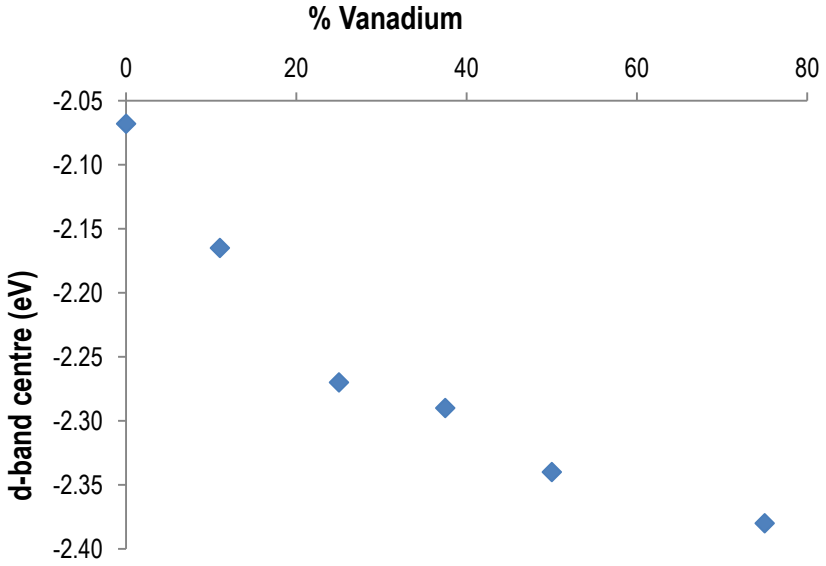

Figure 3.16: D-band centre as a function of Vanadium concentration in Pt-V alloys.

Figure 3.17 shows the change in the Fermi energy as a function of vanadium concentration in Pt-V alloys. Fermi energy is the energy difference between the highest occupied and the lowest orbitals. Figure 3.17 shows a linear variation of the Fermi level as vanadium concentration increases.

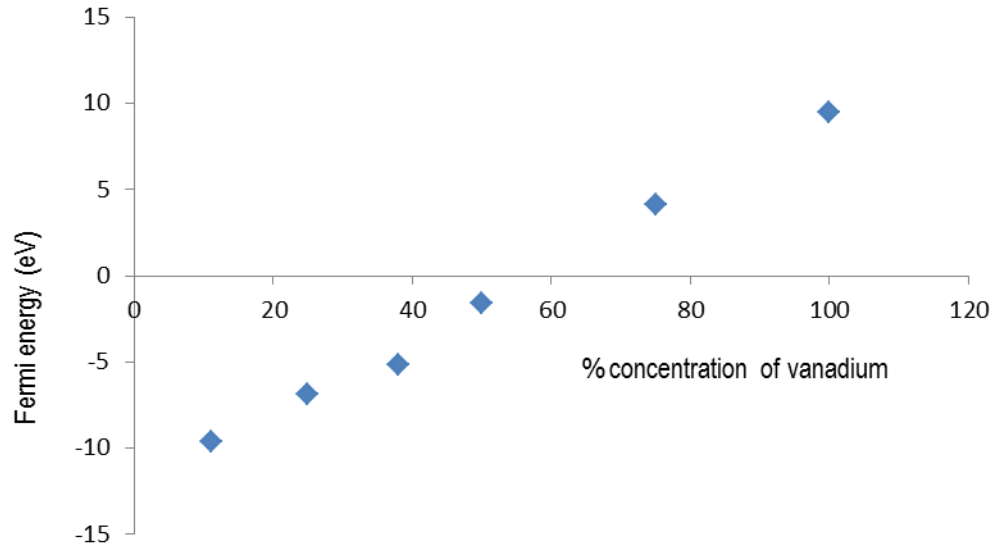

Figure 3.17: Fermi energy as a function of vanadium concentration in Pt-V alloys.

The calculations reported in this chapter show the changes to the electronic structure caused by alloying in bulk structures. However, to understand the effect of changes caused by solute vanadium atoms on catalytic properties of platinum, interaction of the surface with each of the involved gaseous species should be studied. Also creation of a surface introduces more restrictions, and the new boundary conditions result in formation of electronic states that do not appear in bulk solids called surface states. The next chapter discusses the adsorption of an oxygen molecule with platinum surfaces containing vanadium solute atoms.

CHAPTER 4

Pt (111) SURFACES MODIFIED BY SUBSURFACE VANADIUM ATOMS

4.1. Introduction

The electronic and geometrical structures of a metal surface are expected to be perturbed by the presence of foreign subsurface atoms (Stamenkovic et al., 2006). A platinum surface supercell in which the second layer has been replaced by vanadium atoms was used to investigate the modification of surface properties caused by solute elements. The properties investigated are the electronic structure, surface geometry and adsorption on an oxygen molecule.

4.1.1. Pure metal surfaces

The electronic structure of surfaces differs in one prominent way to that of bulk materials. Bulk crystals are considered to extend infinitely in all directions. Thus, the solution for electronic states is determined by periodic boundary conditions in which all solutions are real. However, creation of a surface distorts periodicity in the direction perpendicular to it. In this case, imaginary solutions have to be considered also (Ashcroft and Mermin, 1976). As a result, there exist electronic states confined to the surface region only, called surface states. The electronic density of states for surfaces is much higher compared to that of bulk materials.

The change in electronic structure upon creation of surfaces modifies the surface geometry. Surface atoms are left at a higher energy level compared to their bulk counterparts. To redistribute the excess energy, relaxation and reconstruction may result. In relaxation, the interlayer distance between surface layers change, some layers contracts whilst other layers expand. Reconstruction is a process in which the two dimensional surface geometry changes totally.

The Pt (111) was found to be stable. It does not reconstruct at temperatures below 1329.25K (Sandy et al., 1992). The bulk interlayer distance for platinum in the [111] direction is 2.26Å. The surface layer relaxes by expanding to 2.30Å (Somorjai and Li, 2010).

4.1.2. Alloy surfaces

When solute elements are present in the surface region, segregation and enrichment may result. These processes can be explained by defining segregation energy. This is the energy required to take a solute element form the bulk to the surface of the host. If segregation energy is negative, then the solute will segregate to the surface, and the second layer will be rich with host atoms. Conversely, if the

segregation energy is positive, then the surface is a pristine layer of host atoms whilst the solute atoms segregate to the subsurface layer. Thus the electronic structure of the host surface is modified both by change of geometry and the presence of a foreign atom.

A database for segregation energy of solute-host pairs was constructed (Ruban et al., 1999). It was confirmed that for a system in which platinum is a host and vanadium a solute, vanadium segregates to the subsurface layer and the surface is mainly composed of platinum atoms (Greeley and Mavrikakis, 2004).

The presence of solute atoms also perturbs the surface geometry and may cause reconstruction. There are many studies for geometric structures of pure metals (Da Silva, 2005). However, alloys are complicated, and description of their surface structures in literature is rare. DFT calculations can be used for determining surface relaxations. Such calculations are only efficient for determining the local minima. Reconstruction requires determination of global minima and is computationally expensive.

4.1.3. Adsorption of O_2 on Pt (111)

Adsorption is a process in which a chemical bond is formed between a solid surface and a molecule. Surface adsorption may induce reconstruction. On alloy surfaces, adsorption may also cause segregation of solute from the subsurface layer to the top. Pt (111) is stable in the oxygen environment and is not likely to reconstruct. Also for platinum vanadium surfaces, vanadium is stable in the subsurface layer and is not attracted to the surface by the adsorbate (Greeley and Mavrikakis, 2004).

Adsorption is always exothermic, and configurations that minimises the Gibbs free energy are preferred. Equation 4.1 can be used to calculate the adsorption energy (Eads) using total energies from DFT data:

$$E_{ads} = (E_{slab+O_2} + ZPE) - E_{slab} - (E_{o_2} + ZPE) \quad 4.1$$

where E_{slab+O_2} is the total energy of the slab with an adsorbed molecule, E_{slab} the total energy of the clean slab, E_{o_2} the total energy of the free oxygen molecule supercel and ZPE the zero point energy.

The values of adsorption energy of molecular oxygen on Pt (111) from various surface science experimental techniques are in the range 0.3-0.5 eV (See Table 4.1). Most of these values were measured at high oxygen coverage.

Table 4.1: Experimental adsorption energies of O_2 on Pt (111).

Experiment	Binding energy (eV)
Temperature programmed desorption (Parker et al., 1989)	0.38
Electron Energy Loss Spectroscopy (Steininger et al., 1982)	0.50
Thermal desorption (Gland et al., 1980)	0.30

Adsorption energy values calculated using DFT based techniques from literature surveyed vary between 0.1 to 1.95 eV (Keith et al., 2010). The computational DFT models themselves vary in the combination of calculation settings used. These include exchange and correlation functionals, supercells, energy cut-off and the basis set. Some results from these calculations are displayed in Table 4.2. The differences in the calculated values emphasise the importance of specifying calculation parameters when reporting.

Table 4.2: Calculated adsorption energies of O_2 on Pt (111)

Reference	Binding energy (eV)	
(Eichler et al., 2000)	bridge	0.72
	fcc	0.68
	hcp	0.58
(Ou et al., 2009)	bridge	0.45
	fcc	0.42
	hcp	0.34
(Sha et al., 2010)	bridge	0.41
	fcc	0.48
	hcp	0.36

4.2. Calculation details

Self-consistent DFT calculations were performed to determine the total energy of all supercells. The total energies were calculated for optimised geometries. Electronic settings determined in Chapter 2 were used. A p (2×2) surface supercell with the oxygen molecule adsorbed on the bridge, fcc and hcp sites was used. The k-points were adjusted according the unit cell volume. Vanderbilt ultrasoft

pseudopotentials (Vanderbilt, 1990) were used to model core electrons and the exchange and correlation was described by GGA PBE functional (Perdew et al., 1996).

The surface was cleaved consisting of seven layers. Three top layers were used to represent the surface and were allowed to relax while four bottom layers were used to represent the bulk material and were not allowed to relax. The slab layers were separated by vacuum gaps 12 Å thick. Dipole corrections were implemented. The alloy surface was modelled by a pure platinum host in which the second layer was replaced by vanadium atoms.

Adsorption was tested on the bridge, hcp and fcc sites. The geometry with minimum energy was considered the equilibrium geometry. Equation 4.1 was used to calculate the adsorption energy. However, zero point energy corrections were not performed. The difference between zero point energy of oxygen molecules adsorbed on pure and modified surfaces is expected to be negligible.

The oxygen molecule was modelled with a k-point mesh of $3 \times 3 \times 3$ and cut off energy of 500 eV. The cubical supercell of side length 10Å was used.

All calculations were performed used the Cambridge Serial Total Energy Programme (CASTEP) (Clark *et al*., 2005).

4.3. Results and discussion

4.3.1. The Oxygen molecule

The bond length of the model oxygen molecule was recorded in Table 4.2 and the DOS is displayed in Figure 4.1. The valence π_{2p}^{*} is partially filled and the σ_{2p}^{*} orbital above it is completely empty. Further occupation of these anti-bonding orbitals makes the oxygen bond weaker.

Table 4.3: O-O bond length in Angstroms

CASTEP	Experiment
1.238 (Å)	1.207 (Å)*

*(Lide, 2004)

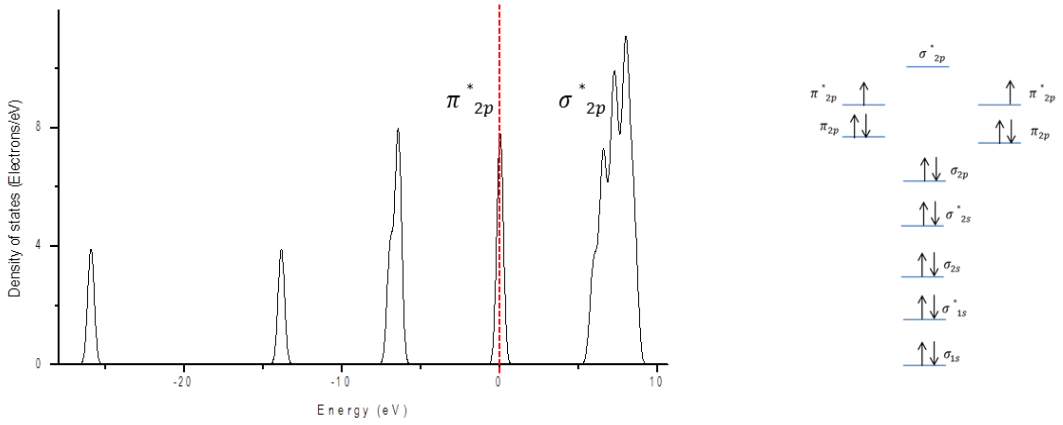

Figure 4.1: The energy levels for an oxygen molecule.

4.3.2. Pure platinum surface

Table 4.4 shows the geometrical and electronic properties of a Pt (111) surface. The surface layer show an expansion of about 1.1%, in agreement with experimental results (Somorjai and Li, 2010). The second and the third interlayer distances were found to contract. The electronic density of states for a Pt (111) surface is displayed in Figure 4.2. The main difference to the bulk platinum is the high density of electronic states for each energy level, owing to the presence of surface states. The d-band centre and width for the surface is almost equal to that of the bulk.

Table 4.4: Surface relaxation and electronic properties of Pt (111) surface. (d_1-d_2 is the vertical distance between layer I and layer 2).

Property		CASTEP (This study)	Experiment
Interlayer distance (Å)	d_1-d_2	2.326	2.30*
	d_2-d_3	2.289	
	d_3-d_4	2.285	
	bulk	2.310	2.26*
d-band centre (eV)		-1.994	
d-band width (eV)		3.050	

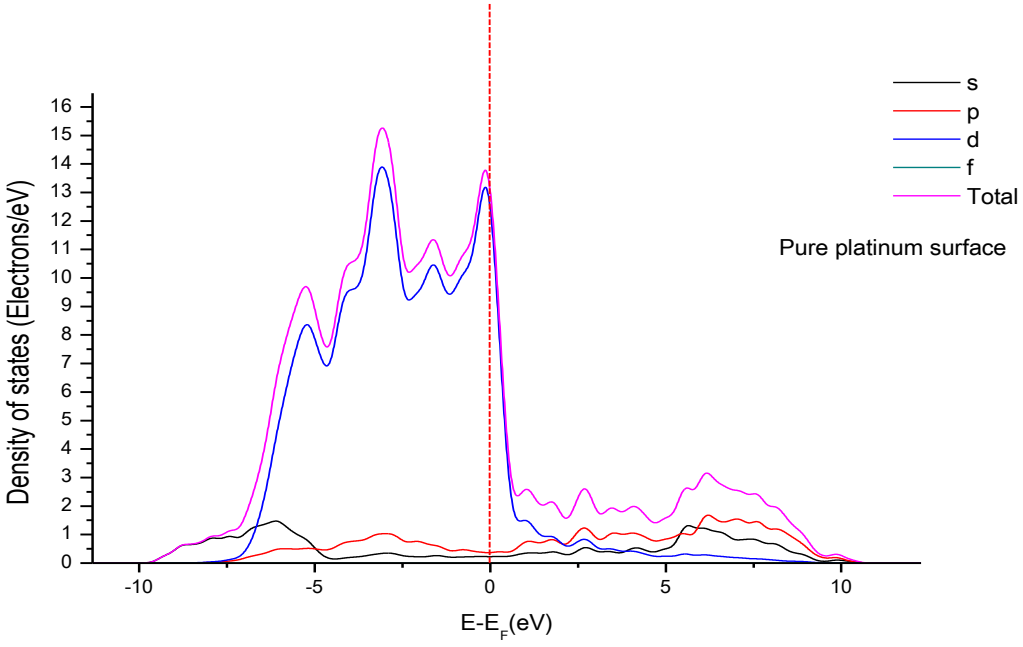

Figure 4.2: The electronic density of states for Pt (111) surface.

4.3.3. Platinum with subsurface vanadium atoms

When the subsurface layer is occupied with vanadium, the first (d_1-d_2) and the second (d_2-d_3) interlayer spacing is reduced. However, the interlayer distance between the third and the fourth layers is increased as shown in Table 4.5.

Table 4.5: Surface relaxation and electronic properties of Pt (111) with a subsurface vanadium layer. (d_1-d_2 is the vertical distance between layer I and layer 2).

Property		CASTEP	Experiment
Interlayer distance (Å)	d_1-d_2	2.076	
	d_2-d_3	2.077	
	d_3-d_4	2.396	
	bulk	2.308	
d-band centre(eV)		-3.23	
d-band width (eV)		4.35	

The density of states diagrams for platinum with a subsurface vanadium layer is displayed in Figure 4.3. The presences of solute vanadium atom cause the bandwidth of the d-band to widen, resulting in a

more negative d-band centre (see Table 4.2). The shifting of the d-band centre is caused by both the contraction of the surface layer and the presence of a foreign atom in the surface region.

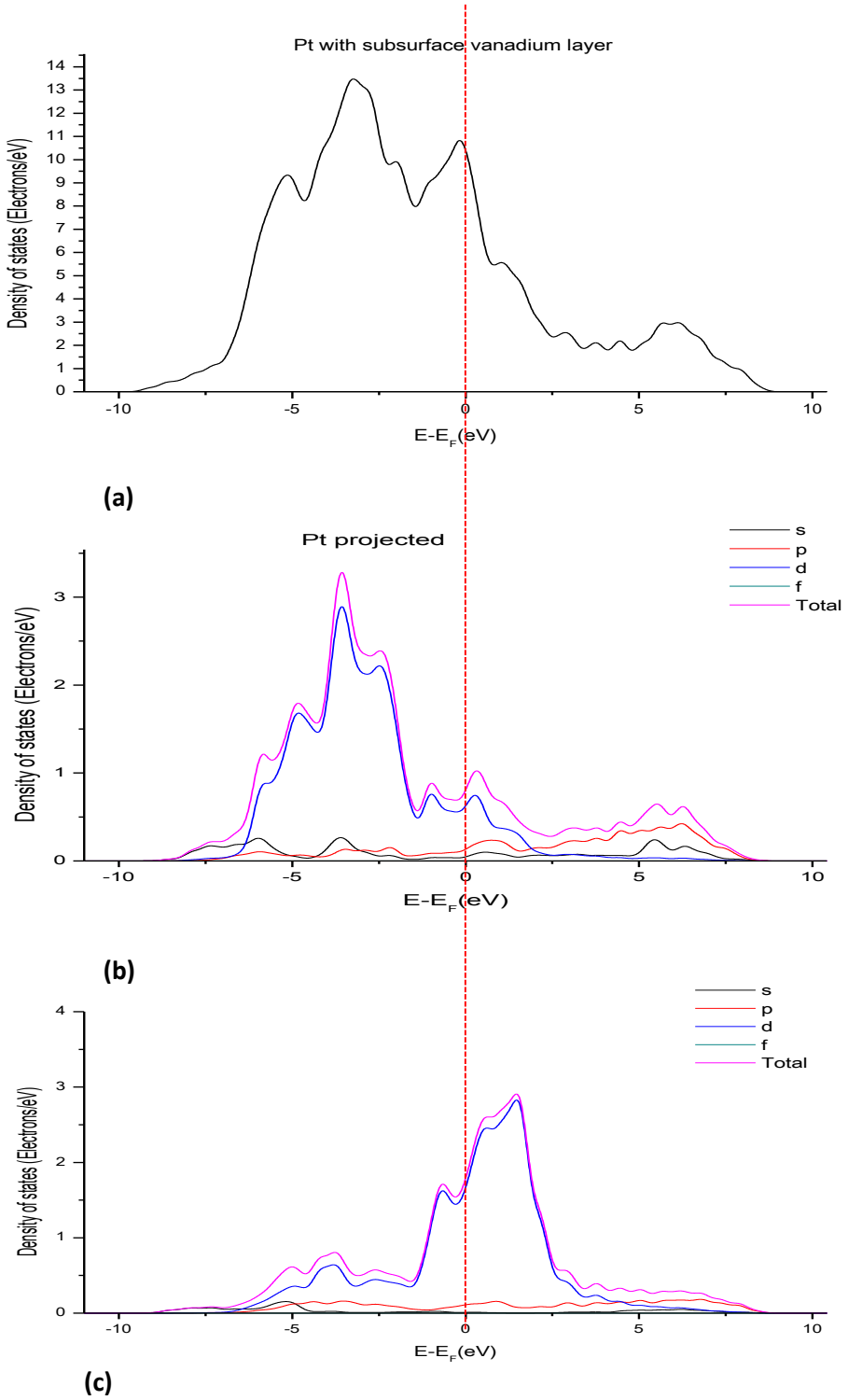

Figure 4.3: The electronic density of states for Pt (111) surface with a vanadium subsurface layer (a) total, (b) Pt-projected and (c) V-projected.

4.3.4. Adsorption of molecular oxygen on Pt (111)

Equilibrium adsorption geometries and energies for the bridge, hcp and fcc site are shown in Tables 4.3, 4.4 and 4.5 respectively. The density of states graphs for oxygen molecules adsorbed on Pt (111) are displayed in Figures 4.5, 4.6 and 4.7 for bridge, hcp and fcc sites respectively. The relationship between the equilibrium surface-molecule distances and the O-O bond length may be worth noting. It is believed the strong adsorption leads to a shorter surface molecule bond and a weaker and longer O-O bond (Xin et al., 2012).

The bridge oxygen molecule is bound to the surface by two covalent bonds 2.056Å above the surface. The O-O bond on the bridge site is 1.36 and the adsorption energy is -1.81 eV.

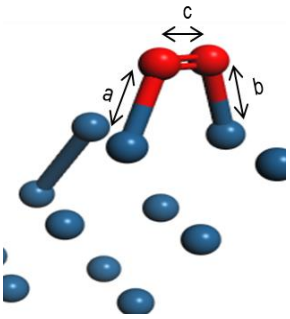

Figure 4.4: Geometry of O_2 adsorbed on the bridge site.

Table 4.6: Geometry and adsorption energy for an oxygen molecule adsorbed on the bridge site

Adsorption geometry	Bond length (Å)	
	a	2.056
	b	2.056
	c	1.360
Adsorption energy (eV)		-1.81

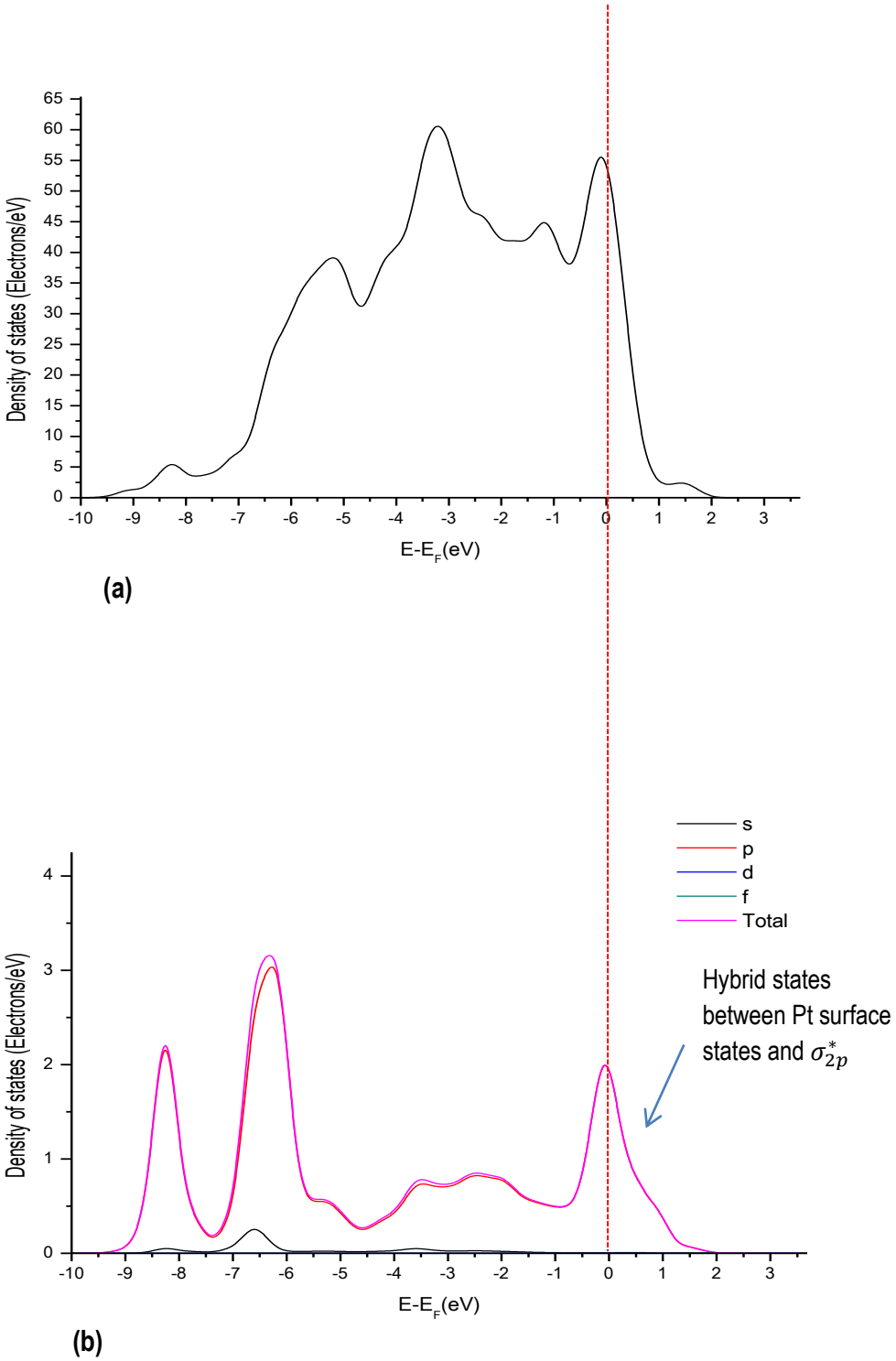

Figure 4.5: The electronic density of states for Pt (111) surface with an adsorbed oxygen molecule on the bridge site (a) total and (b) O_2 projected.

The geometry of the hcp oxygen molecule is shown in Figure 4.5. The equilibrium O-O bond for this site is 1.372Å. Bond lengths and adsorption energy is shown in Table 4.7.

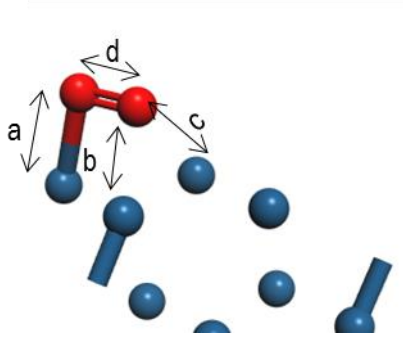

Figure 4.6: Geometry of an oxygen molecule bound on the hcp site.

Table 4.7: Geometry and adsorption energy for an oxygen molecule adsorbed on the hcp site

Adsorption geometry	Bond length (Å)	
	a	2.082
	b	2.256
	c	2.256
	d	1.372
Adsorption energy (eV)		-1.78

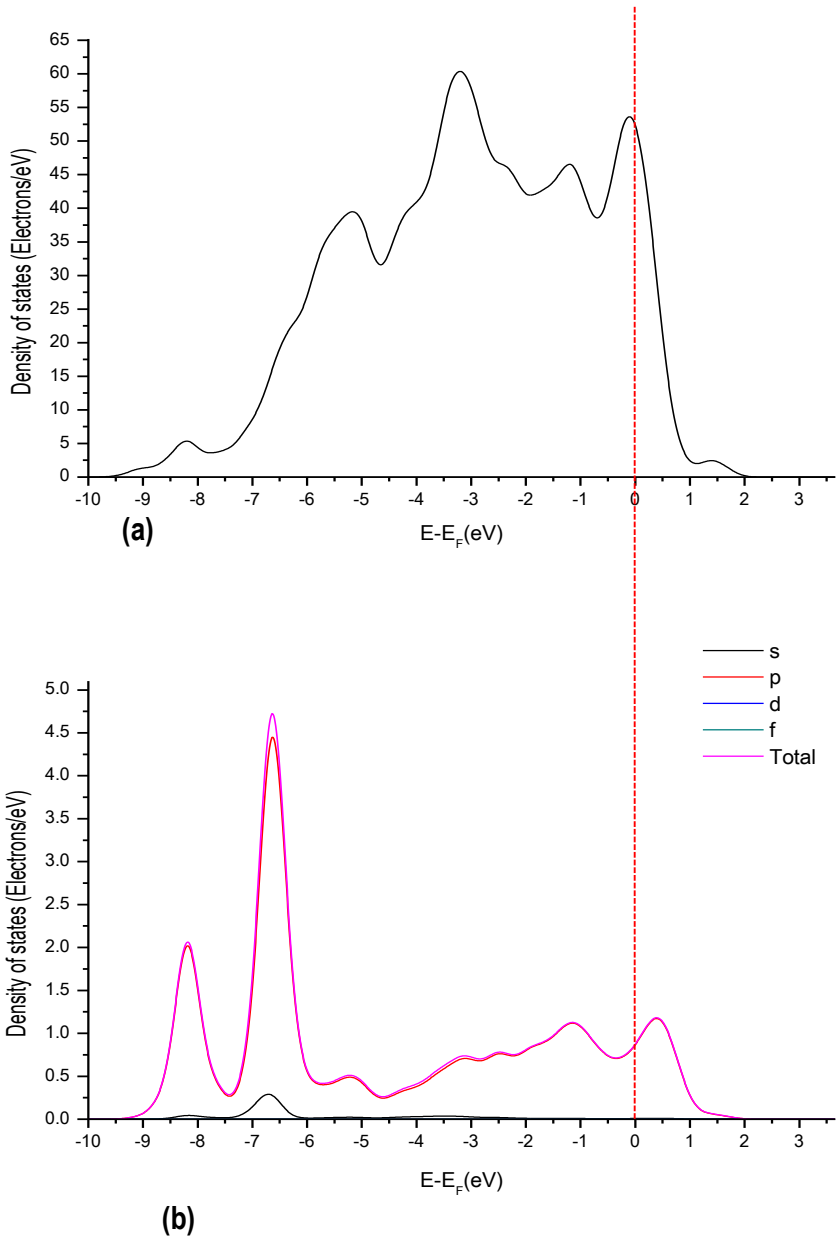

Figure 4.7: The electronic density of states for Pt (111) surface with an adsorbed oxygen molecule on the hcp site (a) total and (b) O_2 projected.

The equilibrium geometry of an oxygen molecule adsorbed on the fcc site is displayed in Figure 4.8. The bond lengths are recorded in Table 4.8. The adsorption energy of the fcc site is -1.91eV is the most stable configuration.

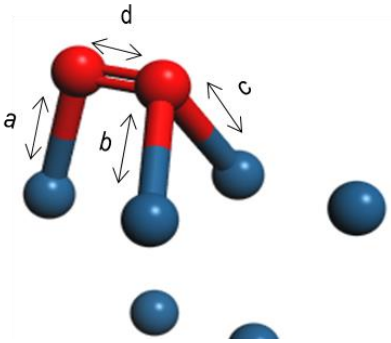

Figure 4.8: Geometry of an oxygen molecule bound on the fcc site.

Table 4.8: Geometry and adsorption energy for an oxygen molecule adsorbed on the fcc site

Adsorption geometry	Bond length (Å)	
	a	2.063
	b	2.200
	c	2.200
	d	1.385
Adsorption energy (eV)		-1.91

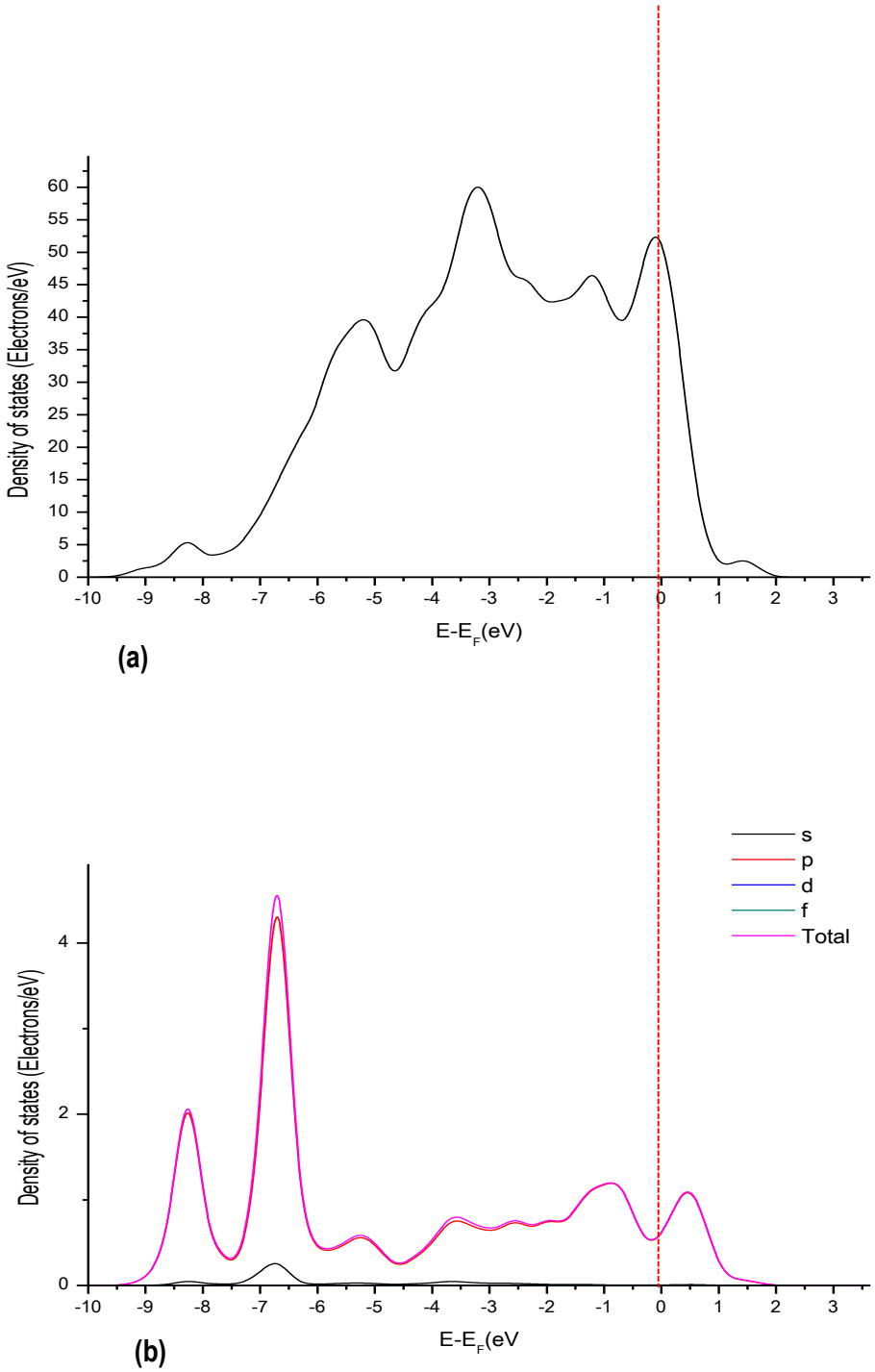

Figure 4.9: The electronic density of states for Pt (111) surface with an adsorbed oxygen molecule on the fcc site (a) total and (b) O_2 projected.

4.3.5. Adsorption of molecular oxygen on Pt (111) with a vanadium subsurface layer

The adsorption geometries and energies for and oxygen molecule adsorbed on a Pt (111) surface with subsurface vanadium atoms is shown in Tables 4.9, 4.10 and 4.11 for the bridge, hcp and fcc sites respectively. The density of states graphs are displayed in Figures 4.10 to 4.12. The fcc has the weakest adsorption energy, followed by the bridge site and the hcp site is the most stable. The adsorption energies range from -1.37 eV for the fcc to -1.45 for the hcp site. The adsorption energies for platinum surface with subsurface vanadium solute are lower than those of pure platinum and the surface-molecule bonds are longer.

The surface-molecule bonds of the Pt (111) surface perturbed by subsurface vanadium atoms for the bridge site are 0.148Å longer compared to a molecule on a pure Pt (111) surface. The O-O bond length for the platinum with vanadium surface is 1.349Å, compared to 1.360Å for a pure surface. The adsorption energy for the modified surface is -1.43eV, which is lower than that of a pure surface, -1.81eV.

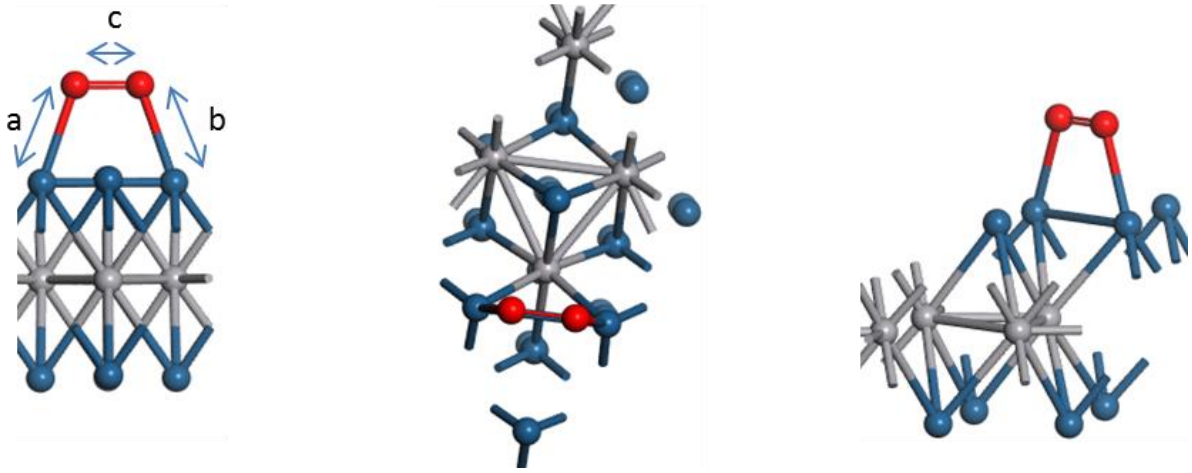

Figure 4.10: Geometry of an oxygen molecule bound on the bridge site of a Pt (111) surface with subsurface vanadium atoms.

Table 4.9: Geometry and adsorption energy for an oxygen molecule adsorbed on the bridge site

Adsorption geometry	Bond length (Å)	
	a	2.204
	b	2.204
	c	1.349
Adsorption energy (eV)		-1.43

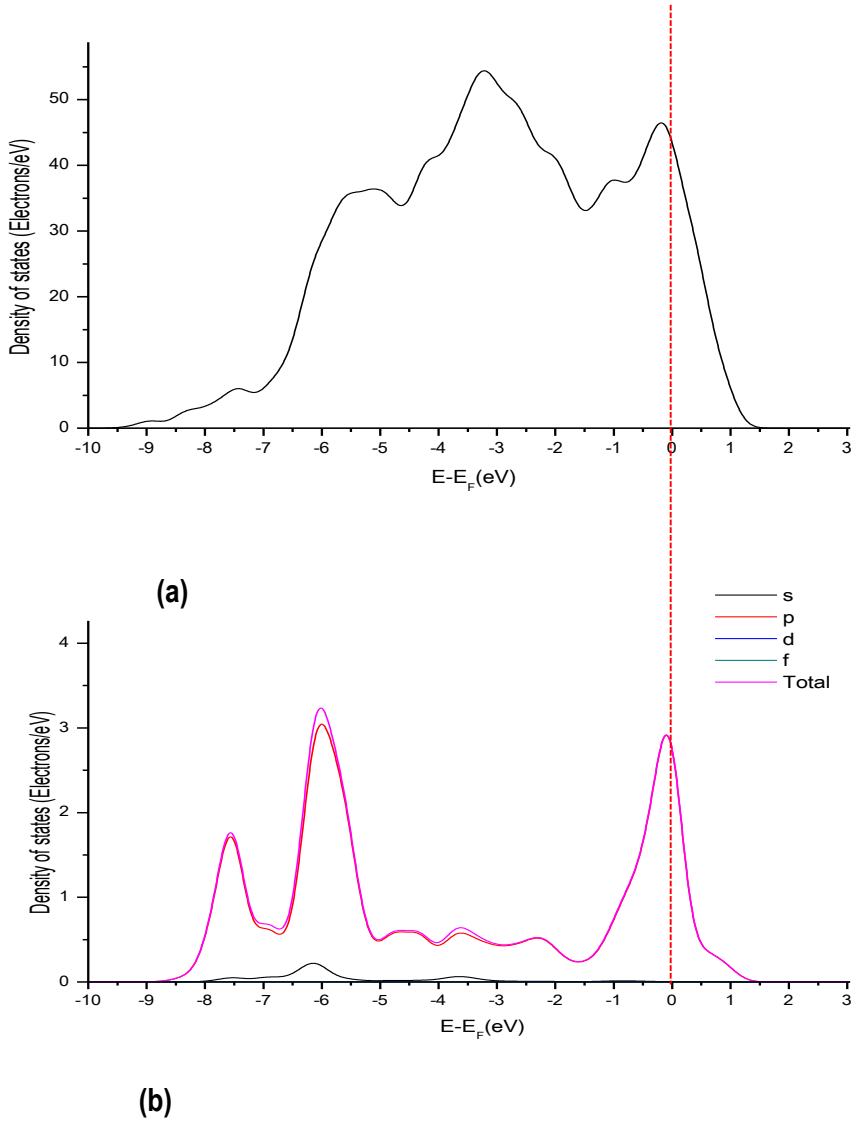

Figure 4.11: The electronic density of states for Pt (111) with a subsurface vanadium layer plus an adsorbed oxygen molecule on the bridge site (a) total and (b) O_2 projected.

Comparing the modified surface with the pure Pt (111) surface at the hcp site, the surface molecule bonds are 2.18Å, 2.40Å and 2.40Å compared to 2.08Å, 2.25Å and 2.25Å respectively for the pure Pt (111) surface. The O-O bond for the modified surface is 1.370Å, and 1.372Å for the pure surface. The adsorption energy is -1.45eV for the modified surface and -1.78eV for a pure surface.

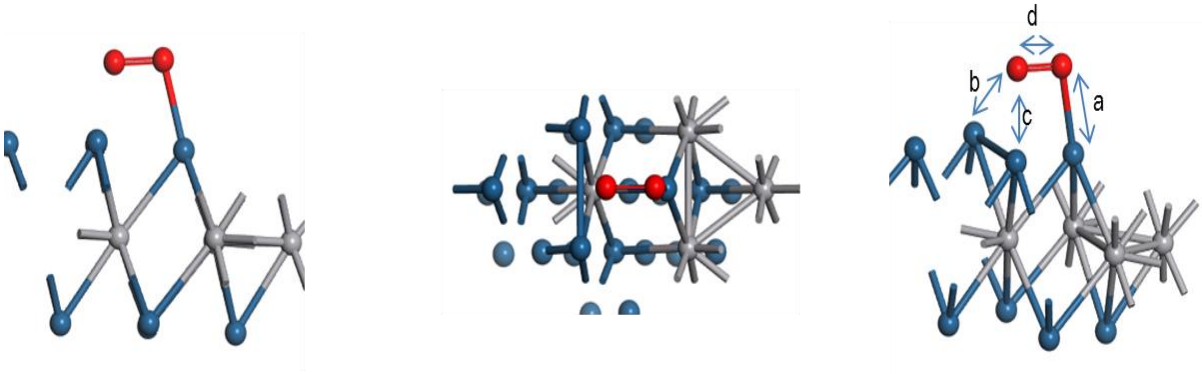

Figure 4.12: Geometry of an oxygen molecule bound on the hcp site of a Pt (111) surface with subsurface vanadium atoms.

Table 4.10: Geometry and adsorption energy for an oxygen molecule adsorbed on the hcp site

Adsorption geometry	Bond length (Å)	
	a	2.18
	b	2.40
	c	2.40
	d	1.37
Adsorption energy (eV)		-1.45

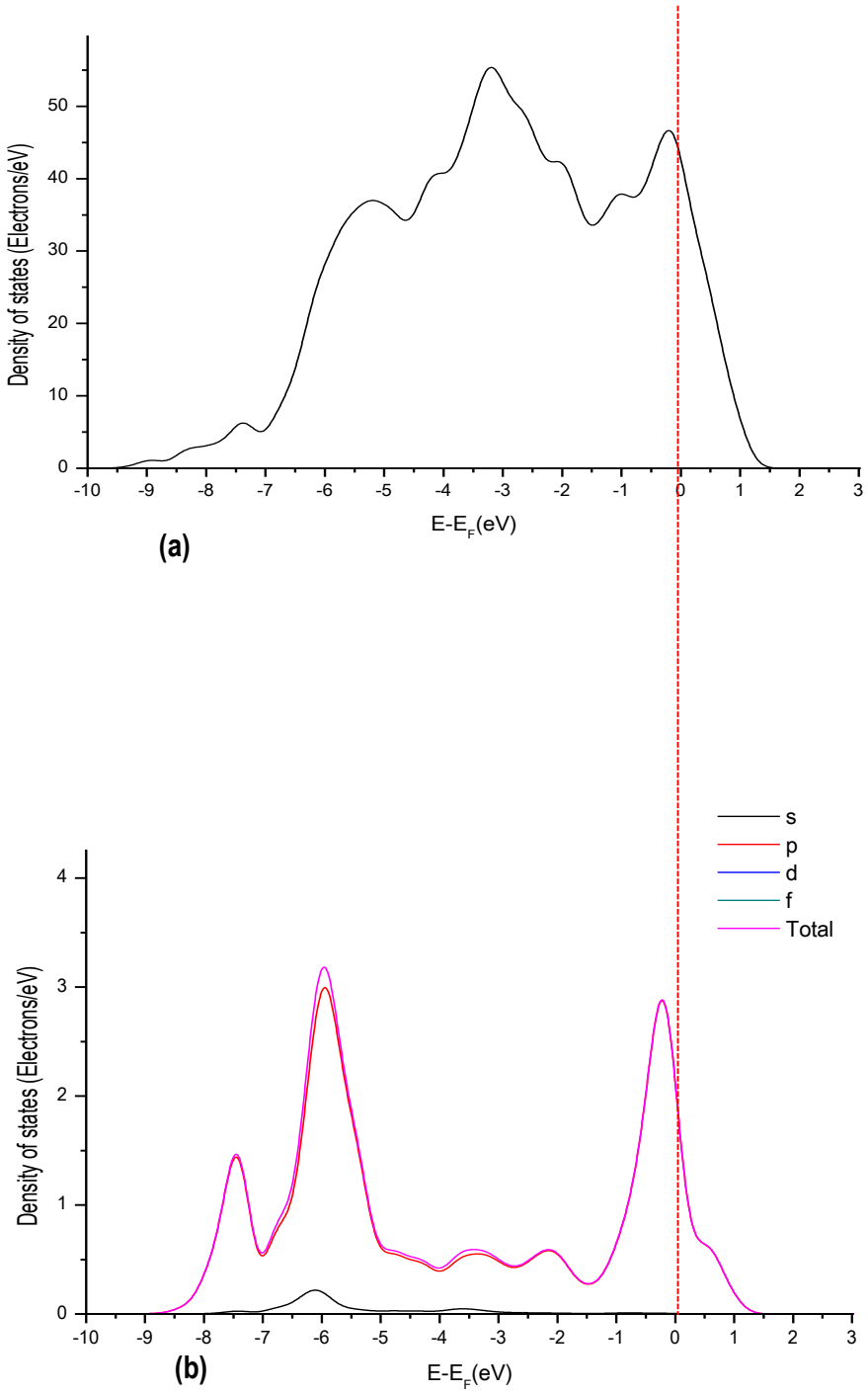

Figure 4.13: The electronic density of states for Pt (111) surface containing a vanadium subsurface layer and an adsorbed oxygen molecule on the hcp site (a) total and (b) O_2 projected.

The surface-molecule bonds for the fcc site were increased from 2.06Å, 2.20Å and 2.20Å on pure Pt (111) to 2.179, 2.468 and 1.395 on a surface modified by vanadium atoms respectively. The O-O bond changed from 2.385 on a pure surface to 2.366 on a modified surface. The adsorption energy changed from -1.91 eV on pure Pt (111) to -1.37 on modified Pt (111).

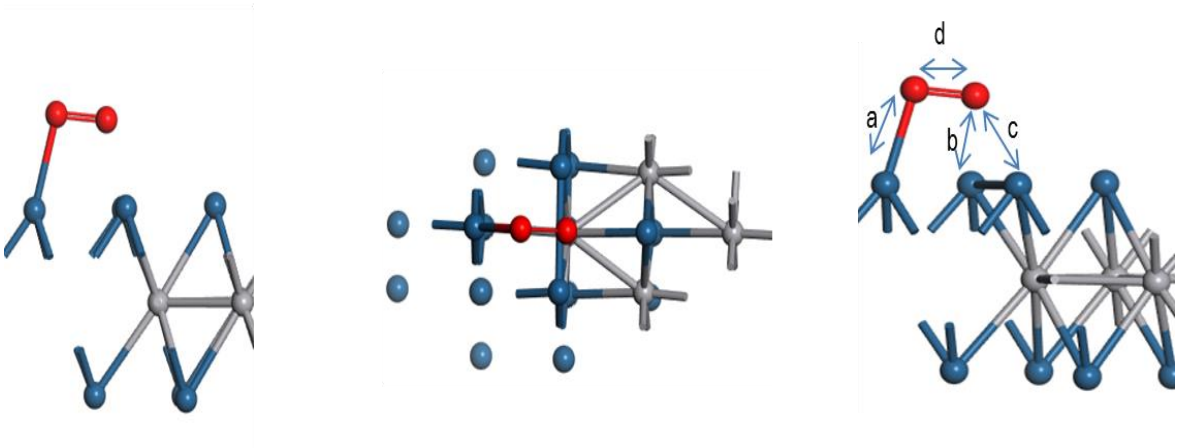

Figure 4.14: The geometry of O_2 on the fcc site of Pt (111) containing subsurface Vanadium atoms.

Table 4.11: Geometry and adsorption energy for an oxygen molecule adsorbed on the fcc site

Adsorption geometry	Bond length (Å)	
	a	2.179
	b	2.468
	c	2.395
	d	1.366
Adsorption energy (eV)		-1.37

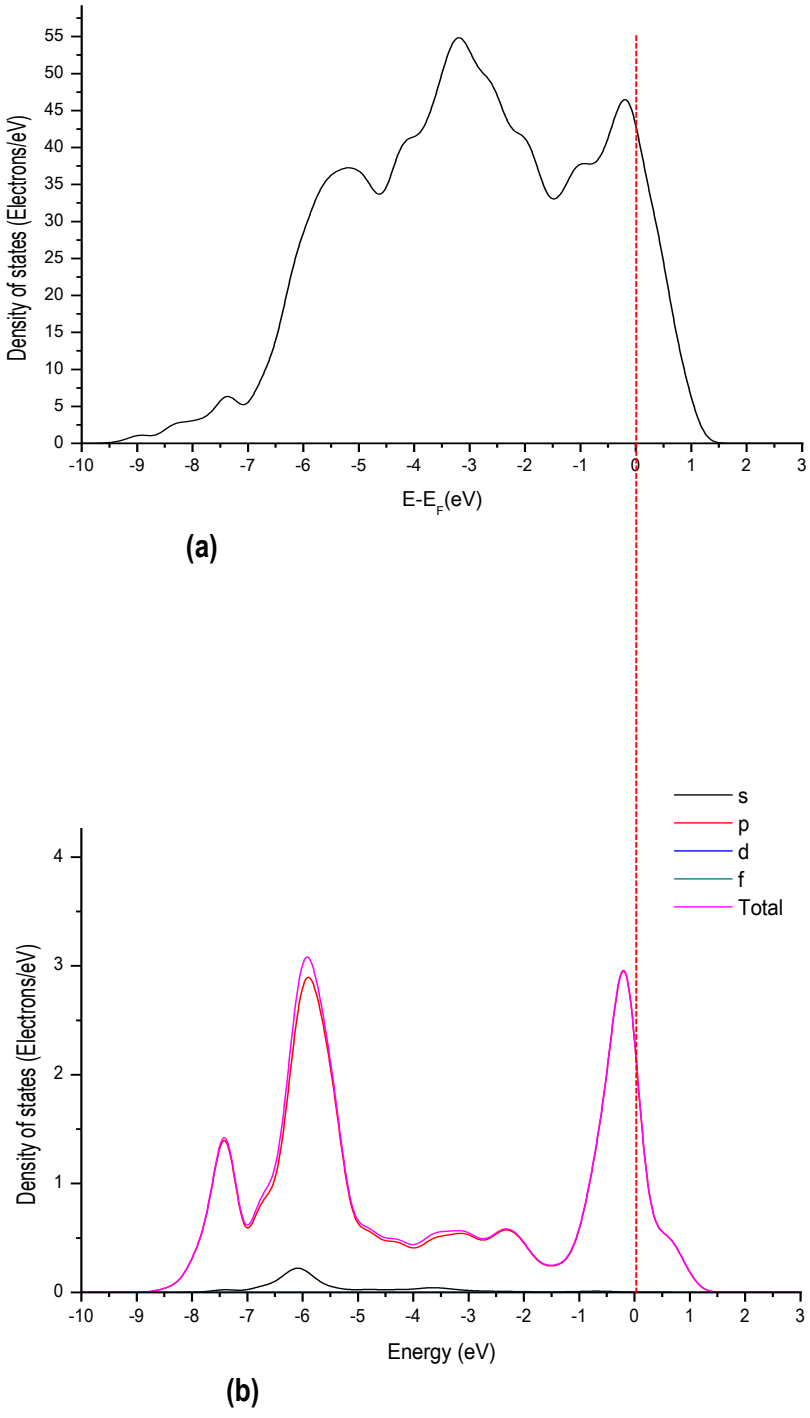

Figure 4.15: The electronic density of states for Pt (111) with a subsurface vanadium layer plus an adsorbed oxygen molecule on the fcc site (a) total and (b) O_2 projected.

4.4. Summary and conclusion

When vanadium atoms are added into the subsurface layer, both the geometrical and electronic structures are modified. A pure Pt (111) does not reconstruct at lower temperatures, but present calculations have confirmed that it relaxes by expanding the top interlayer distance and contracting the distance between the second and the third layers. Adding vanadium to the second layer causes contraction of the distance between both the topmost and the second layer and the second and the third layers.

The resulting modification of the electronic structure is a result of both change in geometry and hybridisation between platinum and vanadium atoms. Hybridisation brings more unoccupied d-orbitals to the platinum structure. The d-band width is widened and the d-band centre is stabilised from a value of -1.99 to -3.22eV.

Also, the presence of vanadium in the subsurface region of a Pt (111) surface repels adsorbed oxygen molecules. Surface-molecule bonds on a modified surface are longer compered to bonds on pure Pt (111) surface, and the adsorption energies is lower on modified compared to pure surfaces. For a pure platinum surface, adsorption is favoured at the fcc site with an adsorption energy of -1.91 eV. The adsorption energies for the bridge and the hcp site are -1.81 and -1.78 eV respectively. On a surface containing subsurface vanadium atoms, the adsorption energy is lower than that of pure platinum. For platinum with vanadium surfaces, the hcp site is the most stable, and the fcc has the weakest binding.

CHAPTER 5

SUMMARY AND CONCLUDING REMARKS

Model platinum vanadium alloys and their surfaces were created by using a Density Functional Theory method implemented in the CASTEP code. The accuracy of the models was tested by comparing their equilibrium lattice parameters and relative phase stability with experimental values reported in the literature. Lastly, model surfaces were used to investigate the effect of putting vanadium atoms into the subsurface region of platinum on its chemisorption and hence catalytic properties.

5.1 Electronic structure of Platinum-Vanadium alloys

DFT total energies of various bcc, fcc, and hcp Pt-V superstructures were used to calculate and compare formation energies. All experimentally determined ordered Pt-V phase had the most negative calculated formation energies, showing that these structures are the real stable geometries, not frozen quasistable structures.

The calculated DOS for Pt-V alloys show hybridisation between platinum and vanadium atoms. The pure platinum valence band is almost fully occupied, with few empty d-states. Hybridisation between platinum and vanadium brings in more empty d-states to the Pt PDOS. The number of empty valence d-states increase with concentration of vanadium atoms.

The first moment of the d-band was used to represent the d-band centre. Pt PDOS d-band centres were calculated. The values of the d-bands centre became more stabilised (more negative) as the concentration of vanadium increased (Figure 3.16). Thus alloys can be used to engineer and modify electronic properties of other metals, platinum in this case.

5.2 Pt (111) modified with subsurface vanadium atoms

Subsurface solute vanadium atoms modify both the geometric and electronic structures of the surface. A pure Pt (111) surface relaxes by expanding its topmost interlayer distance. However, when the second layer is occupied with vanadium atoms, the first topmost and the second interlayer distances contract. Calculations to determine whether the surface will not reconstruct were not performed.

Hybridisation between vanadium and platinum creates more empty states in the valence band of Pt PDOS. The d-band width is widened and the d-band centre lowered. An oxygen molecule on the

surface is repelled by the presence of subsurface vanadium atoms. Surface-molecule bonds increase and the adsorption energy is lowered.

5.3 The effect of alloying platinum catalysts with vanadium

It was shown in this study that presence of vanadium in the surface region of Pt (111) causes it to bind an oxygen molecule less strongly. However, as highlighted in Chapter 1, catalysis involves a number of processes and several adsorbed intermediates. To fully understand the effect of alloying on the catalysts, a detailed study of interaction of modified surface with all intermediates is needed.

Appendix A

Table A 1: Convergence of total energy with respect to the number of irreducible k-points for pure platinum. The cut off energy was maintained at 600$\boldsymbol{eV}$.

Irreducible k-points	Energy difference ($\boldsymbol{meV}$)					
	LDA	GGA PBE	GGA RPBE	GGA PW91	GGA WC	GGA PBESOL
56	14.5041	16.82112	17.00611	15.9019	16.74901	17.25717
84	8.66447	9.11331	9.12399	8.9882	9.11233	9.11494
120	2.59087	1.16187	0.99007	1.77148	1.27531	0.88828
165	0.33982	1.66154	1.81503	1.10258	1.55876	1.87291
220	1.59991	1.93809	1.93644	1.84657	1.944	1.94242
286	1.50287	1.17244	1.07004	1.37873	1.2467	1.06165
364						0

Table A2: Convergence of total energy with respect to the number cut off energy for pure platinum. The number of irreducible k-point was maintained at 120.

Cut-off energy (eV)	Energy difference (eV) Energy difference ($\boldsymbol{meV}$)					
	LDA	GGA PBE	GGA RPBE	GGA PW91	GGA WC	GGA PBESOL
300	36.20143	35.681	35.05411	38.9772	37.39477	36.91032
400	2.66778	3.41919	4.33265	2.80699	2.71469	3.1124
500	0.79685	1.29798	1.30916	0.92674	1.3681	1.43159
600	1.05113	1.06415	1.03473	0.81583	1.13989	1.12501
700	0.67664	0.66168	0.62086	0.79654	0.66973	0.60085
800	0.94517	0.91286	0.80146	0.9116	0.90605	0.76588
900	0.70984	0.7963	0.75038	0.75215	0.75686	0.67913
1000						

Table A3: Convergence of total energy with respect to the number of irreducible k-points for pure vanadium. The cut off energy was maintained at 600$\boldsymbol{eV}$.

Irreducible k-points	Energy difference Energy difference(meV)					
	LDA	GGA PBE	GGA RPBE	GGA PW91	GGA WC	GGA PBESOL
20	8.247	9.883	10.347	10.668	10.952	7.931
35	0.004	1.379	1.662	1.732	0.767	0.287
56	2.242	1.612	1.56	1.649	2.634	1.95
84	1.72	1.963	2.03	2.112	1.977	1.831
120	0.328	0.722	0.779	0.87	0.583	0.374
165	0.587	0.406	0.373	0.324	0.48	0.569
220	0.501	0.473	0.459	0.453	0.51	0.53
286	0.186	0.203	0.191	0.198	0.242	0.251
364	0.017	0.039	0.034	0.045	0.055	
455						

Table A4: Convergence of total energy with respect to the number cut off energy for pure platinum. The number of irreducible k-point was maintained at 120.

Cut-off energy (eV)	Energy difference(meV)					
	LDA	GGA PBE	GGA RPBE	GGA PW91	GGA WC	GGA PBESOL
300	23.519	20.149	24.667	17.415	18.033	25.891
400	1.714	1.488	1.539	5.601	0.919	1.701
500	2.576	1.768	1.818	0.354	2.357	2.165
600	3.919	3.806	3.758	4.207	3.841	3.461
700	1.839	1.628	1.688	2.399	1.785	1.536
800	0.005	0.883	0.807	0.771	1.726	1.186
900	1.09	1.089	1.037	1.044	1.15	1.843
1000						

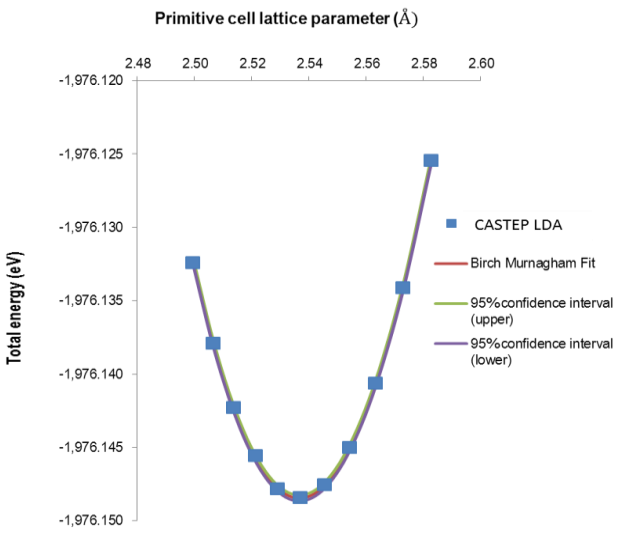
Primitive cell lattice parameter (Å)
2.48 2.50 2.52 2.54 2.56 2.58 2.60
-1,976.120
-1,976.125
-1,976.130
-1,976.135
-1,976.140
-1,976.145
-1,976.150
Total energy (eV)
CASTEP LDA
Birch Murnagham Fit
95%confidence interval (upper)
95%confidence interval (lower)

(a)

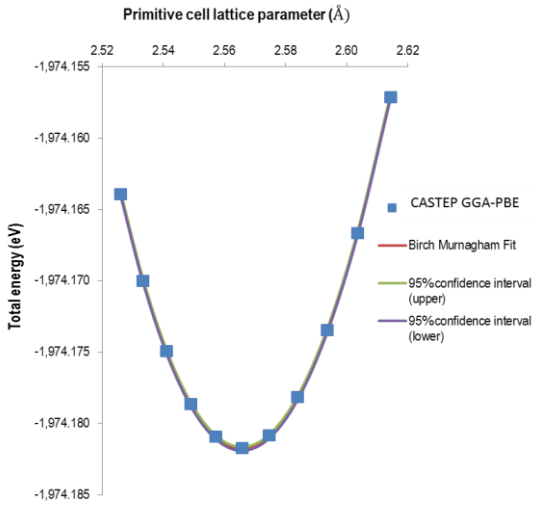
Primitive cell lattice parameter (Å)
2.52 2.54 2.56 2.58 2.60 2.62
-1,974.155
-1,974.160
-1,974.165
-1,974.170
-1,974.175
-1,974.180
-1,974.185
Total energy (eV)
CASTEP GGA-PBE
Birch Murnagham Fit
95%confidence interval (upper)
95%confidence interval (lower)

(b)

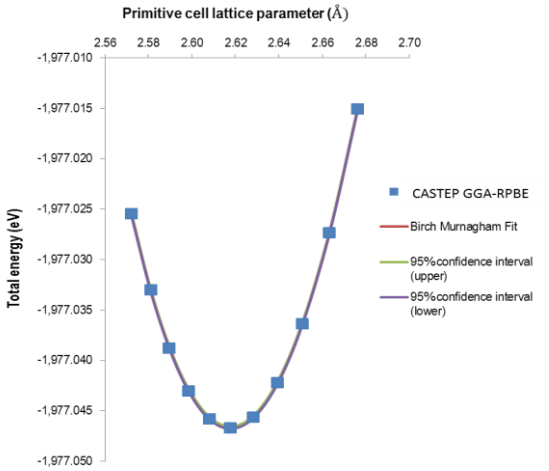
Primitive cell lattice parameter (Å)
2.56 2.58 2.60 2.62 2.64 2.66 2.68 2.70
-1,977.010
-1,977.015
-1,977.020
-1,977.025
-1,977.030
-1,977.035
-1,977.040
-1,977.045
-1,977.050
Total energy (eV)
CASTEP GGA-RPBE
Birch Murnagham Fit
95%confidence interval (upper)
95%confidence interval (lower)

(c)

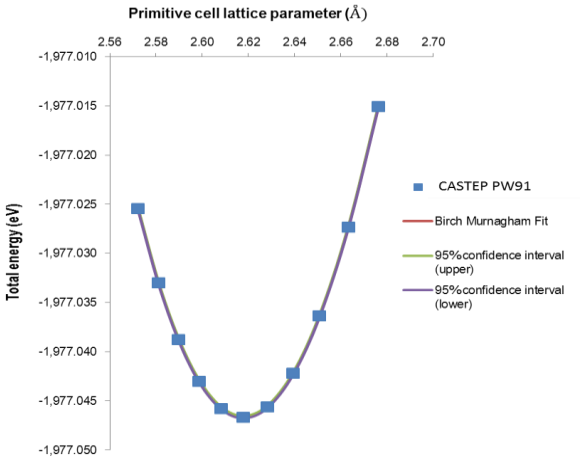
Primitive cell lattice parameter (Å)
2.56 2.58 2.60 2.62 2.64 2.66 2.68 2.70
-1,977.010
-1,977.015
-1,977.020
-1,977.025
-1,977.030
-1,977.035
-1,977.040
-1,977.045
-1,977.050
Total energy (eV)
CASTEP PW91
Birch Murnagham Fit
95%confidence interval (upper)
95%confidence interval (lower)

(d)

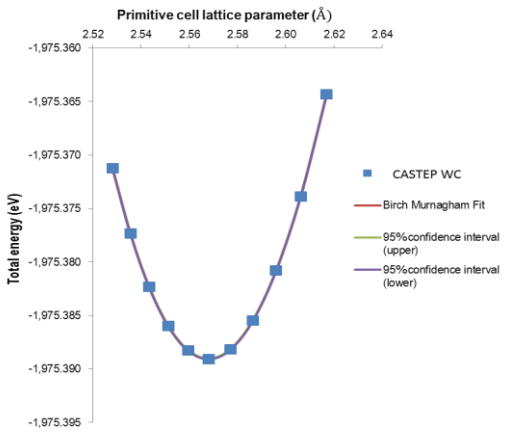
Primitive cell lattice parameter (Å)
2.52 2.54 2.56 2.58 2.60 2.62 2.64
-1,975.360
-1,975.365
-1,975.370
-1,975.375
-1,975.380
-1,975.385
-1,975.390
-1,975.395
Total energy (eV)
CASTEP WC
Birch Murnagham Fit
95%confidence interval (upper)
95%confidence interval (lower)

(e)

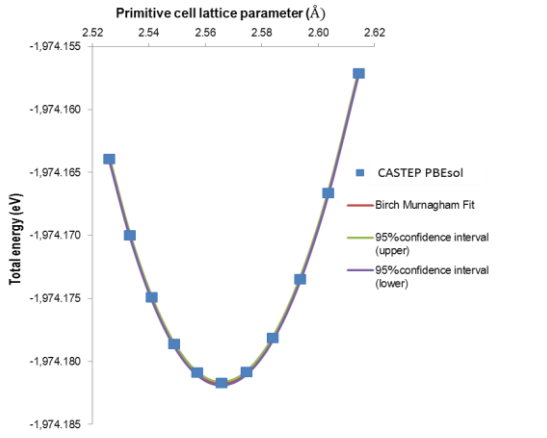
Primitive cell lattice parameter (Å)
2.52 2.54 2.56 2.58 2.60 2.62
-1,974.155
-1,974.160
-1,974.165
-1,974.170
-1,974.175
-1,974.180
-1,974.185
Total energy (eV)
CASTEP PBEsol
Birch Murnagham Fit
95%confidence interval (upper)
95%confidence interval (lower)

(f)

Figure A1: Birch Murnaghan fit for (a) LDA, (b) GGA PBE, (c) GGA RPBE, (d) GGA PW91, (e) GGA WC and (d) GGA PBEsol data for platinum

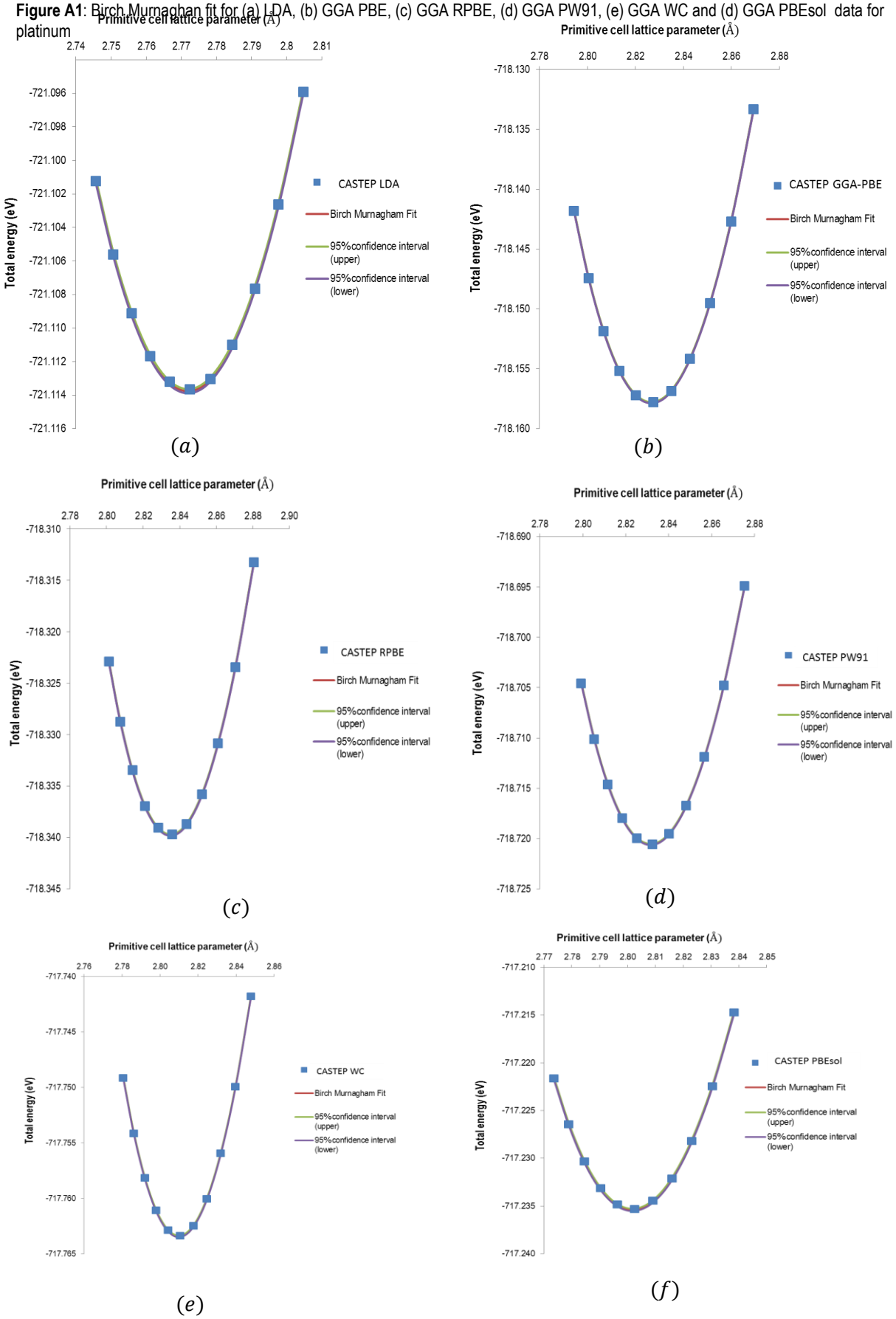

TaFigure A2: Birch Murnaghan fit for (a) LDA, (b) GGA PBE, (c) GGA RPBE, (d) GGA PW91, (e) GGA WC and (d) GGA PBEsol data for waplatinum

Irreducible k-points	Energy difference					
	LDA	GGA PBE	GGA RPBE	GGA PW91	GGA WC	GGA PBESOL
32	29.8282	29.9078	30.0236	30.0568	29.8616	29.8112
41	7.58	6.2854	6.0362	5.9946	6.8548	7.431
50	5.7528	4.9658	4.9158	4.7058	5.2714	5.6496
72	12.0426	5.0392	5.0108	4.92336	5.164	5.2742
98	6.9814	0.0088	0.091	0.08956	0.1588	0.2742
113	0.4506	5.1562	5.3624	5.35	4.8058	4.5694
256	4.7248	7.7278	7.7762	7.829	7.5658	7.4094
289	7.5736	4.873	4.8934	4.9514	4.6984	4.554
361	4.6698	0.3176	0.4644	0.3774		0.0366
441						

Table A6: Convergence of total energy with respect to the number cut off energy for a pure platinum surface. The number of irreducible k-points was maintained at 120.

	Energy difference					
Irreducible k-points	LDA	GGA PBE	GGA RPBE	GGA PW91	GGA WC	GGA PBESOL
300	43.9954	40.8702	51.2212	30.504	33.0982	38.0454
400	0.1002	2.104	2.7892	0.6716	4.1542	2.002
500	2.5822	2.1608	2.3552	3.4598	3.2176	2.6106
600	3.197	2.6304	2.479	4.0376	2.6096	2.259
700	1.7314	1.4054	1.38896	1.467	1.1794	1.3084
800	0.0248	0.367	0.07156	0.3678	0.8404	0.5678
900	1.7148	2.0754	2.052	0.9734	2.0042	1.9642
1000						

Table A7: Convergence of total energy with respect to the vacuum layer thickness.

Vacuum thickness (Å)	Energy difference (eV)					
4	184.94	113.56	70.76	119.99	151.2254	153.41
6	4.62	3.34	1.36	11.31	1.48492	1.93
8	1.77	0.33	2.84	3.31	2.85369	2.32
10	1.96	4.23	3.44	4.15	3.22554	4.81
12	4.44	8.70	0.06	8.13	1.72338	6.52
14	4.16	8.16	3.99	4.81	2.62623	5.99
16	1.32	4.29	0.88	3.07	1.83145	2.36
18	0.93	1.72	4.15	2.94	4.43613	0.80
20	0	0	0	0	0	0

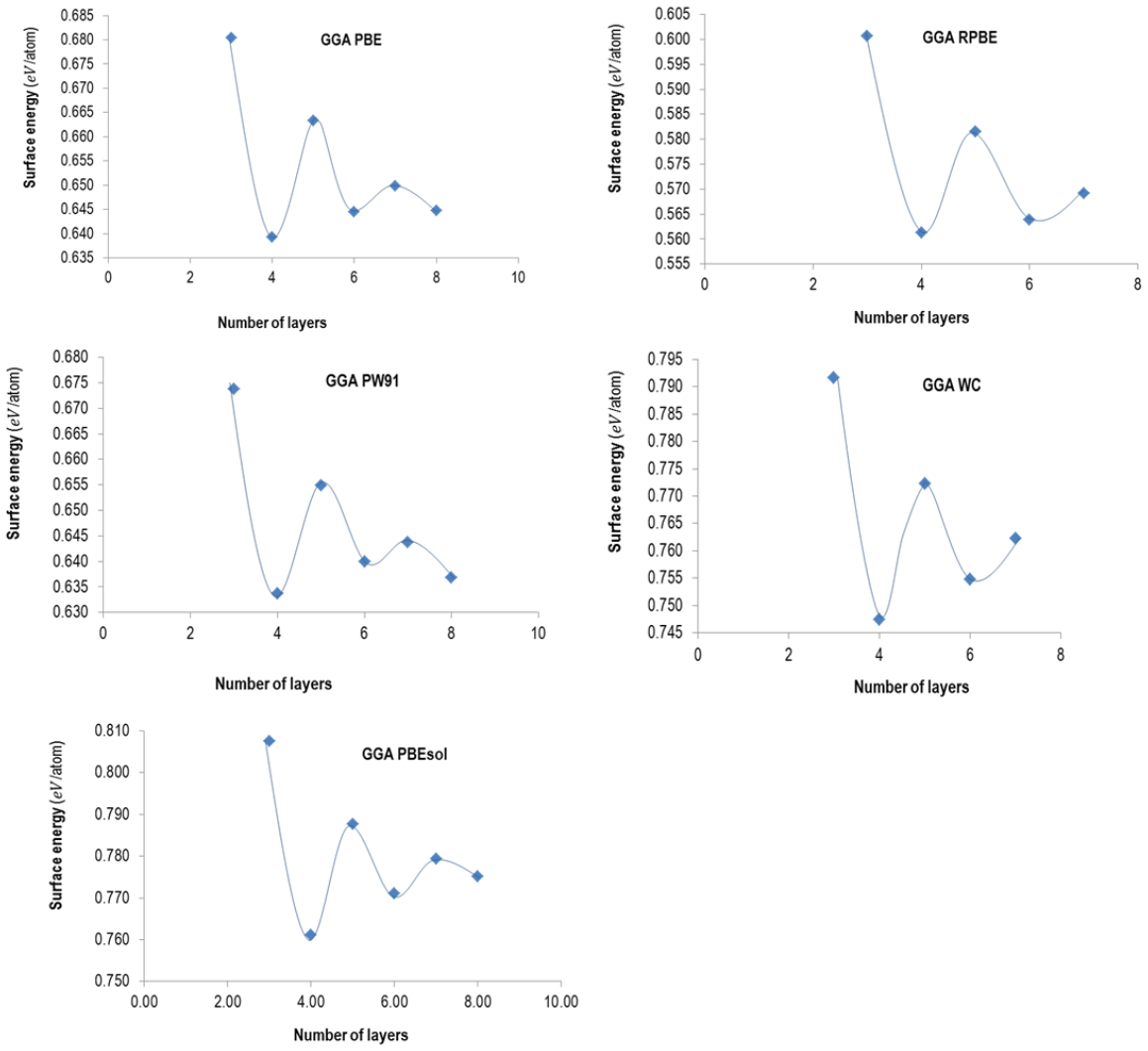

Figure A3: Convergence of surface energy with respect to the number of slab layers

Table A8: Surface interlayer relaxations

No. of Layers	Interlayer relaxation (PBE)		
	Bulk	Surface $_{3-2}$	Surface $_{2-1}$
3		2.325	2.325
4	2.308	2.284	2.318
5	2.308	2.293	2.333
6	2.308	2.337	2.301
7	2.308	2.285	2.322
8	2.308	2.290	2.325

No. of Layers	Interlayer relaxation (RPBE)		
	Bulk	Surface $_{3-2}$	Surface $_{2-1}$
3		2.330	2.331
4	2.316	2.295	2.330
5	2.316	2.300	2.340
6	2.316	2.301	2.342
7	2.316	2.291	2.330

No. of Layers	Interlayer relaxation (PW91)		
	Bulk	Surface $_{3-2}$	Surface $_{2-1}$
3		2.312	2.335
4	2.313	2.280	2.317
5	2.313	2.305	2.339
6	2.313	2.297	2.338
7	2.313	2.286	2.326
8	2.313	2.316	2.314

No. of Layers	Interlayer relaxation (WC)		
	Bulk	Surface $_{3-2}$	Surface $_{2-1}$
3		2.306	2.306
4	2.295	2.271	2.300
5	2.295	2.272	2.310
6	2.295	2.284	2.315
7	2.295	2.278	2.309

No. of Layers	Interlayer relaxation (PBEsol)		
	Bulk	Surface $_{3-2}$	Surface $_{2-1}$
3		2.301	2.301
4	2.289	2.263	2.293
5	2.289	2.266	2.302
6	2.289	2.283	2.310
7	2.289	2.278	2.305
8	2.289	2.278	2.306

References

ADAMS, C. 2009. Applied Catalysis: A Predictive Socioeconomic History. *Topics in Catalysis,* 52**,** 924-934.

ANDERSON, P. W. 1961. Localized magnetic states in metals. *Physical Review,* 124**,** 41.

ASHCROFT, N. & MERMIN, N. 1976. Solid State PhysicsHolt-Saunders. *New York***,** 4.

ATKINS, P. 1998. Physical Chemistry. 6th. Oxford University Press.

ATKINS, P. 2006. Paula J. Atkins' Physical Chemistry. Oxford, New York: Oxford University Press.

BASHYAM, R. & ZELENAY, P. 2006. A class of non-precious metal composite catalysts for fuel cells. *Nature,* 443**,** 63-66.

BECKE, A. D. 1988. Density-functional exchange-energy approximation with correct asymptotic behavior. *Physical Review A,* 38**,** 3098.

BIRCH, F. 1947. Finite elastic strain of cubic crystals. *Physical Review,* 71**,** 809.

BLIGAARD, T. & NØRSKOV, J. K. 2007. Ligand effects in heterogeneous catalysis and electrochemistry. *Electrochimica Acta,* 52**,** 5512-5516.

BØGH, E. & STENSGAARD, I. 1978. Surface relaxation of Pt (111) investigated by ion scattering. *Physics Letters A,* 65**,** 357-359.

CEPERLEY, D. M. & ALDER, B. 1980. Ground state of the electron gas by a stochastic method. *Physical Review Letters,* 45**,** 566.

CHORKENDORFF, I. & NIEMANTSVERDRIET, J. W. 2006. *Concepts of modern catalysis and kinetics*, John Wiley & Sons.

CLARK, S. J., SEGALL, M. D., PICKARD, C. J., HASNIP, P. J., PROBERT, M. I., REFSON, K. & PAYNE, M. C. 2005. First principles methods using CASTEP. *Zeitschrift für Kristallographie,* 220**,** 567-570.

DA SILVA, J. L. 2005. All-electron first-principles calculations of clean surface properties of low-Miller-index Al surfaces. *Physical Review B,* 71**,** 195416.

DA SILVA, J. L., STAMPFL, C. & SCHEFFLER, M. 2006. Converged properties of clean metal surfaces by all-electron first-principles calculations. *Surface science,* 600**,** 703-715.

EICHLER, A. & HAFNER, J. 1997. Molecular precursors in the dissociative adsorption of O_2 on Pt (111). *Physical review letters,* 79**,** 4481.

EICHLER, A., MITTENDORFER, F. & HAFNER, J. 2000. Precursor-mediated adsorption of oxygen on the (111) surfaces of platinum-group metals. *Physical Review B,* 62**,** 4744.

FEIBELMAN, P. J. & HAMANN, D. 1985. Modification of transition metal electronic structure by P, S, Cl, and Li adatoms. *Surface Science,* 149**,** 48-66.

FORD, D. C., NILEKAR, A. U., XU, Y. & MAVRIKAKIS, M. 2010. Partial and complete reduction of O_2 by hydrogen on transition metal surfaces. *Surface Science,* 604**,** 1565-1575.

GASTEIGER, H. A., KOCHA, S. S., SOMPALLI, B. & WAGNER, F. T. 2005. Activity benchmarks and requirements for Pt, Pt-alloy, and non-Pt oxygen reduction catalysts for PEMFCs. *Applied Catalysis B: Environmental,* 56**,** 9-35.

GLAND, J. L., SEXTON, B. A. & FISHER, G. B. 1980. Oxygen interactions with the Pt (111) surface. *Surface Science,* 95**,** 587-602.

GREELEY, J. & MAVRIKAKIS, M. 2004. Alloy catalysts designed from first principles. *Nature materials,* 3**,** 810-815.

GREELEY, J., STEPHENS, I., BONDARENKO, A., JOHANSSON, T. P., HANSEN, H. A., JARAMILLO, T., ROSSMEISL, J., CHORKENDORFF, I. & NØRSKOV, J. K. 2009. Alloys of platinum and early transition metals as oxygen reduction electrocatalysts. *Nature Chemistry,* 1**,** 552-556.

HAAS, P., TRAN, F., BLAHA, P. & SCHWARZ, K. 2011. Construction of an optimal GGA functional for molecules and solids. *Physical Review B,* 83**,** 205117.

HAMMER, B. & NØRSKOV, J. 1995. Electronic factors determining the reactivity of metal surfaces. *Surface Science,* 343**,** 211-220.

HARTREE, D. R. The wave mechanics of an atom with a non-Coulomb central field. Part I. Theory and methods. Mathematical Proceedings of the Cambridge Philosophical Society, 1928. Cambridge Univ Press, 89-110.

JALAN, V. M. 1980. Noble metal/vanadium alloy catalyst and method for making. Google Patents.

KEITH, J. A., JERKIEWICZ, G. & JACOB, T. 2010. Theoretical investigations of the oxygen reduction reaction on Pt (111). *ChemPhysChem,* 11**,** 2779-2794.

KOHN, W. & SHAM, L. J. 1965. Self-consistent equations including exchange and correlation effects. *Physical Review,* 140**,** A1133.

LETEBA, G M., R. VANFLEET R. R., & LANG C. I. 2013. Synthesis of V, Pt and Pt-V colloidal nanoparticles. *International Journal of Nanoparticles* 6, 282-295.

LIDE, D. R. 2004. *CRC handbook of chemistry and physics*, CRC press.

MARTIN, R. M. 2004. *Electronic structure: basic theory and practical methods*, Cambridge university press.

MAVRIKAKIS, M., HAMMER, B. & NØRSKOV, J. K. 1998. Effect of strain on the reactivity of metal surfaces. *Physical Review Letters,* 81**,** 2819.

MONKHORST, H. J. & PACK, J. D. 1976. Special points for Brillouin-zone integrations. *Physical Review B,* 13**,** 5188.

MURNAGHAN, F. 1944. The compressibility of media under extreme pressures. *Proceedings of the national academy of sciences of the United States of America,* 30**,** 244.

NOLAN, P., LUTZ, B., TANAKA, P., DAVIS, J. & MULLINS, C. 1998. Translational energy selection of molecular precursors to oxygen adsorption on Pt (111). *Physical review letters,* 81**,** 3179.

NOLAN, P., LUTZ, B., TANAKA, P., DAVIS, J. & MULLINS, C. 1999. Molecularly chemisorbed intermediates to oxygen adsorption on Pt (111): A molecular beam and electron energy-loss spectroscopy study. *The Journal of chemical physics,* 111**,** 3696-3704.

NØRSKOV, J. K., ROSSMEISL, J., LOGADOTTIR, A., LINDQVIST, L., KITCHIN, J. R., BLIGAARD, T. & JONSSON, H. 2004. Origin of the overpotential for oxygen reduction at a fuel-cell cathode. *The Journal of Physical Chemistry B,* 108**,** 17886-17892.

NXUMALO, S. & LANG, C. 2006. Thermodynamic stability of Pt_8V. *Journal of alloys and compounds,* 425**,** 181-184.

OKAMOTO, H. 2009. Pt-V (Platinum-Vanadium). *Journal of phase equilibria and diffusion,* 30**,** 666-667.

OU, L., YANG, F., LIU, Y. & CHEN, S. 2009. First-principle study of the adsorption and dissociation of O2 on Pt (111) in acidic media. *The Journal of Physical Chemistry C,* 113**,** 20657-20665.

OZAKI, A. 1981. Development of alkali-promoted ruthenium as a novel catalyst for ammonia synthesis. *Accounts of Chemical Research,* 14**,** 16-21.

PARKER, D. H., BARTRAM, M. E. & KOEL, B. E. 1989. Study of high coverages of atomic oxygen on the Pt (111) surface. *Surface Science,* 217**,** 489-510.

PAYNE, M. C., TETER, M. P., ALLAN, D. C., ARIAS, T. & JOANNOPOULOS, J. 1992. Iterative minimization techniques for ab initio total-energy calculations: molecular dynamics and conjugate gradients. *Reviews of Modern Physics,* 64**,** 1045.

PERDEW, J. P. 1986. Density-functional approximation for the correlation energy of the inhomogeneous electron gas. *Physical Review B,* 33**,** 8822.

PERDEW, J. P., BURKE, K. & ERNZERHOF, M. 1996. Generalized gradient approximation made simple. *Physical review letters,* 77**,** 3865.

PERDEW, J. P. & SCHMIDT, K. Jacob's ladder of density functional approximations for the exchange-correlation energy. AIP Conference Proceedings, 2001. IOP INSTITUTE OF PHYSICS PUBLISHING LTD, 1-20.

PREDEL, B. 1998. Pt-V (Platinum-Vanadium). *In:* MADELUNG, O. (ed.) *Ni-Np – Pt-Zr.* Springer Berlin Heidelberg.

RUBAN, A., SKRIVER, H. L. & NØRSKOV, J. K. 1999. Surface segregation energies in transition-metal alloys. *Physical review B,* 59**,** 15990.

SANDY, A. R., MOCHRIE, S. G. J., ZEHNER, D. M., GRÜBEL, G., HUANG, K. G. & GIBBS, D. 1992. Reconstruction of the Pt(111) surface. *Physical Review Letters,* 68**,** 2192-2195.

SEROV, A. & KWAK, C. 2009. Review of non-platinum anode catalysts for DMFC and PEMFC application. *Applied Catalysis B: Environmental,* 90**,** 313-320.

SHA, Y., YU, T. H., LIU, Y., MERINOV, B. V. & GODDARD III, W. A. 2010. Theoretical study of solvent effects on the platinum-catalyzed oxygen reduction reaction. *The Journal of Physical Chemistry Letters,* 1**,** 856-861.

SLATER, J. C., SLATER, J. C., SLATER, J. C., PHYSICIST, C. & SLATER, J. C. 1960. *Quantum theory of atomic structure*, McGraw-Hill New York.

SOMORJAI, G. A. & LI, Y. 2010. *Introduction to Surface Chemistry and Catalysis*, John Wiley & Sons.

STAMENKOVIC, V. R., FOWLER, B., MUN, B. S., WANG, G., ROSS, P. N., LUCAS, C. A. & MARKOVIĆ, N. M. 2007. Improved oxygen reduction activity on Pt3Ni (111) via increased surface site availability. *Science,* 315**,** 493-497.

STAMENKOVIC, V. R., MUN, B. S., MAYRHOFER, K. J., ROSS, P. N. & MARKOVIC, N. M. 2006. Effect of surface composition on electronic structure, stability, and electrocatalytic properties of Pt-transition metal alloys: Pt-skin versus Pt-skeleton surfaces. *Journal of the American Chemical Society,* 128**,** 8813-8819.

STEININGER, H., LEHWALD, S. & IBACH, H. 1982. Adsorption of oxygen on Pt (111). *Surface Science,* 123**,** 1-17.

TURCHI, P., STOCKS, G., BUTLER, W., NICHOLSON, D. & GONIS, A. 1988. First-principles study of ordering properties of substitutional alloys using the generalized perturbation method. *Physical Review B,* 37**,** 5982.

TYSON, W. & MILLER, W. 1977. Surface free energies of solid metals: Estimation from liquid surface tension measurements. *Surface Science,* 62**,** 267-276.

VANDERBILT, D. 1990. Soft self-consistent pseudopotentials in a generalized eigenvalue formalism. *Physical Review B,* 41**,** 7892.

WANG, C., ZHENG, A. & LIU, X. 2008. Thermodynamic assessments of the V–Ge and V–Pt systems. *Intermetallics,* 16**,** 544-549.

WATERSTRAT, R. 1973. The vanadium-platinum constitution diagram. *Metallurgical Transactions,* 4**,** 455-466.

XIN, H., HOLEWINSKI, A., SCHWEITZER, N., NIKOLLA, E. & LINIC, S. 2012. Electronic structure engineering in heterogeneous catalysis: identifying novel alloy catalysts based on rapid screening for materials with desired electronic properties. *Topics in Catalysis,* 55**,** 376-390.

XIONG, L. & MANTHIRAM, A. 2005. Effect of atomic ordering on the catalytic activity of carbon supported PtM (M= Fe, Co, Ni, and Cu) alloys for oxygen reduction in PEMFCs. *Journal of the Electrochemical Society,* 152**,** A697-A703.

ZAMBELLI, T., BARTH, J., WINTTERLIN, J. & ERTL, G. 1997. Complex pathways in dissociative adsorption of oxygen on platinum. *Nature,* 390**,** 495-497.